

NOTE TO USERS

This reproduction is the best copy available.

UMI[®]

University of Alberta

Electrochemical Etching of Carbon Materials:
Applications in Microfabrication, Electroanalysis and
Electrospray Mass Spectrometry

by



Solomon Nnyombi Ssenyange

A thesis
presented to the Faculty of Graduate Studies and Research
in partial fulfillment of the
thesis requirement for the degree of
Doctor of Philosophy

Department of Chemistry
Edmonton, Alberta, Canada, 2004

Spring 2004



Library and
Archives Canada

Bibliothèque et
Archives Canada

Published Heritage
Branch

Direction du
Patrimoine de l'édition

395 Wellington Street
Ottawa ON K1A 0N4
Canada

395, rue Wellington
Ottawa ON K1A 0N4
Canada

Your file *Votre référence*

ISBN: 0-612-96321-7

Our file *Notre référence*

ISBN: 0-612-96321-7

The author has granted a non-exclusive license allowing the Library and Archives Canada to reproduce, loan, distribute or sell copies of this thesis in microform, paper or electronic formats.

L'auteur a accordé une licence non exclusive permettant à la Bibliothèque et Archives Canada de reproduire, prêter, distribuer ou vendre des copies de cette thèse sous la forme de microfiche/film, de reproduction sur papier ou sur format électronique.

The author retains ownership of the copyright in this thesis. Neither the thesis nor substantial extracts from it may be printed or otherwise reproduced without the author's permission.

L'auteur conserve la propriété du droit d'auteur qui protège cette thèse. Ni la thèse ni des extraits substantiels de celle-ci ne doivent être imprimés ou autrement reproduits sans son autorisation.

In compliance with the Canadian Privacy Act some supporting forms may have been removed from this thesis.

Conformément à la loi canadienne sur la protection de la vie privée, quelques formulaires secondaires ont été enlevés de cette thèse.

While these forms may be included in the document page count, their removal does not represent any loss of content from the thesis.

Bien que ces formulaires aient inclus dans la pagination, il n'y aura aucun contenu manquant.

Canada

ABSTRACT

The research presented in this work explores the implementation of electrochemical etching to graphitic carbon materials, with a broad focus on the fields of microfabrication, electroanalysis and mass spectrometry. A method is presented for the etching of glassy carbon (GC) and pyrolyzed photoresist films (PPF) that opens pathways enabling the creation of new devices and electrode patterns. This was accomplished through standard lithography to transfer a pattern onto a photoresist layer and electrochemical oxidation of the exposed graphitic surface in basic electrolyte. The reaction at the carbon electrode results in the breakdown of the carbon lattice, which likely involves the intercalation of hydroxide anions. The depth achieved during etching was found to be dependent on the applied potential, anodization time, and the charge that is delivered during the anodization. The presented etching process was found to be isotropic due to the nano-scale graphitic microcrystalline size of GC.

Three proposed applications for the electrochemical etching of carbon material are explored and presented through the design and characterization of various structures in carbon material. The first application illustrates the fabrication of microchannel structures. This represents the first time that a wet etching method has been used in the fabrication of structures into carbon material. The second application involved the electrochemical fabrication and characterization of arrays of sub-micron sized carbon electrodes and band electrodes for their potential use in electroanalysis. Finally, design, fabrication, and operation of a GC microchip interfaced to nanoelectrospray ionization mass spectrometry was explored. This platform was designed to be coupled to an external separation technique, followed by on-chip ionization and spray, culminating in quadrupole mass spectrometric identification of the sample. By analysis of the outlined applications, the electrochemical etching method is presented as a feasible mode of carbon microfabrication.

“Natulenge Juu”

(Let's Aim High)

To my mom who provided me with the greatest training ground that anyone possibly could have. The things that I learned from you, both in Africa and North America will continue to serve me every day in everything that I do.

ACKNOWLEDGEMENTS

There are many people that I would like to thank for their help during my time in Edmonton. First and foremost, my supervisor, Dr. M. T. McDermott who has provided me with the scholarly guidance to explore the world of electroanalytical chemistry, and given me tremendous advice at all stages of my studies at the University of Alberta. It is impossible to imagine that this thesis could ever have become what it has without his example and role as my mentor throughout this entire intellectual journey. Through his generosity, he has given me the opportunity to travel far and wide in order to fully experience the research practice. I will always be grateful for the friendly, yet disciplined environment that you nurtured in our research lab. One of my greatest wishes is for the continued success of the McDermott research group and the best in life for you and your family.

Next, I extend my sincerest gratitude to the McDermott group members, both past and present, for their encouragement and the spirited discussions that we had during various occasions. For the current group members, Vishal, Aaron, Francis, Bushra, Chris, Dwayne, it has been an honor to work with you. To the former McDermott group members namely, Dr. Michael Finot, Dr. Truong Ta, Dr. James Kariuki, Dr. Gregory Kiema, Dr. Mirwais Aktary, Dr. Beatrice Leveugle, and Dr. Abbas Rostami: the path that you created for my success as a McDermott group member, with respect to my being welcome and the large amount of support received, leaves me indebted to your good heartedness. To the summer students, Ryan C. and Erin B., the time that you spent in this lab was thoroughly enjoyable. Without your company, those long summers and the graduate school experience would surely have not been the same. I wish you all success in your future endeavors.

Many thanks also go to the Department of Chemistry support staff, which without their help, the work in this thesis would never have been accomplished. Thanks to the gentlemen in the Glass and Machine Shops who put up with my

urgent demands for the various artifacts that I needed for my projects. Thanks to Ed Feschuk, Al Chilton and Kim Do for the help they provided each time an electronic device needed fixing as well as the hours spent fixing my endlessly malfunctioning TV remote (Oops--I should not say that). I will forever be grateful for the kindness and patience that you showed. Thanks to Kevin Wipf and Tobi Gardner for the laughs and shared camaraderie in both my academic and sporting endeavors; Carolyn Leoung, Bill Donahue, Shandra Doran for their advice and friendship during my tenure at the University of Alberta.

A very special thank you goes to my family, and my girlfriend, Erin Van Overloop. To my Mom, thank you for teaching me the importance of an education, but most importantly, for your endless love, support and the faith. I could never have asked for a better mom and hope that I have made you proud. I love you very much. To my girlfriend, Erin, thank you for your love, patience and support during my studies. The joy that you have brought into my life makes each day that much brighter. Much love goes to my two brothers, Herbert and Daniel, and my sister, Esther. Thank you all for your love and encouragement.

Finally, I would like to acknowledge the Natural Science and Engineering Research Council (NSERC) of Canada for funding of our research group. I wish to express my gratitude George Braybook of Earth and Atmospheric Science, University of Alberta for the SEM images, and all the staff at the University of Alberta's Nanofab Facility for providing the facilities and knowledge for doing the microfabrication work presented in my thesis. This has been a long journey and there stands the possibility that I have forgotten to thank some people that have been instrumental to my success. In which case, I hope you accept my sincerest apologies.

TABLE OF CONTENTS

CHAPTER 1: LITERATURE REVIEW AND TOPIC INTRODUCTION

1.1	INTRODUCTION.....	2
1.2	SUBSTRATE MATERIALS.....	2
1.3	BASIC MICROFABRICATION PROCESSES	5
1.3.1	<i>Film Deposition</i>	7
1.3.2	<i>Lithography</i>	10
1.3.3	<i>Etching</i>	13
1.3.4	<i>Doping</i>	14
1.4	POLYMER MICROFABRICATION TECHNIQUES.....	15
1.4.1	<i>Hot Embossing</i>	15
1.4.2	<i>Injection Molding</i>	19
1.4.3	<i>Soft lithography</i>	20
1.4.4	<i>Laser Photoablation</i>	21
1.4.5	<i>X-ray lithography</i>	22
1.4.6	<i>Miscellaneous techniques</i>	23
1.5	CARBON MATERIALS IN MICROFABRICATION	25
1.5.1	<i>Glassy Carbon in Electroanalytical Chemistry</i>	26
1.5.2	<i>Treatment of GC Surfaces</i>	29
1.6	PYROLYZED PHOTORESIST CARBON FILMS	35
1.7	OBJECTIVES OF THIS THESIS	36
1.8	REFERENCES:.....	39

**CHAPTER 2: MICROFABRICATION OF GLASSY CARBON BY
 ELECTROCHEMICAL ETCHING**

2.1	INTRODUCTION	54
2.2	EXPERIMENTAL.....	56
2.2.1	<i>Materials</i>	56
2.2.2	<i>Mask Preparation</i>	56
2.2.3	<i>Etching of GC substrates</i>	57
2.2.4	<i>Gas Analysis</i>	59
2.2.5	<i>Microscopy</i>	59
2.3	RESULTS AND DISCUSSION	60
2.4	CONCLUSION	73
2.5	REFERENCES.....	74

**CHAPTER 3: ELECTROCHEMICAL FABRICATION OF MICROFLUIDIC
 NETWORKS IN CARBON SUBSTRATES**

3.1	INTRODUCTION.....	83
3.2	EXPERIMENTAL.....	86
3.2.1	<i>Materials</i>	86
3.2.2	<i>Mask Preparation</i>	87
3.2.3	<i>Etching and Sealing of GC Substrates</i>	87
3.2.4	<i>Microscopy</i>	90
3.2.5	<i>Instrumentation for Flow Injection Analysis</i>	93
3.3	RESULTS AND DISCUSSION	94

3.4	CONCLUSION	105
3.5	REFERENCES.....	110

**CHAPTER 4: A GLASSY CARBON MICROCHIP FOR ELECTROSPRAY
MASS SPECTROMETRY**

4.1	INTRODUCTION.....	117
4.2	EXPERIMENTAL.....	119
4.2.1	<i>Fabrication of GC Device</i>	119
4.2.2	<i>Chip-MS Interfacing</i>	120
4.2.3	<i>Mass Spectrometry</i>	121
4.3	RESULTS AND DISCUSSION	122
4.4	CONCLUSION	131
4.5	REFERENCES:.....	132

**CHAPTER 5: ELECTROCHEMICAL FABRICATION AND
CHARACTERIZATION OF PYROLYZED PHOTORESIST
FILM MICRO- AND BAND ARRAY ELECTRODES**

5.1	INTRODUCTION.....	137
5.2	EXPERIMENTAL.....	141
5.2.1	<i>Reagents and Materials</i>	141
5.2.2	<i>Mask Preparation</i>	142
5.2.3	<i>Preparation of the Carbon Films</i>	142
5.2.5	<i>SEM Characterization</i>	143
5.2.6	<i>Electrochemical Experiments</i>	144

5.3	RESULTS ND DISCUSSION.....	144
5.4	CONCLUSIONS.....	161
5.5	REFERENCES.....	164

**CHAPTER 6: CONCLUSIONS AND FUTURE WORK INVOLVING THE
APPLICATION OF ELECTROCHEMICAL ETCHING**

6.1	ELECTROGENERATED CHEMILUMINESCENCE DETECTION ON A GLASSY CARBON MICROCHIP	172
6.2	MICROFABRICATED ELECTROLYSIS PUMP SYSTEM	174
6.3	MODIFIED CARBON SUBSTRATES FOR ELECTROSPRAY MASS SPECTROMETRY STUDIES.....	174
6.4	REFERENCE	176

LIST OF TABLES

Table 1.1	Comparisons of Substrate Materials.....	6
Table 1.2	An overview of the existing master fabrication methods between the different technologies available for fabricating masters [8]. These important aspects should be considered when selecting the described fabrication processes.....	24

LIST OF FIGURES

Figure 1.1	Flow diagram of an integrated circuit fabrication process using the four basic microfabrication techniques: deposition, photolithography, etching, and doping [12]	8
Figure 1.2	Illustration of the steps involved in the lithography of patterns into positive and negative photoresists.....	12
Figure 1.3	Schematic of anisotropic and isotropic etching of a thin film.....	16
Figure 1.4	Schematic illustrating the production of metal electroform and polymer molds using a micromachined silicon master.....	18
Figure 1.5	Schematic representation of glassy carbon [59].....	28
Figure 1.6	Illustration of the surface architecture for (A) polished GC, (B) polished GC with phenolic, carbonyl, and carboxylate functionalities on a diminished polishing layer after electrochemical pretreatment in acid and (C) polished GC with surface oxides after electrochemical pretreatment in base	34
Figure 1.7	Schematic showing the protocol for the preparation of pyrolyzed photoresist films and the resultant high-resolution AFM image taken of a near-atomic flatness carbon film [98].....	37
Figure 2.1	Illustration of the scheme used to microfabricate glassy carbon...	58
Figure 2.2	(A) 110 × 110 μm tapping mode SFM image of the surface of a GC substrate after etching through a TEM grid pattern that was transferred to a layer of photoresist. The line traversing the image corresponds to the cross-sectional profile below the image. (B) SEM image of microwells etched in GC.....	62
Figure 2.3	(A) Plot of etch depth vs. anodization potential at a constant time of 2 min. (B) Plots of current vs. time in response to a potential step. (a) GC, 2.0 V vs. Ag/AgCl, (b) GC, 2.5 V, (c) GC, 3.0 V, (d) Pt, 2.5 V.....	67

Figure 2.4	10 × 10 μm STM images of GC. (A) As polished GC, RMS = 5.4 ± 0.9 nm. (B) Following etching for 8 min. at 2.0 V, RMS = 4.5 ± 1.0 nm.....	69
Figure 2.5	(A) SEM image illustrating the measurement of etch depth. (B) Plot of etch depth vs. time at a constant potential of 2.5 V. (C) Plot of etch depth vs. charge. Experiment was carried out at a constant current of 100mA.....	70
Figure 2.6	SEM image of a microchannel etched in GC at 2.0 V for 30 min. The semicircular profile is indicative of isotropic etching.....	72
Figure 3.1	Illustration of the scheme used to fabricate the microchannels in glassy carbon by electrochemical-wet etching.....	88
Figure 3.2	Schematic describing the procedure used to prepare PDMS sealing and glass bonding for a GC microchip for fluorescence detection. For glass bonding, after etching was completed, adhesive was applied and cured with a UV lamp.....	91
Figure 3.3	The experimental set-up for the flow injection analysis with laser induced fluorescence of fluorescein. An argon ion laser was used as the source, followed by a focusing lens, GC microchip and the emitted light focused into a PMT detector. The optical image is an illustration of the GC substrate that was used in the experiments.....	92
Figure 3.4	SEM image of a single "T" glassy carbon microchannel fabricated by electrochemical etching at 2.0V for 30 min.....	95
Figure 3.5	SEM image of a single "T" microchannel fabricated in glassy carbon at a constant current of 100mA for 80 min. The inset shows a close-up view of the slanted channel wall which was indicative of mask undercutting.....	96
Figure 3.6	SEM image of a microchannel networks etched in GC at 2.0V for 30min.....	97
Figure 3.7	SEM image of a 1cm x 2.5 cm glassy carbon chip showing an etched electrolysis pump device. Channels are ~30μm deep and either 300μm or 600μm wide as illustrated by the 2 different line widths. The chevron barrier is shown to the left of the device. Anodization was carried out at 2.0V for 80 min.....	99

Figure 3.8	Fluorescence micrograph of a single microchannel containing FITC labeled IgM. The channel is $\sim 300\mu\text{m}$ wide and shows the resultant poor seal achieved with PDMS elastomer.....	102
Figure 3.9	Fluorescence micrograph of 2 channels containing 10mM PBS buffer and FITC labeled IgM. The channels, which illustrate excellent sealing achieved using bonded glass are also $\sim 300\mu\text{m}$ wide and are separated by a barrier wall.....	103
Figure 3.10	Figure 3.10 Flow injection analysis (FIA) of (a) 100% methanol (b) $1\mu\text{M}$ fluorescein, (c) $2\mu\text{M}$ fluorescein, (d) $5\mu\text{M}$ fluorescein, (e) $7\mu\text{M}$ fluorescein, (f) $10\mu\text{M}$ fluorescein at 530nm following suction of fluorescein samples through GC chip. FIA was performed in a mobile phase composed of 100% methanol.....	107
Figure 3.11	A calibration curve of the various fluorescein solutions that were pressure driven a channel of the GC based FIA-LIF device shown in figure 3.7.....	108
Figure 3.12	SEM image of a single meandering microchannel fabricated in a pyrolyzed photoresist film (PPF). The channel is $300\mu\text{m}$ wide and $2.5\mu\text{m}$ deep. The inset shows a close-up view of the channel wall from which we can observe its morphology. Anodization was carried out at a constant voltage of 2.0V for 8 min.....	109
Figure 4.1	Illustration of the scheme used to fabricate the glassy carbon chip	123
Figure 4.2	Experimental setup of the GC nanoelectrospray device. The sample is introduced via a syringe pump and the high voltage is applied to the glassy carbon chip. The nanospray tip creates a spray that is directed into a quadrupole mass spectrometer.....	124
Figure 4.3	Resulting spectrum from infusion of the PPG standard. Spectrum is the sum of 50 scans. The main plot shows m/z range 550 to 2800 and the inset 50 to 550 both at a step size of 0.1 amu. ESI voltage was 3850 V.....	126
Figure 4.4	Long-term stability of the signal collected from the device for the PPG standard. The m/z range was 750 to 1400 at a step size of 0.5 amu. ESI voltage was 3900V.....	127

- Figure 4.5 Mass spectra from infusion of angiotensin II at various concentrations. A single spectrum is shown in plots A-C. The peak at $m/z = 524$ corresponds to the doubly charged state of angiotensin. In all plots the m/z range was 504-544 at a step size of 0.1 amu and ESI voltage was 3200 V. (A) Infusion of 6.69 μM angiotensin II (B) The black trace represents infusion of 134 nM angiotensin II. The grey trace is the running buffer alone collected immediately before injection. (C) The black trace represents infusion of 26.8 nM angiotensin II. The grey trace is the running buffer alone collected immediately before injection. The black traces in both B and C have been offset in the y direction for ease of comparison to the buffer trace. (D) Total ion chromatogram for infusion of 26.8 nM angiotensin at a scan rate of 2.5 spectra s^{-1} . **129**
- Figure 5.1 Schematic showing the lithographic and electrochemical procedure used to fabricate the microband and microelectrode arrays.....**145**
- Figure 5.2 Scanning electron micrographs of electrochemically etched carbon microelectrode arrays. A) SEM image of ~ 1600 carbon microelectrode arrays. B) SEM image of a single cube shaped carbon microelectrode.....**146**
- Figure 5.3 Two sets of microelectrode arrays etched for two different periods of time in identical solutions. The SEM image in (A) is an illustration of an array etched for 30min while the one in (B) represents an array etched for 60 min.....**148**
- Figure 5.4 Schematic illustrating the three diffusion regimes associated with microelectrode arrays. (a) overlapping spherical diffusion to microelectrodes (b) spherical diffusion to microelectrodes and (c) planar diffusion to microelectrodes.....**150**
- Figure 5.5 Typical cyclic voltammograms acquired with a carbon microelectrode array using potassium ferricyanide and 1M KCl. (a) CV of silicon substrate (b) CV collected at 20mV/s and (c) CV collected at 200mV/s.....**151**
- Figure 5.6 Log (cathodic peak current) vs. Log (scan rate) for cyclic voltammograms of 5mM ferricyanide in potassium chloride. Curve a represents the theoretically expected relation where $m=0.5$ while curve b, represents the observed relationship when data was collected using the carbon microelectrode arrays**152**
- Figure 5.7 SEM image of electrochemically etched carbon microband arrays. A) Array with width $\sim 10 \mu\text{m}$ and an interband distance of $\sim 50 \mu\text{m}$.

The inset represents the junction between the bulk PPF pad and a single microband electrode. B) Array with band width of $\sim 20 \mu\text{m}$ and an interband distance of $\sim 200 \mu\text{m}$. The inset represents the junction between the bulk PPF pad and a single microband electrode.....**157**

- Figure 5.8 Cyclic voltammograms acquired with carbon microband array electrodes as shown in Figure 5.7A using $500 \mu\text{M}$ potassium ferricyanide and 1M KCl**158**
- Figure 5.9 Cyclic voltammograms acquired with carbon microband array electrodes as shown in Figure 5.7B using $500 \mu\text{M}$ potassium ferricyanide and 1M KCl**159**
- Figure 5.10 Cyclic voltammograms for the reduction of 4-nitrobenzene (NB) diazonium tetrafluoroborate in 0.1M H_2SO_4 (a) A wave corresponding to the reduction of nitrobenzene on the carbon surface and (b) A smaller wave on a second scan after the initial deposition wave was acquired. All CV's were acquired at a scan-rate of 100mV/s**162**
- Figure 5.11 Figure 5.11 Cyclic voltammograms showing the blocking of the surface by NB of the carbon microband arrays as diagnosed with dopamine voltammetry (A) and the typical dopamine voltammogram acquired with unblocked (bare) carbon microband array electrodes. The microband array used was as shown in Figure 5.7B. All CV's were acquired at a scan-rate of 100mV/s**163**

ABBREVIATIONS, SYMBOLS AND UNITS

Å	angstrom (10 ⁻¹⁰)
σ	standard deviation
Ω	ohms
v	scan rate
≥	greater than or equal to
<i>i</i> _{pa}	anodic peak current
APCVD	atmospheric pressure chemical vapor deposition
AFM	atomic force microscopy
amu	atomic mass unit
O/C	atomic oxygen to carbon ratio
BOE	buffered oxide etch
CVD	chemical vapor deposition
CAD	computer-assisted design
c.p.s	counts per second
<i>iR</i>	current times resistance
CV	cyclic voltammetry
DRIE	deep reactive ion etching
°C	degrees celsius
EGO	electrochemical graphitic oxide
ECP	electrochemical pretreatment
ECL	electrogenerated chemiluminescence
ESI	electrospray ionization
F	faraday's constant
FIA	flow injection analysis
FITC	fluorescein-6-isothiocyanate
GC	glassy carbon
Hz	hertz
HPLC	high performance liquid chromatography
IgM	immunoglobulin class M
L _c	interplanar microcrystalline size
L _a	intraplanar microcrystallite size
IBE	ion beam etching
LIGA	lithography and electro-deposition machining
LPCVD	low pressure chemical vapor deposition
MS	mass spectrometry
m/z	mass-to-charge ratio
MOSFETs	metal oxide semiconductor field effect transistors
μ-EDM	micro electro-discharge machining
MEMS	microelectromechanical systems
min	minute
NB	4-nitrobenzene
NEEs	nano electrode ensembles
PMT	photo-multiplier tube

PVD.....	physical vapor deposition
PECVD.....	plasma-enhanced chemical vapor deposition
PECVD.....	plasma-enhanced chemical vapor deposition
PDMS.....	poly(dimethylsiloxane)
PMMA.....	poly(methyl-methacrylate)
PPG.....	polypropylene glycol
PPF.....	pyrolyzed photoresist films
RIE.....	reactive ion etching
RSD.....	relative standard deviation
RC.....	resistive-capacitive
RMS.....	root-mean-square
rpm.....	rotations per minute
SCE.....	saturated calomel electrode
SEM.....	scanning electron microscopy
SPM.....	scanning probe microscopy
STM.....	scanning tunneling microscopy
s.....	seconds
TM SFM.....	tapping mode scanning force microscopy
2-D.....	two-dimensional
TIC.....	total ion chromatogram
UV.....	ultra violet
XPS.....	X-ray photoelectron spectroscopy

Mathematical prefixes

k.....	kilo (10^3)
c.....	centi (10^{-2})
m.....	milli (10^{-3})
μ	micro (10^{-6})
n.....	nano (10^{-9})
p.....	pico (10^{-12})
f.....	femto (10^{-15})
a.....	atto (10^{-18})

CHAPTER 1

LITERATURE REVIEW AND TOPIC INTRODUCTION

1.1 INTRODUCTION

The desire to create structures and patterns on micro- and nano-scale lengths has triggered a wide range of scientific investigations. This interest has led to the development of many devices to pattern surfaces as well as to transport and manipulate fluids. Microfabrication or micromachining, refers to the fabrication processes employed in the manufacture of micro-electro-mechanical systems (MEMS) and is the foundation of the manufacturing processes for silicon and glass-based chemical and biological microchips. The field of microfabrication comprises the use of a set of tools, commonly used in semiconductor engineering, for creating small multidimensional structures with dimensions ranging from a millimeter to a few nanometers [1]. Within the realm of microfabrication technology, there are several approaches that are utilized in fabricating microchips for chemical and biological analysis. They are divided into two categories: (1) Microfluidic technology, which uses all facets of the microfabrication processes to create three dimensional (3-D) structures for chemical reactions and separations through the manipulation of fluid movement; and (2) Microarray technology, which uses microlithography, contact, or drop-on-demand printing to form 2-D biologically active arrays on flat substrate surfaces for biological assays [2].

1.2 SUBSTRATE MATERIALS

Since the advent of bulk micromachining, silicon has been at the forefront of microfabrication. The first known use of silicon as a micromechanical

substrate can be traced back to an innovation and an idea from the mid-1950s and early 1960's, respectively. The innovation was the large piezoresistance in silicon and germanium [3] while the idea stems from a proposed diffusion technique for the fabrication of silicon piezoresistive sensors for stress, strain and pressure [4].

As a substrate and structural material in the fabrication of chemical and biological sensor devices, such as the lab-on-a-chip technology, silicon often presents an excellent substrate choice due to its intrinsic mechanical stability and the viability of integrating sensing and circuitry components on the same substrate. However, the choice of silicon as a substrate is not always straightforward and therefore, it is important to consider criteria such as ease of metallization (referring to the metal layers that electrically interconnect the various device structures fabricated on the silicon substrate), cost and machinability (referring to a measure of the ease with which a substrate can be machined or etched satisfactorily) in ranking silicon against other readily available substrates for microfabrication. These criteria are important because they aid in determining the feasibility of using the various substrates for a variety of devices such as chemical sensors, optical devices and micro-instrumentation. With an increasing need for all types of micromachines with a wide variety of functions, a comparison of these criteria among the various micromachining materials can help improve efficiency in production, aid in the choice of protocol for optimal device fabrication and provide a focus on the vital properties of the

various substrates that could be exploited for a specific application.

Table 1.1 shows a comparison of substrate materials in terms of cost, metallization ease, and machinability [2]. As observed, substrate materials such as ceramics and glass are challenging to microfabricate while plastics are not readily amenable to metallization without extensive modification. Conversely, silicon is extremely easy to micromachine, with features on the order of a few microns easy to fabricate. Silicon is also extremely flat and has well established coating procedures, which afford its preference especially in the formations of thin films. Disadvantages of using silicon as a substrate stem from its high cost per unit area, which becomes distinct with increasing device size and low production volume. This is the reason why glass (e.g. quartz, fused silica, and borosilicate) has been the dominant substrate for the fabrication of miniaturized analytical systems in the early 1990s [5,6]. A better insulator than silicon, glass is also less expensive and can be fabricated using similar methodologies. Also, surface properties and the derivatization methods used for the modification of glass surfaces have been well developed and characterized [7].

The cost of producing systems in glass in combination with its lack of machinability is driving commercial producers to seek other materials. Manufacturers of miniaturized analytical systems such as microfluidic devices see many benefits in employing plastics or polymers. These include reduced cost, and simplified manufacturing procedures particularly when compared to silicon and glass. Also, an added advantage is the wide range of available

plastic materials, which allows the manufacturer to choose material properties that are suitable for their specific application. Plastics, unlike glass, can be manufactured containing a number of additives that impact their mass-production processing and shelf life. These can include fillers, plasticizers, heat stabilizers, antioxidants, and UV stabilizers [8].

Ceramics have been extensively used as substrates for hybrid microelectronics and are common in microelectronics packaging [9]. The standard material is alumina (Al_2O_3) and other materials include beryllium oxide (BeO) and aluminum nitride (AlN). Chemical inertness, biocompatibility and mechanical rigidity make ceramics a very interesting material for miniaturized analytical systems [9].

1.3 BASIC MICROFABRICATION PROCESSES

Microfabrication processes are used to produce devices with dimensions in the micrometer to millimeter range. These processes can be effectively applied to yield single device or thousands of devices. Microfabrication processes therefore, significantly differ from conventional, sequential machining process. With regard to the properties of the material being used, different microfabrication protocols have different and very specific constraints.

Substrate	Cost	Metallization	Machinability
Ceramic	Medium	Fair	Poor
Plastic	Low	Poor	Fair
Silicon	High	Good	Very Good
Glass	Low	Good	Poor

TABLE 1.1 Comparisons of Substrate Materials

The semiconductor industry originated a set of standard processing steps for the fabrication of silicon and glass substrates. Four basic microfabrication techniques are used for integrated circuitry fabrication and shown in Figure 1.1. These include film (metal, silicon nitride, silicon dioxide, diamond and polymer) deposition, patterning, etching and doping. Figure 1.1 illustrates how these techniques are combined to build a device, layer by layer. A brief overview of the four basic microfabrication techniques will be given in the following sections [10-12].

1.3.1 Film Deposition

Thin films are essential building materials in microchip technology. Usually 0.05-50 μm thick, several types of films have been shown to achieve different properties on the various substrate materials. Dielectric layers, such as silicon dioxide, and silicon nitride can be used as insulators. Metal layers, such as gold, copper, silver, aluminum, tungsten, and titanium can be used as electrodes, electrical interconnects or as mirror surfaces while highly doped polycrystalline silicon can be used as gate material and resistor material for MOSFETs and piezoresistive sensors respectively. Various polymers are also utilized as thin films in microchip fabrication with the most utilized polymer noted to be spin-coated photoresist.

Two film deposition techniques are commonly used in the microfabrication of silicon and glass substrates. They can either be physical, such as in physical

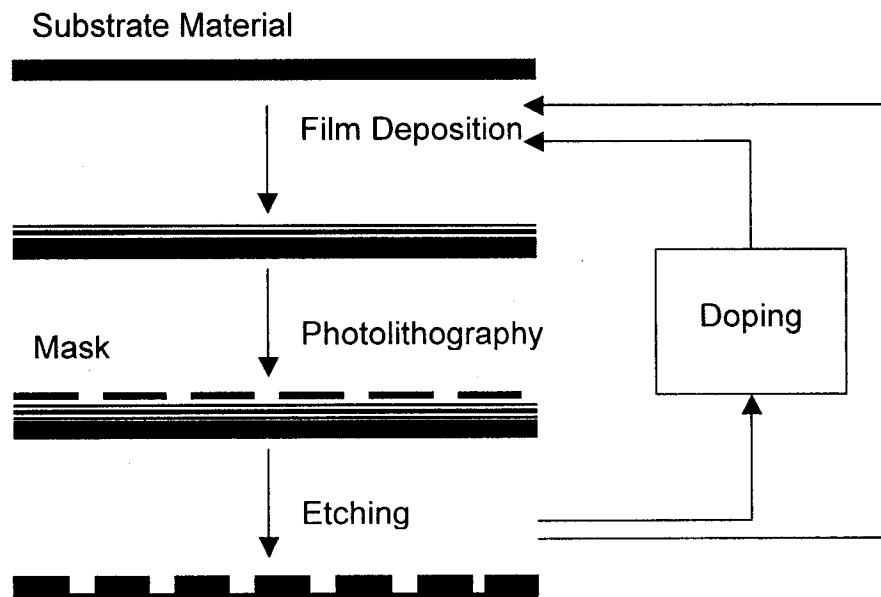


Figure 1.1: Flow diagram of an integrated circuit fabrication process using the four basic microfabrication techniques: deposition, photolithography, etching, and doping [13].

vapor deposition (PVD) or chemical, as in chemical vapor deposition (CVD). PVD occurs when either of sputtering, spin coating and evaporations are performed while CVD can be carried out at low pressure (LPCVD), atmospheric pressure (APCVD) or plasma-enhanced (PECVD).

In CVD, mass transport of reactant and diluent gases occurs in the deposition zone of a furnace. Homogeneous gas phase reactions lead to the formation of film precursors and by-products. Finally, adsorption of film precursors and reactants leads to nucleation and growth onto a surface forming a film. Many different thin films can be deposited using this method including polycrystalline silicon, silicon nitride and metals like tungsten. PECVD is a special CVD technique in which a gas decomposes into its components with the aid of plasma which speeds up the process. Advantages include faster deposition rates and lower deposition temperatures than regular CVD. The technique is mainly used to deposit inter-metal dielectric layers and organic layers.

In the PVD method of sputtering, a high vacuum chamber (10^{-7} to 10^{-8} mTorr) with either argon, helium or xenon forms a plasma using a direct current or resonant frequency power supply. Upon ignition, positive ions from this plasma bombard the target material designated as the cathode. This process sputters material away from the target as neutral atoms and deposits them onto a substrate, designated as the anode. This coats a thin film onto the substrate. It is advantageous to use sputtering because one can use multiple substrates and

materials, thereby increasing its feasibility in mass production, and also, most materials can be sputtered. Evaporation requires heating of a crucible in which the material to be deposited is placed. A shutter acts as a shield that can be open or shut to let the material of interest reach the substrate. Like sputtering, the process is carried out under high vacuum. Relatively simple and inexpensive, evaporation suffers from shadow effects on most of the deposited thin films when not rotated. The shadowing is a result of the point source, which is used for the deposition. It is also hard to deposit films with high melting points, such as tungsten, with evaporation. There are also several other deposition techniques, which include electroplating of thin metal films such as gold, spin- or spray-coating of polymeric films such as photoresist, and reactive growth of thin films.

1.3.2 Lithography

Lithography is the standard process of transferring a pattern onto a substrate. If light is used to transfer patterns from a mask onto a wafer, then this is referred to as photolithography. Briefly, a mask with the desired pattern is created. Generally, the mask is a glass plate with two layers deposited onto it. The middle layer, usually a thin metal film such as chromium, is sandwiched by an outside layer, in most cases photoresist. A pattern that has previously been designed with computer-assisted design program is then written into the photoresist layer using a laser by a pattern-generating machine. The photoresist on the glass plate is developed and the underlying metal film finally etched to

give a patterned opaque layer on the surface of the plate.

On the substrate, a photoresist layer is first spin-coated and then exposed to UV light through a mask. Depending on whether positive or negative photoresist was used, the exposed or unexposed photoresist areas are removed during the resist development process. As illustrated in Figure 1.2, when positive photoresist is exposed to UV light, the polymer is degraded and is easily washed away using a developer solution. Conversely, when negative photoresist is exposed to UV light, the polymer cross-links, thereby forming stable structures that are not easily removable with developer solution. In both cases, the remaining photoresist acts as a protective mask during the etching process or as a mask for subsequent ion implantation during a doping process.

Common in photolithography is a *lift-off* technique that is used to structure thin films that would be difficult to etch. In this technique, a thin-film material is deposited on top of the patterned photoresist. To avoid a continuous film, the thickness of the deposited film must be less than the resist thickness. Removal of the underneath photoresist “lifts off” the thin-film material on top thereby leaving a structured thin film on the substrate. Another technique that has recently come of age in micro- and nanofabrication is known as microcontact printing or soft lithography [14,15]. Microcontact printing uses a soft polymeric material to reproduce a desired pattern directly on a substrate. The polymeric material, in most cases made from poly (dimethylsiloxane) (PDMS), is formed by a molding process using a master fabricated with conventional microfabrication

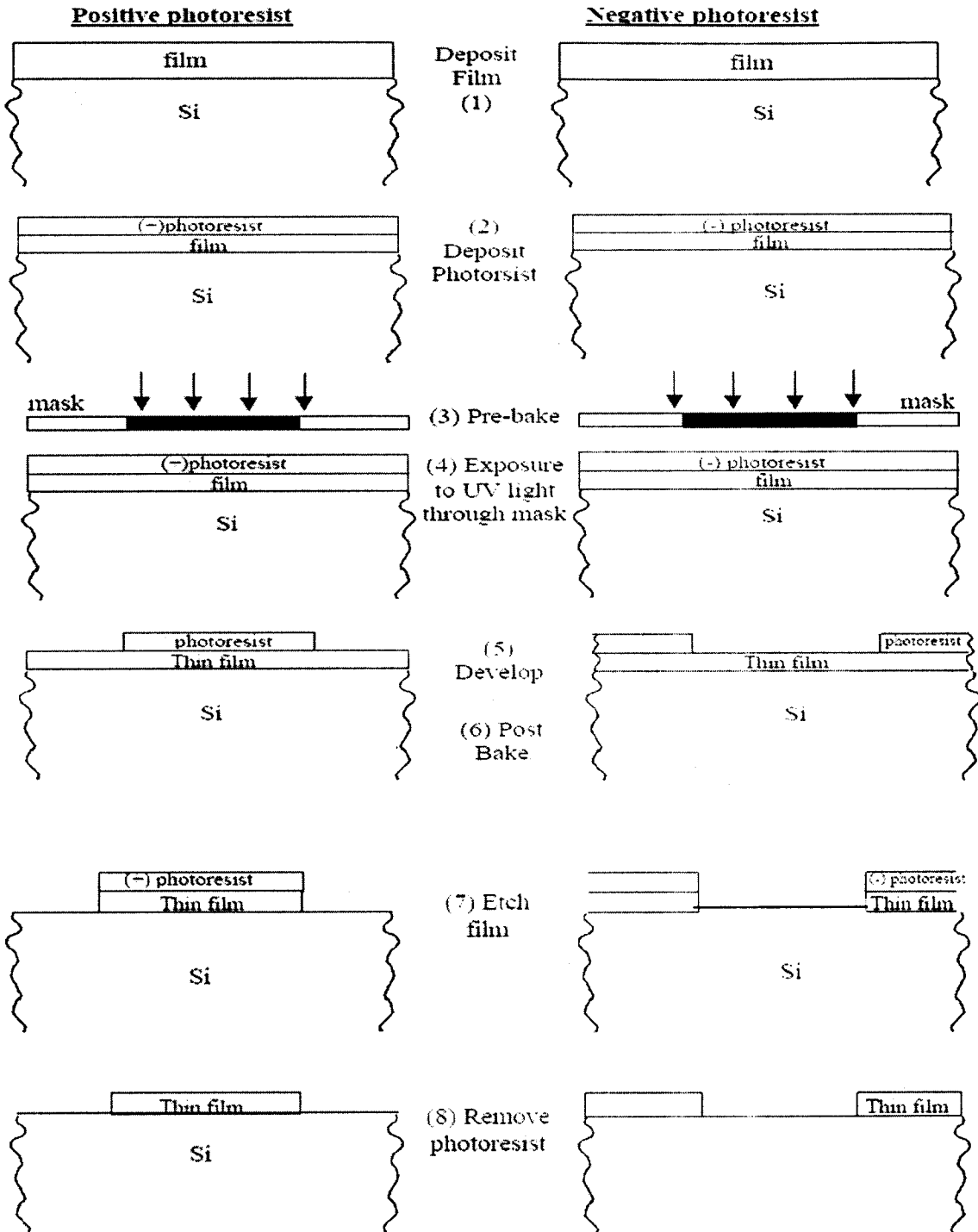


Figure 1.2: Illustration of the steps involved in the photolithography of patterns into positive and negative photoresists.

techniques. After “inking” the stamp with material to be printed, the stamp is brought in contact with the substrate and the pattern of the stamp is reproduced.

1.3.3 Etching

Microfabrication of silicon and glass consists of two different categories of etching processes known as wet chemical etching and dry (plasma) etching. In wet chemical etching, a substrate with patterned photoresist is immersed in basic or acidic etchants. The process serves to remove material from a substrate. Agitation or heat can be used to speed up and control the performance of the etching (e.g. when several different shapes are being etched). In dry or plasma etching, a chemical etchant in its plasma state, such as gas-phase fluorine or chlorine, is instead used to remove material from the substrate [10,11]. Wet etching and dry etching can either be anisotropic or isotropic. In the anisotropic case, etching occurs at different etch rate in different directions. In the case of isotropic etching, the same etch rate occurs in all directions. Illustrated clearly in Figure 1.3, these modes of etching are widely used in silicon and glass microfabrication. It should be noted that the choice for using a particular etching process over another includes material etch rate, selectivity of the material to be etched versus other material such as the resist and isotropy/anisotropy of the etching process.

Wet etching is often isotropic with the important exception of anisotropic silicon etching in the alkaline solution of potassium hydroxide. Wet etching also provides better etch selectivity for the material to be etched in comparison to

accompanying other materials. An example includes wet etching of glass using hydrofluoric-acid-based chemistry. Silicon dioxide is isotropically etched in diluted hydrofluoric acid (HF: H₂O) or buffered oxide etch (BOE) (HF: NH₄F).

However, dry etching is often anisotropic, resulting in a better pattern transfer, as mask undercutting is averted as illustrated in Figure 1.3. Several anisotropic dry etching processes, such as reactive ion etching (RIE) and deep reactive ion etching (DRIE), are common in the field of microfabrication. In an RIE system, reactive ions are generated in a plasma and are accelerated toward the surface to be etched thereby providing directional etching characteristics. Higher ion energies typically result in more anisotropic etching characteristics but also lead to reduced etching selectivity. In a DRIE system, two distinct gases, such as SF₆ for etching and C₄F₈ for passivation, are used to achieve higher selectivity (indicating the directionality of the etching process) for silicon and glass substrates. Typically, DRIE machines cycle between an etching cycle and a passivating cycle in a time multiplexing scheme to create features with an aspect ratio greater than 70:1.

1.3.4 Doping

The introduction of ions into substrate materials is known as doping. This is carried out by either implantation or diffusion from a gaseous, liquid or solid source into a substrate material such as silicon, germanium or gallium arsenide [16]. Primarily, doping is used for the modification of the electrical conductivity of semiconductor materials and is one of the key processes during the fabrication of

semiconductor devices such as diodes and transistors. In the case of silicon, doping with phosphorus or arsenic yields *n*-type silicon whereas doping with boron results in *p*-type silicon. By varying the dopant concentration of *n*-type silicon from 10^{14} to 10^{20} ions per cm^{-3} , the resistivity at room temperature can be reduced from $\sim 40 \text{ } \Omega\text{cm}$ to $7 \times 10^{-4} \text{ } \Omega\text{cm}$ [13], which is approximately 350 times more resistant than copper.

1.4 POLYMER MICROFABRICATION TECHNIQUES

In addition to existing microfabrication technologies for the manufacturing of silicon or glass-based microsystems, the increase in demand for low cost polymer-based devices established technologies for the micromachining of polymer substrates in the late 1990s. Microstructures with dimensions in the range of 15-30 μm [8] have been realized using polymer microfabrication techniques, which can be divided into two fields: processing and replication. Processing begins with the design and structuring of positive relief known as the “master”. Replication of the master design is then followed by back-end processing, i.e., drilling, metallization, and bonding of the fabricated substrate. A brief review of some of the fabrication technologies is given below.

1.4.1 Hot Embossing

Hot embossing and imprinting of plastics in the fabrication of polymeric microstructures was first described in the late 1990s by several groups [17-21]. The first technique described the use of wires for imprinting plastic [20] but in

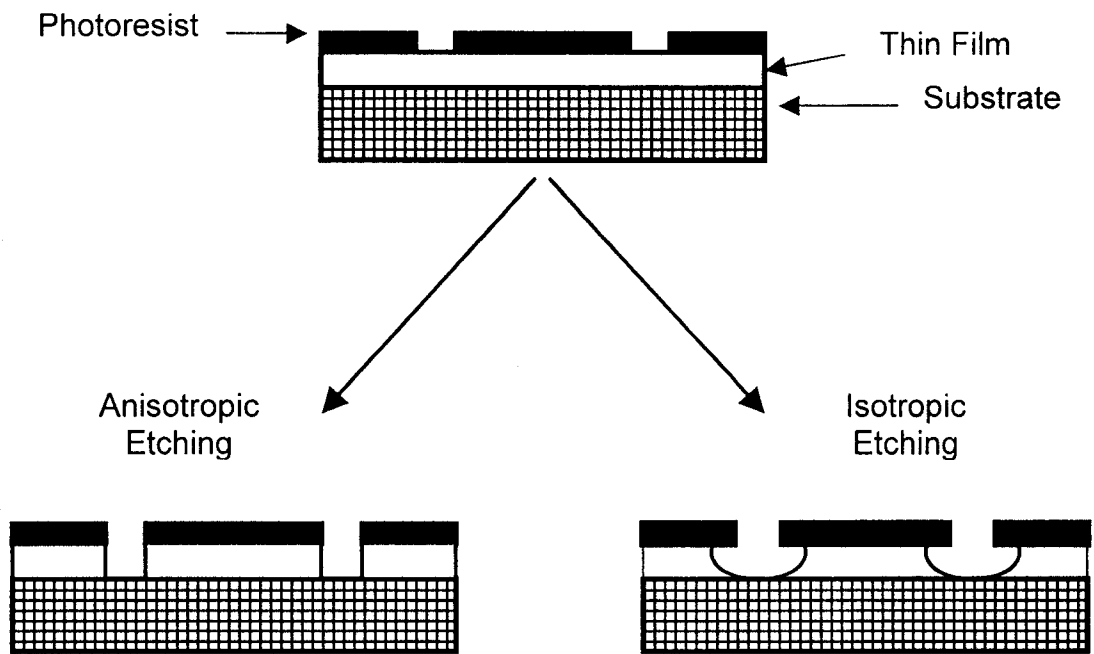


Figure 1.3: Schematic of anisotropic and isotropic etching of a thin film.

recent times it has been common to use a silicon stamp as an imprinting tool for the fabrication of polymer microsystems. In making a silicon stamp, a drawing of the channels is first created using a CAD tool, and the image transferred to a photomask or alternatively to a high contrast resolution transparency if features greater than 20 μm are desired.

Typically, a single crystal silicon wafer is coated with a masking material such as silicon dioxide or silicon nitride, and then coated with a layer of photoresist. A transparency is then placed on top of the wafer and upon exposure to the UV light, the photoresist is developed revealing the transferred image. The image is then transferred to the exposed masking layer by etching in a solution of hydrofluoric acid (HF) and potassium hydroxide (KOH) for silicon dioxide and silicon nitride, respectively. The exposed silicon is then anisotropically etched and the result is a raised three-dimensional inverted image of the initial image. The height and the width of the positive image may be controlled by the amount of time the wafer is etched. The etched silicon stamp may then be used to imprint features, such as microchannels, in plastic materials at room temperature [22], or at elevated temperature [20].

Alternatively, a micromachined silicon wafer may be used to fabricate a stamp in metal as illustrated in Figure 1.4 [23]. In this process, a metal electroform is produced using the micromachined silicon wafer as the master. The first metal electroform is the mirror image of the master. Then, a second metal electroform is created using the first electroform as a template. The second

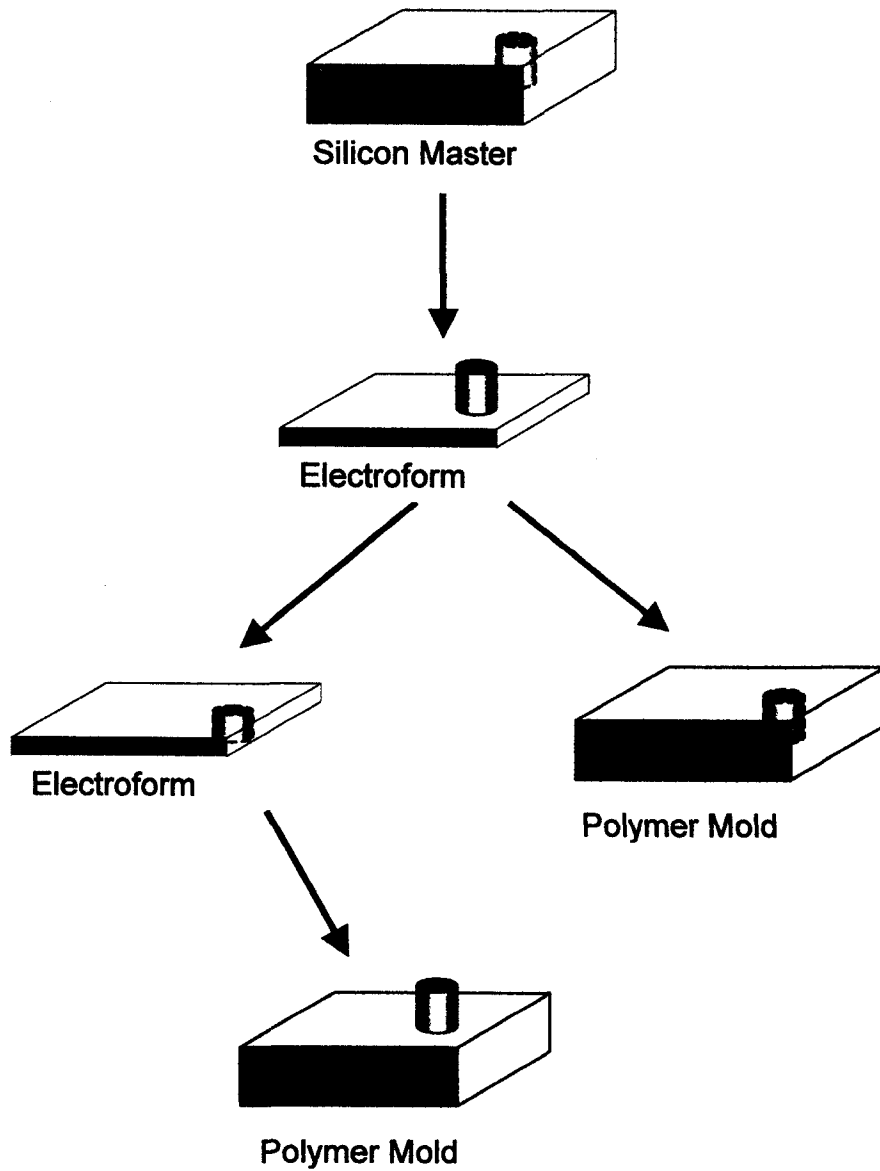


Figure 1.4: Schematic illustrating the production of metal electroform and polymer molds using a micromachined silicon master.

electroform is then a replica of the original silicon master. Thus, micrometer features are transposed to the more robust metal substrate. The metal stamp can be used to fabricate microchannels in plastic substrates by imprinting or injection molding.

To imprint or emboss microstructures, a hard polymeric material is thoroughly cleaned, dried, and then placed on top of the silicon or metal stamp. The stamp and plastic are then placed in a hydraulic press and pressure is applied for a specific time. Hot embossing is performed at temperatures close to the softening temperature of the plastic and at lower pressures. When devices are hot embossed, the resulting polymer microstructure dimensions are mirror images of the silicon stamp. When devices are imprinted at room temperature, the microchannel dimensions are much more dependent on parameters including imprinting pressure, imprinting time and properties of the polymer itself [20]. However, an advantage of imprinting at room temperature is that fabrication time is reduced when compared to hot embossing.

1.4.2 Injection Molding

Injection molding techniques for fabricating microchannels were first described by researchers at Aclara [23]. Silicon masters are fabricated using a wet etch procedure, however, the silicon wafers can also be processed using DRIE to provide structures with higher aspect ratios [24]. As previously described, a nickel electroform is used to transfer micro features from the silicon master to an injection molding suitable substrate. The nickel electroforms from a

single silicon master can be used to produce thousands of injection molded parts. In the injection molding process, the nickel electroform is mounted onto a mold insert and the polymer resin introduced to produce the microstructured parts. During the injection process, the polymer solution has relatively low viscosity, which leads to good contact with the mold resulting in well-defined features. Variables that can impair the replication of micron-sized features include mold temperature and relaxation of the polymer after release from the mold. By adjusting the process time and temperature, injection molded parts can be fabricated with excellent precision. Advantages of using injection molding over imprinting or hot embossing include the ability to create three-dimensional structures and the implantation of pre-formed polymer structures during the molding process.

1.4.3 Soft lithography

As previously described, a significant advancement in microfabrication technologies was the introduction of polymer molding techniques, known as soft lithography [25-27]. As with the methods described thus far, a positive relief master must be fabricated. An elastomeric polymer, in most cases PDMS, is then cast onto the silicon stamp and allowed to cure. After curing, either at room temperature or at a slightly elevated temperature (generally 40–70 °C for PDMS), the polymer is peeled off the stamp. Since the stamp is not exposed to excessive pressure, as with imprinting, or excess heat, as with injection molding, fabrication of a metal electroform is unnecessary. A unique advantage of this

fabrication technique is that elastomeric polymers can easily be bonded to each other or to plastic or glass substrates by conformal contact. The simplicity inherent with the sealing procedure has made this fabrication technology one of the most widely used for prototyping microfluidic systems.

1.4.4 Laser Photoablation

Laser ablation was first introduced as a method for fabricating polymer microfluidic channels by Roberts and coworkers [28] in 1997. In the laser ablation process, a polymer is exposed to a pulsed UV laser source, and the absorption of that light induces bond-breakage in the polymer backbone [29]. The exact mechanism of polymer decomposition in the ablation process is unknown, however, it has been widely accepted that either photodegradation or thermal degradation, or a combination of the two occurs. Local temperatures on the polymer surface during ablation have been reported to be very high, i.e. 427 °C for poly (methyl-methacrylate) (PMMA) [30].

Micromachining using laser ablation can be achieved by exposing a polymer substrate to a laser through a mask that defines the area to be ablated. The mask must be made from a material that does not have significant absorption at the laser wavelength, such as chromium metal. Alternatively, microstructures can be defined and micromachined using a direct-write, maskless process. In this process, the polymer substrate is placed on a programmed-moveable stage, and the substrate is moved under the focused laser beam to create the desired structure. The direct-write micromachining

process is advantageous in that a mask does not have to be created to change the design of desired microstructures therefore, the design can be changed rapidly during the prototyping process. The disadvantage to this approach is that parts are made in a sequential manner thereby limiting the ability to mass-produce devices for commercial applications. In the fabrication of microstructures, their roughness and depth is dependent on parameters, which including polymer absorption, laser power, pulse rate, and number of passes made across the structure. Fabricated microstructures, such as microchannels are generally square or rectangular shaped with straight walls, however, in very deep channels, walls can become slanted due to laser defocusing effects with each successive pass.

1.4.5 X-ray lithography

Over the last decade, X-ray lithography has been modified for fabricating polymer microchannels [31-33]. The most common substrate material used in this process is PMMA because it exhibits high X-ray absorption (soft X-rays of 0.7–0.8 nm) and is sensitive to X-ray degradation. For the fabrication of microstructures using X-ray lithography, a quartz–chrome mask is first generated to define the pattern. For the process to be successful, a reusable gold/Kapton™ mask has to be created since the Kapton layer is transparent to X-rays. The Kapton layer is then coated with photoresist and the image from the quartz–chrome mask is transferred photolithographically to the photoresist over the Kapton layer. Once the photoresist is developed, a thick layer of gold is

deposited onto the Kapton surface in the open areas in the photoresist. Thick gold layer absorbs X-rays thereby protecting the polymer substrate that lies beneath it. Regions of the Kapton without the thick gold layer are transparent to the X-rays. The photoresist is removed, and the polymer substrate material is irradiated with X-rays through the gold/Kapton mask to degrade the exposed polymer. The exposed, degraded polymer is dissolved with developing solvent leaving the fabricated microstructures. The process has been shown to yield high aspect ratio structures with straight and smooth walls. The channel depth depends on the X-ray energy and on the exposure time.

1.4.6 Miscellaneous techniques

Several other techniques have been reported for the fabrication of microfluidic channels in polymers. Lee and coworkers described the use of low energy ion beam etching (IBE) with Ar⁺ ions (500 eV, 0.5 mA cm⁻²) to fabricate high aspect ratio microchannels in a variety of fluoropolymers [34]. Rossier and coworkers described the use of a plasma etch the for mass-production of microfluidic devices in polymer substrates [35] while several groups have reported UV-patterning of SU-8 negative photoresist for microfluidics and MEMS applications [36-38]. Also, Mastrangelo and coworkers described a sacrificial etch process to fabricate polymer microchannels in parylene-C [39].

Technology	Choice of Geometry	Minimum feature size	Height	Total surface area	Aspect ratio	Lifetime	Cost	Availability
Wet silicon etching	-	+	0	++	-	+	+	++
Dry silicon etching	+	++	+	++	+	-	0	+
Optical lithography and electroforming	+	++	+	++	0	+	0	0
Laser ablation and electroforming	++	+	+	-	+	+	-	-
LIGA	+	++	++	-	++	+	--	--
Mechanical micromachining	+	0	+	+	0	++	-	-
μ -EDM	-	0	+	-	+	++	-	-

Legend: + = good selectivity, - = bad selectivity, 0 = neutral

Abbreviations: LIGA = lithography and electro-deposition machining, μ -EDM = micro electro-discharge machining.

Table 1.2: An overview of the existing master fabrication methods between the different technologies available for fabricating masters [8]. These important aspects should be considered when selecting the described fabrication processes.

1.5 CARBON MATERIALS IN MICROFABRICATION

The carbon materials that are commonly used as solid electrodes are predominantly comprised of sp^2 -hybridized carbon (e.g. carbon fibers, glassy carbon, pyrolytic graphite). These materials generally exhibit a wide potential window, low cost, mechanical stability and applicability to a wide range of redox systems. Several reviews are available discussing its utility in electroanalytical chemistry, electrosynthesis, energy storage, and energy conversion [40-44]. However, sp^3 -hybridized carbon material such as diamond, have recently come into use as robust electrode material that offer significant advantages over the sp^2 -hybridized carbon electrodes. These advantages include linear-dynamic range, limit of detection, response time, response precision, and response stability [45]. A number of electrochemical technologies have been proposed to benefit from the use of diamond as an electrode material. These include electroanalysis, electrocatalysis, spectroelectrochemistry and bioelectrochemistry.

Over the past decade, microfabrication of low-cost and disposable electrodes has received attention in the development of electrochemical sensors [46-47]. Thick-film, screen-printed carbon electrodes have been prepared using carbon inks [47-52] and a majority of the glucose sensors currently available use such electrodes [47]. While Schueller and coworkers have proposed the fabrication of freestanding glassy carbon microstructures after the pyrolysis of various polymeric precursors for applications in microelectromechanical systems (MEMS) [53-56], carbon inks have thus far been the only carbon substrates that

have been applied in large-scale microfabrication process. This thesis proposes the implementation of microfabricated glassy carbon and carbon films prepared by the pyrolysis of photoresist as alternatives to the use of carbon ink in microfabrication. In the subsequent sections of the thesis, a detailed overview of these two carbon materials with respect to structure and ability to be microfabricated, is given.

1.5.1 Glassy Carbon in Electroanalytical Chemistry

Glassy Carbon (GC) has been a widely utilized in electroanalytical chemistry due to its importance in electrocatalysis [57], in electroanalysis [43], and in biological sensing [44, 58-62]. Its extensive usage is due to its attractive properties such as low porosity, chemical stability, wide potential window, mechanical stability, and relatively low cost. The rich surface chemistry of GC allows tailoring of its interfacial properties by physisorption or chemisorption of molecules, polymers, and metals [43, 44, 57, 58]. Chemical sensors and biosensors have been prepared by immobilization of recognition elements and enzymes on the GC electrode surface [43].

GC is made from a controlled thermal decomposition of polymeric resins such as phenol-formaldehyde or polyacrylonitrile under an inert atmosphere. These precursor materials are used because of their high carbon yield upon pyrolysis. The polymer is heated to a temperature, in the range of 1000-3000°C resulting in an extensively conjugated sp^2 carbon structure [43, 44, 58-60]. Graphitization starts to occur at a temperature above 300°C. Non-carbon atoms

such as nitrogen, chlorine and oxygen present in the precursor polymer are released and only carbon is left. Further heating results in an extensively conjugated sp^2 structure. Depending on the processing temperature and polymer resin used, the yields of GC are usually 40-60% [60, 61]. The widely accepted schematic representation of the structural model of GC proposed by Jenkins and coworkers is shown in Figure 1.5 [60]. Although the high temperatures produce local graphitic domains, the tangled ribbon-like structure is a result of the precursor polymer and prevents long-range graphitization. The physical properties of GC material are dependent on the final temperature at which the polymer is heated. Higher heat treatment temperature generally results in greater ordering of the GC. Three grades of GC are commonly available based on this final temperature: GC-10 (1000°C), GC-20 (2000°C), GC-30 (3000°C). A GC-20 substrate was utilized for the research presented in this thesis.

The microcrystallite size of sp^2 hybridized carbon material can be defined by the intraplanar microcrystallite size, L_a , and the interplanar microcrystallite size, L_c . These parameters provide a measure of the extent of graphitization. L_a defines the extent of the crystal in the plane of the hexagonal lattice (a-axis) while L_c defines the extent of the crystal plane perpendicular to the hexagonal lattice (c-axis). The plane along the a-axis is commonly referred to as the basal

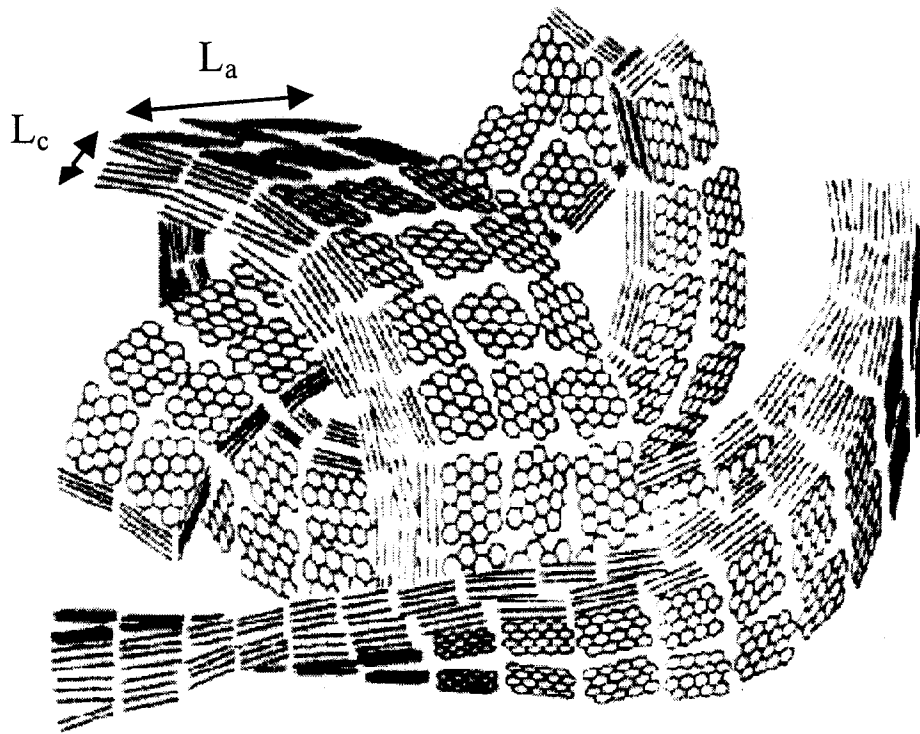


Figure 1.5: Schematic representation of glassy carbon [60].

plane while the plane perpendicular to the graphite lattice is termed the edge plane. X-ray diffraction studies have shown significant change in the microcrystalline size when the final heat treatment temperature is varied [44]. The values of L_a have been reported to change from 25Å to 55Å and that of L_c from 12Å to 70Å when the final temperature is varied from 2000°C to 3000°C respectively. GC is isotropic on a scale greater than ca. 200Å and has a lower density (1.3-1.5g/cm³) than graphite (2.27g/cm³), which reflects its porous microstructure [43]. However, the voids constituting the pores are not connected. This property accounts for the low gas permeability observed for glassy carbon.

1.5.2 Treatment of GC Surfaces

A number of pretreatment and activation methods have been developed to increase the reactivity and reproducibility of the GC electrode surfaces. Most pretreatment methods to date have involved polishing of the GC surface with various grades, sizes and types of abrasive materials. Polishing improves reproducibility of "as received" GC surfaces via the removal of gross surface defects and impurities that arise during the production processes. Activation procedures are additional steps that are undertaken to increase the reactivity of the electrode surface. Procedures such as electrochemical pretreatment (ECP) [61-66], ambient or vacuum heat treatment [60, 68-73], laser irradiation [66, 74-78], and sonication in an isopropanol/activated carbon mixture [77] have often been employed to activate GC electrodes. These activation procedures alter the final surface structure of GC electrodes and are often found to be crucial to

electrochemical performance [62, 63, 65, 69, 71, 73, 74, 78-80] of the GC substrate. After polishing, ECP of the GC electrode is usually the most utilized treatment method. Since both polishing and ECP methods were employed in the research presented, only these pretreatment methods will be discussed further in this chapter.

1.5.2.1 *Polishing Glassy Carbon*

Polishing procedures have been extensively used for GC electrodes [68, 70, 78, 80-83]. Polished GC is by far the most often used starting surface for other activation procedures. Generally, the procedure begins by grinding the “as received” GC with fine grit silicon carbide paper to level any large-scale roughness. The surface is then polished in aqueous slurries of alumina particles or in a paste of diamond particles. The polishing material is supported on a felt polishing cloth. The particle size of the abrasive powders used is typically in the micron to sub-micron range and produces a mirror like surface once polishing is completed. Kazee and coworkers have shown that the final surface of a polished GC electrode is covered with a thin layer of finely divided carbon microparticles and polishing contaminants [83]. This layer has been found to remain even after ultrasonication in water bath [73, 80, 83].

1.5.2.2 *Electrochemical Pretreatment (ECP) of Glassy Carbon*

Electrochemical methods for the pretreatment of carbon material have been the subject of many studies involving carbon fibers and GC electrodes [43, 44]. The terms anodization and cathodization are frequently used to describe the

ECP process. Anodization indicates that the electrode is subjected to positive potentials and an oxidation reaction is occurring at the working electrode. Conversely, cathodization means that the electrode is subjected to negative potentials a reduction reaction occurring at the working electrode. Electrochemical methods for the pretreatment of glassy carbon have been used extensively, as they are convenient, inexpensive and quick while offering an added advantage of being able to be performed within an electrolyte solution. The procedure involves application of one or several potential waveforms to the carbon electrode in some suitable solvent.

Lord and coworkers first demonstrated that anodization of a graphite electrode significantly altered the shape of a slow scan voltammetric curve for the reduction of Fe^{3+} in 0.1M HCl [84]. Thereafter, more studies were done on the effects of ECP on carbon electrodes in acidic solutions [64, 65, 85-90], in neutral buffered or salt solutions [62, 63, 66, 68, 92, 93], and in basic solutions [87, 88, 90, 94, 95]. As with the polishing procedure, there has not been a standardized ECP procedure. Differences in ECP procedure arise from electrolyte composition, applied potential waveform and magnitude of the applied potential. One of the most widely applied ECP procedures involves anodization of the carbon surface at potentials between 1.6 to 2.2V versus the standard calomel electrode (SCE). For the research presented here, ECP was performed by applying a voltage of $\geq 1.8\text{V}$ versus the silver/silver chloride (Ag/AgCl) reference electrode on a working GC surface.

Several studies have reported on the effects of ECP on the surface structure of carbon electrodes. ECP of GC in acidic or neutral buffered/salt solutions at high positive potentials compositionally transforms the surface of the GC with a layer of graphitic oxide referred to as electrochemical graphitic oxide (EGO) [65, 83]. Investigation by Kepley and coworkers revealed that the EGO layer thickness increased monotonically with activation time to a thickness of at least 1 μm [65]. It was also noted that the oxide film was observed to be porous, hydrated, anionic and non-conductive.

Nagaoka and coworkers have established that the EGO film absorbs ions and can undergo ion exchange of cations [96]. XPS studies of the EGO film have also indicated an increase of oxygen/carbon (O/C) ratio from 0.08 for polished GC to 0.24 after ECP in acid, confirming formation of an oxygen rich film [63]. High-resolution XPS studies revealed that the majority of the surface oxide groups exist as phenolic, carbonyl and carboxylate functionalities, [63, 82, 92, 94]. However, Engstrom and Strasser have reported that the amount of charge in the cathodic stripping peak indicates a multilayer structure and that cathodization reduction of the oxides did not entirely eliminate them [63]. In the same study, contact angle measurements following ECP indicated an increase in hydrophilicity of the acid anodized GC surface.

Electrochemical pretreatment of GC in basic solutions shows significant differences when compared to ECP in acidic or neutral buffered/salt solutions [63, 94, 95]. Kozlowski and Sherwood [88] reported the formation of surface

oxides by anodization of carbon electrodes in basic solutions. However, ECP of GC in basic electrolytes does not result in an EGO film [86, 94]. Reported results imply that if an EGO film was produced by ECP in base, it was immediately removed, possibly by dissolution in the alkaline solution [86, 95]. ECP of GC in basic media at high positive potentials has been observed to result in lower background current values than those observed on acid electrochemical pretreated GC surfaces [65, 94]. The high background noted on acid modified GC surfaces has been attributed to redox functional groups produced by ECP and the increased porosity and anionic character of the EGO film.

Figure 1.6 illustrates the proposed surface structures of polished, acid and base anodized GC surfaces. ECP of carbon electrodes in basic electrolytes at mild conditions (≥ 1.8 V versus SCE) has been found to etch away the carbon material and this phenomenon has not been observed in acidic media [88, 94]. Beilby and Carlsson have also reported on the removal of pyrolytic carbon films deposited on polished GC substrates upon ECP in NaOH. The authors stated that they were able to visually observe the underlying GC substrate following anodization in basic electrolyte [94]. A study by Kozłowski and Sherwood supported this observation when they reported the presence of carbon fragments in the working electrode solution after electrochemical oxidation of carbon fibers in NaOH solution [88]. Their observation suggested the breakup of the carbon fiber lattice. The only change observed during acid anodization of GC surfaces has been a display of different colors [64, 86, 94] attributable to optical

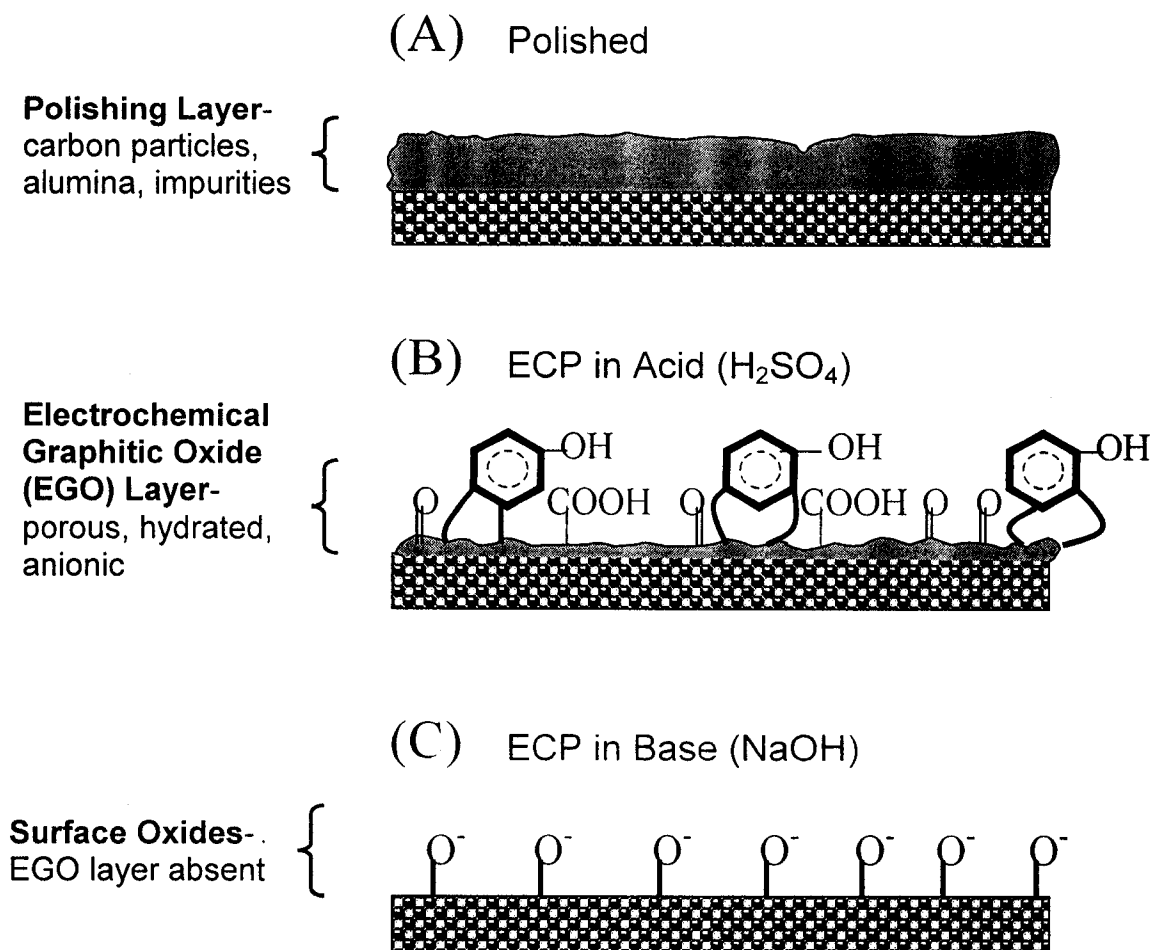


Figure 1.6: Illustration of the surface architecture for (A) polished GC, (B) polished GC with phenolic, carbonyl, and carboxylate functionalities on a diminished polishing layer after electrochemical pretreatment in acid and (C) polished GC with surface oxides after electrochemical pretreatment in base.

interferences of a permanently in-place transparent EGO film [65, 86].

Previous work in this group has shown that an electrochemical oxidative procedure removes polishing contaminants from polished carbon surfaces [91]. It has been observed that for this ECP procedure, anodization of GC in a basic solution for short times (~10s) initially removes the ubiquitous layer of polishing debris via an etching process [90]. Longer anodization in basic electrolyte results in significant etching of the GC surface. The work presented in this thesis expands on the observations made during longer anodization in basic electrolyte and applies it to a novel carbon electrode material known as pyrolyzed photoresist films.

1.6 PYROLYZED PHOTORESIST CARBON FILMS

Pyrolyzed photoresist films (PPF) are carbon films obtained by pyrolyzing commercially available photoresist. To form PPF, photoresist is spin-coated onto a silicon wafer and pyrolyzed at 1000⁰C in a reducing atmosphere (95% nitrogen and 5% hydrogen) to produce conducting carbon films as illustrated in Figure 1.7. The carbon films show unusual surface properties when compared to other carbon electrodes. With no observable porosity, the PPF surface is exceptionally smooth (<0.5 nm rms) compared to other carbon electrode surfaces, such as polished glassy carbon (GC) and vacuum heat-treated GC disks, whose root-mean-square surface roughness was found by STM to be 4.1 and 4.5 nm, respectively [97, 98].

In addition, curing the films in a reducing atmosphere minimizes carbon oxidation, leading to a low oxygen/carbon (O/C) atomic ratio thereby rendering the films relative stability towards air oxidation. The smoothness and low O/C ratio result in a surface with unusually low capacitance ($\sim 8.1 \mu\text{F}/\text{cm}^2$), contributing to the low background levels observed [96]. PPF also has a resistivity comparable to that of GC [99].

Analytical devices based on pyrolysis of lithographic patterns may be mass-produced, in principle, and could form the basis of high volume electrochemical sensors. The practicality of creating sensitive carbon electrodes through lithographically patterning photoresist opens up many useful possibilities. For example, PPF electrodes can be fabricated in a planar arrangement that allows for placement in the separation channel of a capillary electrophoresis microchip [100]. Although this detection geometry is not optimal [101], the rigidity and stability of alignment are necessary to create a truly integrated device. Therefore, integrating a low capacitance electrode at a microchannel outlet decreases peak asymmetry and increases efficiency, as well as increasing sensitivity when the electrophoresis and electrochemical circuits are decoupled [100].

1.7 OBJECTIVES OF THIS THESIS

Due to the impact of microfabrication technology on chemistry and biology, new methods to pattern and etch a variety of materials have been explored in a number of laboratories. For this thesis, attention is focused on

Pyrolyzed Photoresist Films (PPF)

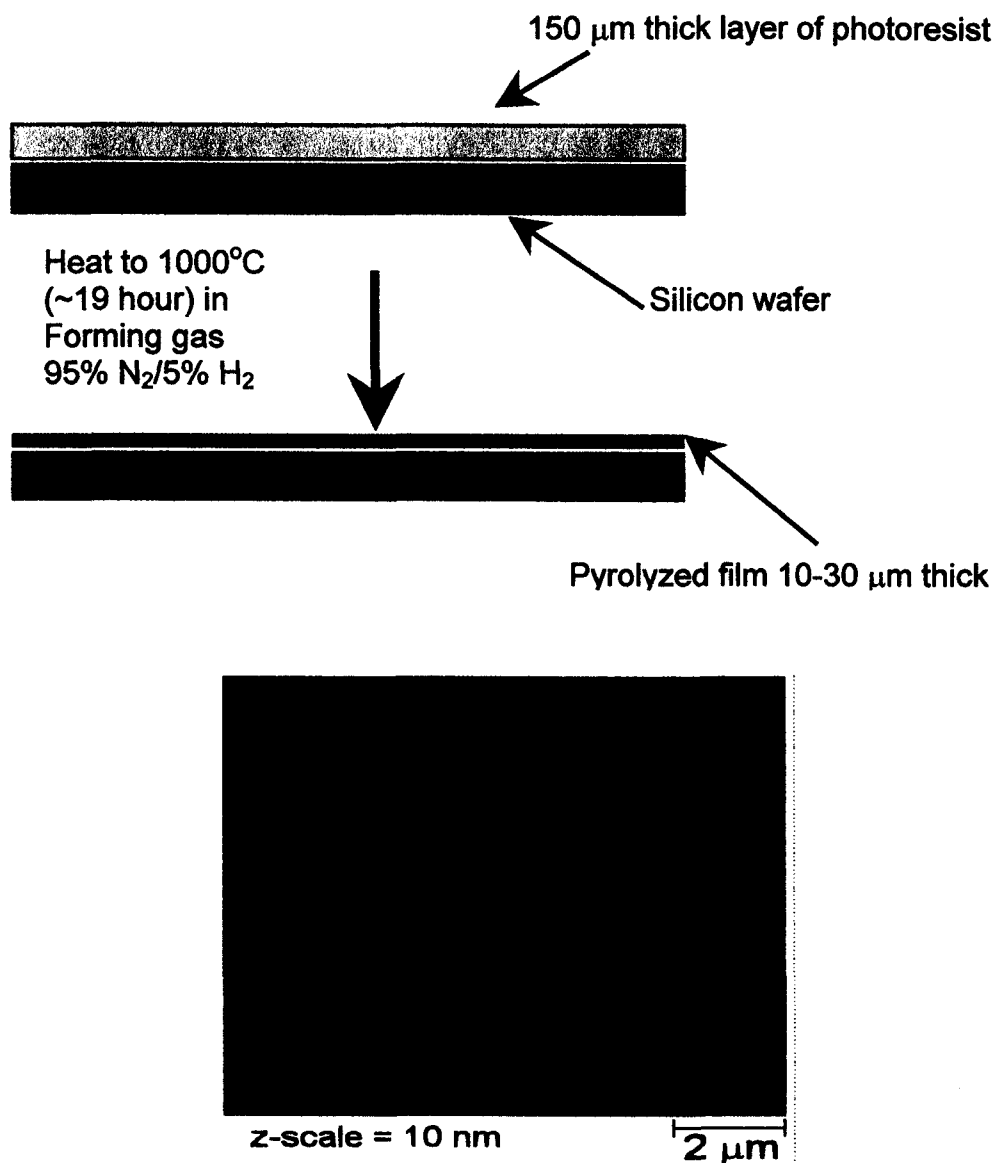


Figure 1.7 Schematic showing the protocol for the preparation of pyrolyzed photoresist films and the resultant high-resolution AFM image taken of a near-atomic flatness carbon film [98].

fabricating microstructures of glassy carbon and pyrolyzed photoresist films.

Glassy carbon and pyrolyzed photoresist film structures could be used in lieu of silicon in applications where less density, high chemical resistance to strong bases or thermal stability are required properties. These physical properties make both these substrates potential candidates for the preparation of MEMS and application in microfluidics.

The first objective of this thesis was the detailed study of an electrochemical etching technique for the microfabrication of carbon material, with a broad focus on glassy carbon substrates. This work developed to include the investigation of the mechanism of etching and the parameters that control the etching process. Results demonstrating the successful implementation of this method are presented in Chapter 2.

The second aim of this work was to fabricate and develop functional devices that could have applications in chemical and biological analysis. This was to include microfluidic devices to be used for nano-liter analysis and the fabrication of a carbon-based chip-electrospray-ionization interface. The first prototypes of these devices are explored in detail in Chapters 3 and 4. Finally, novel miniaturized carbon-based electroanalytical systems were developed by the fabrication of arrays of microelectrodes and microbands. Chapter 5 gives a detailed evaluation of these electrochemically-etched systems. Suggestions for future work and applications of this technique are presented in Chapter 6.

1.8 REFERENCES:

1. Madou, M., *Fundamentals of Microfabrication*. 1st ed, ed. P. Gottehrer. 1997, Boca Raton: CRC Press LLC. 589
2. Various authors., *Biochip Technology*. 1st ed. Cheng J. and L. J. Kricka eds., 2001, Bridgeport: Harwood Academic Publishers. 363
3. Smith, C.S., *Piezoresistance Effect in Germanium and Silicon*. Physical Review, 1954. 94: p. 42-49.
4. Pfann, W.G., *Improvement of Semiconducting Devices by Elastic Strain*. Solid State Electron, 1961. 3: p. 261-267.
5. Manz, A., et al., *Planar Chips Technology for Miniaturization and Integration of Separation Techniques into Monitoring Systems - Capillary Electrophoresis on a Chip*. Journal of Chromatography A, 1992. **593**(1-2): p. 253-258.
6. Harrison, D.J., et al., *Micromachining a Miniaturized Capillary Electrophoresis-Based Chemical Analysis System on a Chip*. Science, 1993. **261**: p. 895-897.
7. [Anon], *Glass Surface Modification*. Ceramics, 1968. **19**(227): p. 34-&.
8. Becker, H. and L.E. Locascio, *Polymer Microfluidic Devices*. Talanta, 2002. **56**(2): p. 267-287.

9. Tummala, R.R., *Fundamentals fo Microsystems Packaging*, Ed. R.R. Tummala. 2001, New York: McGraw-Hill.
10. Chang, C.Y. and S.M. Sze, *ULSI Technology*, ed. C.Y. Chang and S.M. Sze. 1996, New York: McGraw-Hill.
11. Sze, S.M., *VLSI Technology*. 2nd ed, Ed. S.M. Sze. 1988, New York: McGraw-Hill.
12. Sze, S.M., *Semiconductor Devices: Physics and Technology*. 2nd ed. 2002, New York: Wiley.
13. Hierlemann, A., et al., *Microfabrication Techniques for Chemical/Biosensors*. Proc. of the IEEE, 2003. **91**(6): p. 839-863.
14. Quake, S.R. and A. Scherer, *From Micro- to Nanofabrication with Soft Materials*. Science, 2000. **290**: p. 1536-1539.
15. Whitesides, G.M., et al., *Soft Lithography in biology and biochemistry*, in Annual Review of Biomedical Engineering, 2001. p. 335-373.
16. Campbell, S.A., *The Science and Engineering of Microelectronic Fabrication*. 2nd ed. 2001, New York: Oxford University Press. 624.
17. Lin, L., et al., *Seventh International Symposium of MicroMachine and Human Science*. 1996. p. 67-71.
18. Becker, H., W. Dietz, and P. Dannberg, *Microfluidic Manifolds by Polymer*

- Hot Embossing for Micro-TAS Applications*, in *MicroTotal Analysis Systems '98*, D.J. Harrison and A.v.d. Berg, Editors. 1998, Kluwer: Dordrecht. p. 253-256.
19. Becker, H. and U. Heim, *Polymer Hot Embossing with Silicon Master Structures*. *Sensor and Materials*, 1999. **11**(5): p. 297-304.
 20. Martynova, L., et al., *Fabrication of Plastic Microfluid Channels by Imprinting Methods*. *Analytical Chemistry*, 1997. **69**(23): p. 4783-4789.
 21. Locascio, L.E., et al., *Plastic Microfluid Devices for Clinical Measurements*, in *MicroTotal Analysis Systems '98*, D.J. Harrison and A.v.d. Berg, Editors. 1998, Kluwer: Dordrecht. p. 367-370.
 22. Xu, J.D., et al., *Room-Temperature Imprinting Method for Plastic Microchannel Fabrication*. *Analytical Chemistry*, 2000. **72**(8): p. 1704-1706.
 23. McCormick, R.M., et al., *Microchannel Electrophoretic Separations of DNA in Injection-Molded Plastic Substrates*. *Analytical Chemistry*, 1997. **69**(14): p. 2626-2630.
 24. Ekstrand, G., et al., *Integrated Cell Based Assay in Microfabricated Disposable CD Devices*, in *MicroTotal Analysis Systems 2000*, A.v.d. Berg, W. Olthius, and P. Bergveld, Editors. 2000, Kluwer: Dordrecht. p. 249-252.

25. McDonald, J.C., et al., *Fabrication of Microfluidic Systems in Poly(dimethylsiloxane)*. *Electrophoresis*, 2000. **21**(1): p. 27-40.
26. Effenhauser, C.S., et al., *Integrated Capillary Electrophoresis on Flexible Silicone Microdevices: Analysis of DNA Restriction Fragments and Detection of Single DNA Molecules on Microchips*. *Analytical Chemistry*, 1997. **69**(17): p. 3451-3457.
27. Duffy, D.C., et al., *Rapid Prototyping of Microfluidic Systems in Poly(dimethylsiloxane)*. *Analytical Chemistry*, 1998. **70**(23): p. 4974-4984.
28. Roberts, M.A., et al., *UV Laser Machined Polymer Substrates for the Development of Microdiagnostic Systems*. *Analytical Chemistry*, 1997. **69**(11): p. 2035-2042.
29. Srinivasan, R., *Controlled Degradation and Ablation of Polymer Surfaces by Ultraviolet Laser Radiation*. *Polymer Degradation and Stability*, 1987. **17**(3): p. 193-203.
30. Schmidt, H., et al., *Modeling of Velocity and Surface Temperature of the Moving Interface during Laser Ablation of Polyimide and Poly(methyl methacrylate)*. *Applied Surface Science*, 1999. **139**: p. 102-106.
31. Ueno, K., et al., *Fabrication and Characteristic Responses of Integrated Microelectrodes in Polymer Channel Chip*. *Chemistry Letters*, 2000(8): p. 858-859.

32. Ford, S.M., et al., *Microcapillary Electrophoresis Devices Fabricated using Polymeric Substrates and X-ray Lithography*. *Journal of Microcolumn Separations*, 1998. **10**(5): p. 413-422.
33. Ford, S.M., et al., *Micromachining in Plastics using X-ray Lithography for the Fabrication of Micro-Electrophoresis Devices*. *Journal of Biomechanical Engineering-Transactions of the Asme*, 1999. **121**(1): p. 13-21.
34. Lee, L.P., et al., *Key Elements of a Transparent Teflon Microfluidic System*, in *MicroTotal Analysis Systems '98*, D.J. Harrison and A.v.d. Berg, Editors. 1998, Kluwer: Dordrecht. p. 245-248.
35. Rossier, J.S., et al., *Polymer Microstructures: Prototyping, Low-Cost Mass Fabrication and Analytical Applications*, in *MicroTotal Analysis Systems 2000*, A.v.d. Berg, W. Olthius, and P. Bergveld, Editors. 2000, Kluwer: Dordrecht. p. 159-162.
36. Lorenz, H., et al., *High-Aspect-Ratio, Ultrathick, Negative-Tone near-UV Photoresist and its Applications for MEMS*. *Sensors and Actuators A-Physical*, 1998. **64**(1): p. 33-39.
37. Renaud, P., et al., *Polymer Microstructures: Prototyping, Low-Cost Mass Fabrication and Analytical Applications*, in *MicroTotal Analysis Systems '98*, D.J. Harrison and A.v.d. Berg, Editors. 1998, Kluwer: Dordrecht. p. 17-22.

38. Lee, K.Y., et al., *Micromachining Applications of a High Resolution Ultrathick Photoresist*. Journal of Vacuum Science & Technology B, 1995. **13**(6): p. 3012-3016.
39. Webster, J.R., et al., *An Inexpensive Plastic Technology for Microfabricated Capillary Electrophoresis Chips*, in *MicroTotal Analysis '98*, D.J. Harrison and A.v.d. Berg, Editors. 1998, Kluwer: Dordrecht. p. 249-267.
40. McCreery, R.L., *Chapter 35*, in *Interfacial Electrochemistry*, A. Wieckowski, Editor. 1999, Dekker: New York.
41. McCreery, R.L., *Chapter 10*, in *Laboratory Techniques in Electroanalytical Chemistry*, P.T. Kissinger and W.R. Heineman, Editors. 1996, Dekker: New York.
42. McCreery, R.L., et al., *Control of Reactivity at Carbon Electrode Surfaces*. Colloids and Surfaces A-Physicochemical and Engineering Aspects, 1994. **93**: p. 211-219.
43. Kinoshita, K., *Carbon, Electrochemical and Physicochemical Properties*. 1988, John Wiley & Sons Inc.: New York. p. 226 - 292.
44. McCreery, R.L., *In Electroanalytical Chemistry*, A.J. Bard, Editor. 1991, Marcel Dekker: New York. p. 221-374.
45. Hubert, M., Muck, A., Wang, J., Stotter J., et al., *Conductive Diamond*

- Thin-Films in Electrochemistry*. Diamond and Related Materials, 2003. **12**: p. 1940-1949.
46. Alvarezicaza, M. and U. Bilitewski, *Mass-Production of Biosensors*. Analytical Chemistry, 1993. **65**(11): p. A525-A533.
 47. Lindner, E. and R.P. Buck, *Microfabricated Potentiometric Electrodes and their in vivo Applications*. Analytical Chemistry, 2000. **72**(9): p. 336A-345A.
 48. Wang, J., et al., *Metal-Dispersed Screen-Printed Carbon Electrodes*. Electroanalysis, 1995. **7**(11): p. 1032-1034.
 49. Wang, J., P.V.A. Pamidi, and D.S. Park, *Screen-printable Sol-Gel Enzyme-containing Carbon Inks*. Analytical Chemistry, 1996. **68**(15): p. 2705-2708.
 50. Wang, J., et al., *Electrochemical Activation of Screen-Printed Carbon Strips*. Analyst, 1996. **121**(3): p. 345-350.
 51. Wang, J., et al., *Performance of Screen-Printed Carbon Electrodes Fabricated from Different Carbon Inks*. Electrochimica Acta, 1998. **43**(23): p. 3459-3465.
 52. Wang, J., B.M. Tian, and E. Sahlin, *Micromachined electrophoresis chips with thick-film electrochemical detectors*. Analytical Chemistry, 1999. **71**(23): p. 536-5440.
 53. Schueller, O.J.A., et al., *Fabrication and Characterization of Glassy*

Carbon MEMS. Chemistry of Materials, 1997. 9(6): p. 1399-1406.

54. Schueller, O.J.A., S.T. Brittain, and G.M. Whitesides, *Fabrication of Glassy Carbon Microstructures by Pyrolysis of Microfabricated Polymeric Precursors*. Advanced Materials, 1997. 9(6): p. 477-&.
55. Schueller, O.J.A., S.T. Brittain, and G.M. Whitesides, *Fabrication of Glassy Carbon Microstructures by Soft Lithography*. Sensors and Actuators A-Physical, 1999. 72(2): p. 125-139.
56. Shah, H.V., et al., *Bis-o-diynylarene (BODA) derived Polynaphthalenes as Precursors to Glassy Carbon Microstructures*. Chemistry of Materials, 1999. 11(10): p. 2623-2625.
57. Pocard, N.L., et al., *Doped Glassy-Carbon-A New Material for Electrocatalysis*. Journal of Materials Chemistry, 1992. 2(8): p. 771-784.
58. van der Linden, W.E. and J.W. Dieker, *Glassy-Carbon as Electrode Material in Electroanalytical Chemistry*. Analytica Chimica Acta., 1980. 119(1): p. 1-24.
59. Yamada, S. and H. Sato, Nature, 1962. 193: p. 261.
60. Jenkins, G.M. and K. Kawamura, *Structure of Glassy Carbon*. Nature, 1971. 231(5299): p. 175-&.
61. McKee, D.W., *Carbon and Graphite Science*. Annual Review of Materials Science, 1973. 3: p. 195-123.

62. Engstrom, R.C., *Electrochemical Pretreatment of Glassy Carbon Electrodes*. Analytical Chemistry, 1982. **54**(13): p. 2310-2314.
63. Engstrom, R.A. and V.A. Strasser, *Characterization of Electrochemically Pretreated Glassy Carbon Electrodes*. Analytical Chemistry, 1984. **56**(2): p. 136-141.
64. Cabaniss, G.E., et al., *Electrocatalysis of Proton-Coupled Electron-Transfer Reactions at Glassy Carbon Electrodes*. Journal of the American Chemical Society, 1985. **107**: p. 1845-1853.
65. Kepley, L.J. and A.J. Bard, *Ellipsometric, Electrochemical, and Elemental Characterization of the Surface Phase Produced on Glassy Carbon Electrodes by Electrochemical Activation*. Analytical Chemistry, 1988. **60**(15): p. 1459-1467.
66. Gonon, F.G., et al., *Electrochemical Treatment of Pyrolytic Carbon-Fiber Electrodes*. Analytical Chemistry, 1981. **53**(9): p. 1386-1389.
67. Falat, L. and H.Y. Cheng, *Graphite Epoxy Electrode*. Analytical Chemistry, 1982. **54**(12): p. 2108-2111.
68. Wightman, R.M., et al., *Methods to Improve Electrochemical Reversibility at Carbon Electrodes*. Journal of Electrochemical Society, 1984. **131**(7): p. 1578-1583.
69. Stutts, K.J., et al., *Enhanced Electrochemical Reversibility at Heat-Treated*

- Glassy Carbon Electrodes*. Analytical Chemistry, 1983. 55: p. 1632-1634.
70. Hu, I.-F., D.H. Karweik, and T. Kuwana, *Activation and Deactivation of Glassy Carbon Electrodes*. Journal of Electroanalytical Chemistry, 1985. 188: p. 59 - 72.
 71. Deakin, M.R., K.J. Stutts, and R.M. Wightman, *The Effect of pH on Some Outer-Sphere Electrode Reactions at Carbon Electrodes*. Journal of Electroanalytical Chemistry, 1985. 182: p. 113-122.
 72. Chen, P. and R.L. McCreery, *Control of Electron Transfer Kinetics at Glassy Carbon Electrodes by Specific Surface Modification*. Analytical Chemistry, 1996. 68: p. 3958-3965.
 73. Fagan, D.T., I. Hu, and T. Kuwana, *Vacuum Heat Treatment for Activation of Glassy Carbon Electrodes*. Analytical Chemistry, 1985. 57: p. 2759-2763.
 74. Poon, M. and P. McCreery, *In Situ Laser Activation of Glassy Carbon Electrodes*. Analytical Chemistry, 1986. 58: p. 2745-2750.
 75. Rice, R.J. and R.L. McCreery, *Quantitative Relationship between Electron Transfer Rate and Surface Microstructure of Laser-Modified Graphite Electrodes*. Analytical Chemistry, 1989. 61: p. 1637-1641.
 76. Rice, R.J., N.M. Pontikos, and R.L. McCreery, *Quantitative Correlations of Heterogenous Electron - Transfer Kinetics with Surface Properties of*

- Glassy Carbon Electrodes*. Journal of the American Chemical Society, 1990. **112**(12).
77. Ranganathan, S., T.-C. Luo, and R.L. McCreery, *Facile preparation of active glassy carbon electrodes with activated carbon and organic solvents*. Analytical Chemistry, 1999. **71**(16): p. 3574-3580.
 78. Tse, D. and T. Kuwana, *Electrocatalysis of Dihyronicotinamide Adenosine-Diphosphate with Quinones and Modified Quinone Electrodes*. Analytical Chemistry, 1978. **50**(9): p. 1315-1318.
 79. Hu, I.F. and T. Kuwana, *Oxidative Mechanism of Ascorbic-Acid at Glassy-Carbon Electrodes*. Analytical Chemistry, 1986. **58**(14): p. 3235-3239.
 80. Kamau, G.N., W.S. Willis, and J.F. Rusling, *Electrochemical and Electron Spectroscopic Studies of Highly Polished Glassy Carbon Electrodes*. Analytical Chemistry, 1985. **57**: p. 545-551.
 81. Thornton, D.C., et al., *Pretreatment and Validation Procedure for Glassy-Carbon Voltammetric Indicator Electrodes*. Analytical Chemistry, 1985. **57**(1): p. 150-155.
 82. Evans, J.F. and T. Kuwana, *Radiofrequency Oxygen Plasma Treatment of Pyrolytic-Graphite Electrode Surfaces*. Analytical Chemistry, 1977. **49**(11): p. 1632-1635.
 83. Kazee, B., D.E. Weisshaar, and T. Kuwana, *Evidence for the Presence of*

- a Thin Carbon-Particle Layer on Polished Glassy Carbon Electrodes.* Analytical Chemistry, 1985. 57: p. 2736-2739.
84. Lord, S.S. and L.B. Rogers, *Polarographic Studies with Gold, Graphite, and Platinum Electrodes.* Analytical Chemistry, 1954. **26**(2): p. 284-295.
85. Rojo, A., A. Rosenstratten, and D. Anjo, *Characterization of a Conductive Carbon-Film Electrode for Voltammetry.* Analytical Chemistry, 1986. **58**(14): p. 2988-2991.
86. Anjo, D.M., et al., *Electrochemical Activation of Carbon Electrodes in Base: Minimization of Dopamine Adsorption and Electrode.* Analytical Chemistry, 1989. 61: p. 2603-2608.
87. Noel, M. and P.N. Anantharaman, *Voltammetric Studies on a Glassy Carbon Electrode Part II. Factors Influencing the Simple Electron-transfer Reactions.* Analyst, 1985. 110: p. 1095-1103.
88. Kozlowski, C. and P.M. Sherwood, *X-Ray Photoelectron-spectroscopic Studies of Carbon-fiber Surfaces.* Journal of Chemical Society, Faraday Trans. 1, 1985. 81: p. 2745-2756.
89. Sundberg, K.M., et al., *Surface Modification and Oxygen Reduction on Glassy-Carbon in Chloride Media.* Journal of the Electrochemical Society, 1989. **136**(2): p. 434-439.
90. Kiema, G.K., G. Fitzpatrick, and M.T. McDermott, *Probing Morphological*

and Compositional Variations of Anodized Carbon Electrodes with Tapping-Mode SFM. Analytical Chemistry, 1999. 71: p. 4306-4312

91. Kiema, G. K., M. Aktary and M. T. McDermott, *Preparation of reproducible electrodes by removal of polishing impurities.* Journal of Electroanalytical Chemistry, 2003, 540:p.7-15.
92. Nagaoka, T. and T. Yashino, *Surface-Properties of Electrochemically Pretreated Glassy-Carbon.* Analytical Chemistry, 1986. **58**(6): p. 1037-1042.
93. Freund, M.S., et al., *Scanning Tunneling Microscopy and Atomic Force Microscopy in the Characterization of Activated Graphite Electrodes.* Analytical Chemistry, 1991. **63**(10): p. 1047-1049.
94. Beilby, A.L. and A. Carlsson, *A Pyrolytic Carbon Film Electrode For Voltammetry: Characterization and Comparison with the Glassy Carbon Electrode by Electrochemical Pretreatment in Basic Solution.* Journal of Electroanalytical Chemistry, 1988. **248**(2): p. 283-304.
95. Bielby, A.L., T.A. Sasaki, and H.M. Stern, *Electrochemical Pretreatment of Carbon Electrodes as a Function of Potential, pH, and Time.* Analytical Chemistry, 1995. **67**(5): p. 976 - 980.
96. Nagaoka, T., T. Fukunaga, and T. Yoshino, *Uptake of Ions into Electrochemically Treated Glassy Carbon.* Analytical Chemistry, 1988. 60:

p. 2766-2769.

97. McDermott, M.T. and R.L. McCreery, *Scanning-Tunneling-Microscopy of Ordered Graphite and Glassy-Carbon Surfaces - Electronic Control of Quinone Adsorption*. *Langmuir*, 1994. **10**(11): p. 4307-4314.
98. Ranganathan, S. and R.L. McCreery, *Electroanalytical Performance of Carbon films with Near-Atomic Flatness*. *Analytical Chemistry*, 2001. **73**(5): p. 893-900.
99. Ranganathan, S., et al., *Photoresist-Derived Carbon for MEMS and Electrochemical systems*. *Journal of the Electrochemical Society*, 2000. **147**(1): p. 277-282.
100. Hebert, N.E., et al., *Performance of Pyrolyzed Photoresist Carbon Films in a Microchip Capillary Electrophoresis Device with Sinusoidal Voltammetric Detection*. *Analytical Chemistry*, 2003. **75**(16): p. 4265-4271.
101. Zeng, Y., et al., *Microchip Capillary Electrophoresis with Electrochemical Detection*. *Analytical Chemistry*, 2002. **74**(10): p. 2441-2445.

CHAPTER 2

MICROFABRICATION OF GLASSY CARBON BY ELECTRO- CHEMICAL ETCHING

A version of this chapter has been published. Kiema, G. K., Ssenyange, S., McDermott, M. T., *Journal of The Electrochemical Society*. **2004**, 151 (2), C142-C148. "Microfabrication of Glassy Carbon by Electrochemical Etching"

2.1 INTRODUCTION

Microfabrication has had a considerable impact in many areas of chemistry and biology as discussed in chapter 1. The application of processes such as metal deposition, lithographic pattern transfer, and etching techniques to a variety of materials has enabled, for example, the development of lab-on-a-chip devices, [1, 2] microelectromechanical systems (MEMS), [3] miniaturized sensor systems, [4, 5] and methods to easily and reliably pattern surfaces [6, 7]. It is reasonable to believe that further developments of microfabrication processes and materials will lead to additional useful applications. This chapter reports on a technique for the microfabrication of structures in glassy carbon (GC). Previous work in this group had shown that the application of anodic potentials to GC electrodes in basic media removes material from the surface [8]. The procedure was applied to remove the thin layer of impurities from a polished GC electrode to produce a reproducible electrode surface [9]. Here we investigate the mechanism and parameters of this etching procedure and apply it to photolithographically patterned GC substrates to fabricate microstructures.

GC has been a widely utilized material in electrochemistry due to a number of attractive properties [10-15]. The physical properties of GC such as good electrical conductivity, thermal stability, low gas permeability, low coefficient of thermal expansion, and low density, all provide a framework for GC as an appealing complementary material to glass and silicon for designing miniature systems. In addition, a number of convenient methods have been reported to

chemically tailor the surface of GC [16-20], thereby opening pathways for the development of microsensors and microsystems for controlled fluid flow. Micromachined GC structures may also find applications as microbatteries, [21] and microcapacitors [22-24].

Relevant to the current work, Whitesides and coworkers have reported the fabrication of GC microstructures by procedures based on micromolding of polymeric precursor resins, followed by heating (400–1800°C) under an inert atmosphere [25-27]. This procedure is extremely successful at fabricating large area structures with high aspect ratio [25] and even freestanding microstructures. [26] However, the final size and shape of the structures can be compromised by the drastic weight and volume reduction (~50%) that occurs during carbonization. [27] In earlier work, Morita and Shimitzu prepared recessed microelectrode arrays by etching carbon fibers embedded in non-conductive epoxy [28, 29]. In this case, the etching was accomplished by anodization in acidic electrolyte to a depth of 500 μm .

This chapter demonstrates the efforts aimed at micromachining GC via a combination of photolithographic pattern transfer and anodization in basic media. We investigate the mechanism of carbon removal, the parameters available to control the etching, and the morphology of the resultant surface. Scanning electron microscopy (SEM) and scanning probe microscopy (SPM) are both used to track the amount of material removed, and to image the microfabricated structures. Results obtained in this study show that this etching procedure can

be implemented for the fabrication of microfluidic devices.

2.2 EXPERIMENTAL

2.2.1 Materials

Sodium hydroxide pellets (Fisher) were used as received. Aqueous NaOH solutions were prepared in distilled/deionized (18 M Ω /cm) water (Nanopure, Barnstead, Dubuque, IA) and purged with nitrogen gas for 10 min. prior to use. Glassy carbon plates (10 × 10 cm, 3 mm thick) were obtained from Tokai Carbon Co., Ltd. (Tokai GC-20S, Tokyo, Japan) and diced into various sizes. GC-20 refers to a pyrolysis temperature of 2000°C. The positive photoresist (Microposit SJR 5740) was obtained from OCG Chemicals (Providence, RI).

2.2.2 Mask Preparation

In some cases, transmission electron microscopy (TEM) grids (Ted Pella Inc., Redding, CA) were used as masks for lithography. Masks for specific structures (e.g., channels) were created by designing the initial pattern in L-Edit TM Student Version (Pasadena, CA) software. The design was written on a Nanofilm chrome photomask blank (Westlake Village, CA) using a Heidelberg Instruments DWL 66 (Heidelberg, Germany) mask generator. After the mask generation, the photoresist was developed (Shipley 354 developer) and the chromium etched using Chrome Etch Semi-grade (Arch Chemicals Inc., Norwalk CT). The remaining photoresist was removed with HPLC grade acetone (Fisher).

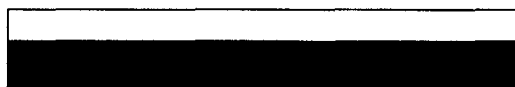
2.2.3 Etching of GC substrates

The GC substrates were polished with successive slurries of 1.0, 0.3 and 0.05 μm alumina (Buehler) in distilled/deionized (dd) water on polishing microcloth (Buehler). The GC plates were sonicated in dd water for 10 min. between polishing and then dried with a stream of argon. Mask patterns were transferred to polished GC substrates as shown in Figure 2.1. The SJR 5740 photoresist was once spin-coated on the surface. The coated GC substrate was illuminated through a lithographic mask with UV light (~ 405 nm) at an intensity of $2.5\text{mW}/\text{cm}^2$. The photoresist subsequently was developed with Shipley 354 developer (0.01M NaOH). Electrochemical anodization of the surface was accomplished in a three-electrode cell with a Ag/AgCl (3 M KCl) reference electrode and a Pt wire counter electrode. A positive potential (≥ 1.8 V) was applied to the GC surface for a controlled period of time in 0.1 M NaOH solution (pH ~ 13) at room temperature (23°C). For patterns covering a small area of the substrate (< 0.2 cm^2), an inverted cell with the electrode area defined by a Viton O-ring (geometric area = 0.28 cm^2) was used. For larger patterns, the entire substrate was immersed in the electrolyte solution. The cell was connected to a Model AFCBP1 (Pinechem Instrument Co., PA) bipotentiostat. Anodized GC substrates were sonicated in acetone for 10 min to remove the remaining photoresist and for a further 5 min. in dd water.

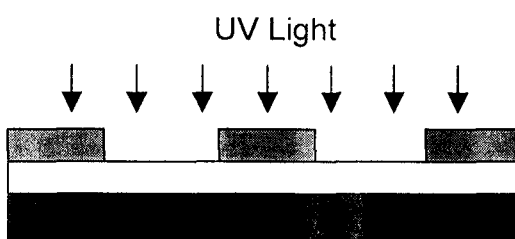
1. GC Substrate



2. Deposit Photoresist



3. Pattern



4. Develop Photoresist with 0.01M NaOH



5. Anodize in 0.1M NaOH



6. Remove Photoresist



Figure 2.1: Illustration of the scheme used to microfabricate glassy carbon.

2.2.4 Gas Analysis

The analysis of the gas that evolved during etching was accomplished using the Rae Systems LP-1200 Hand Pump (Sunnyvale, CA) and gas detection tubes purchased from Dräger Sicherheitstechnik GmbH (Revalstrabe, Germany). The electrochemical cell was completely purged with nitrogen prior to the experiment and then the cell tightly sealed with parafilm. Anodization of a 0.28 cm² GC electrode at 2.5 V vs Ag/AgCl for 15 min. at room temperature was used to accumulate gas in the gas cell headspace. A fixed volume (100 mL) of the headspace was drawn into the gas detection tube (O₂ or CO₂) where a color change is diagnostic for the particular gas. The percent volumes of oxygen and carbon dioxide within the sampled gas volumes were read directly from the calibrated tube. The error in these measurements, as reported by the manufacturer, is 10-15% relative standard deviation.

2.2.5 Microscopy

Scanning tunneling microscopy (STM) images were collected with a Multimode (Digital Instruments, Santa Barbara CA) stage and a Nanoscope III controller. Cut Pt-Ir tips were employed. Images were collected with bias voltages of 5 to 200 mV (sample positive) and currents of 50 to 100 nA. The images presented are representative of at least 10 images taken at different points on each sample. Root mean square (RMS) roughness values for whole images were determined with the manufacturer's software provided. Tapping mode scanning force microscopy (TM SFM) images were obtained in air using a

Quadrex Bioscope with Nanoscope IV controller (Digital Instruments). Images were collected under constant amplitude with silicon cantilevers oscillating at their resonance frequency (~300 kHz). All images shown here were collected with moderate tapping force at a rate between 0.5 and 1.0 Hz. Scanning electron microscopy (SEM) of the GC substrates was carried out using a JEOL model 6301FXV scanning electron microscope at an acceleration voltage of 3-5 kV. The samples were attached to a silver holder with conductive carbon tape. Image analysis was performed with commercial software (Image Tool, version 2.00, University of Texas Health Science Center in San Antonio) for measuring dimensions of features.

2.3 RESULTS AND DISCUSSION

The procedure for combining lithographic pattern transfer and electrochemical etching to microfabricate features in GC is shown in Figure 2.1. A mask pattern was transferred into a layer of photoresist that had been deposited on a polished GC electrode. The substrate was then anodized in 0.1 M NaOH and the photoresist dissolved in acetone. We found that 0.1 M NaOH solutions produced well-defined features without a metal film between the substrate and photoresist, thus minimizing the number of steps required. Higher concentrations of NaOH tend to dissolve the photoresist during etching, while concentrations lower than 0.1 M require longer etching times.

Figure 2.2 demonstrates the result of this procedure. Figure 2.2A is a TM SFM image of a GC electrode anodized at 3.0 V for 15 min. in a stagnant

solution through a pattern transferred from a TEM grid consisting of 25 μm square openings. As highlighted in the cross sectional profile, the regions that were exposed to the anodization appear 400 nm lower in topography than those that were masked with the photoresist. Figure 2.2B is a SEM image of a similar GC substrate providing a different view of the well-like structures that can be fabricated with this procedure. The combination of lithographic patterning and electrochemical oxidation in basic solution results in spatially selected etching of GC and provides a pathway for microfabrication.

Electrochemical pretreatment (ECP) of GC is a widely used procedure to activate the surface toward electron transfer for a number of redox species. This procedure involves anodization of GC via the application of a variety of potential waveforms in acidic [32-36], neutral [12, 37-41], or basic [36, 42, 43] media. For electron transfer activation, ECP is generally carried out in acidic or neutral electrolytes and results in a layer of oxygen-containing function groups (graphitic oxide) on the GC surface [10, 32, 33]. Although the structure and reactivity of GC following anodization in hydroxide electrolytes has been studied, only a few reports have explored morphological changes and details of the electrode processes. Kiema and coworkers have reported that anodization in 0.1 M NaOH does not increase the XPS measured O/C ratio appreciably from the initial polished surface, implying that the etched surface is not significantly oxidized [9]. An earlier XPS study has shown that the surface oxides that form upon anodization in NaOH at potentials >2.0 V are primarily $-\text{OH}$ groups [44].

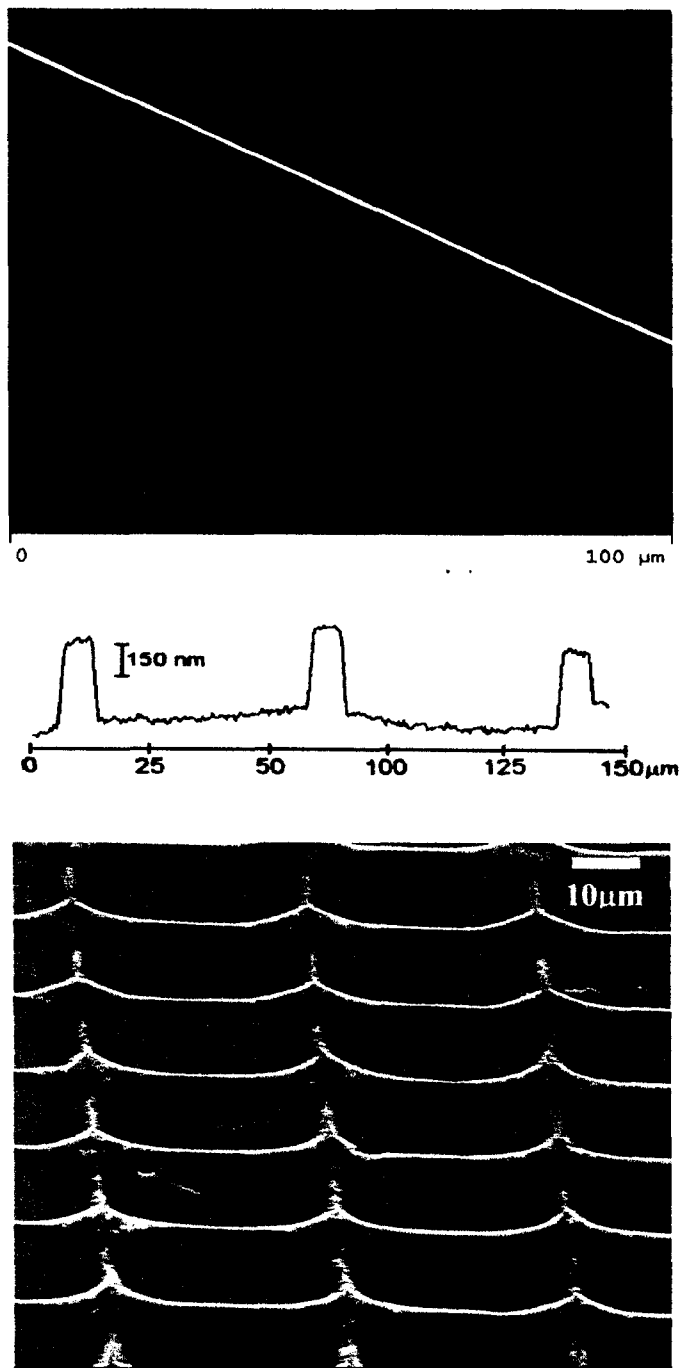
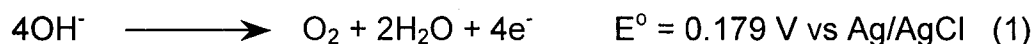
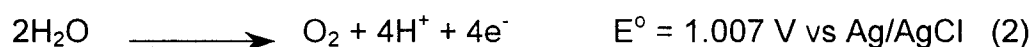


Figure 2.2 (A) $110 \times 110 \mu\text{m}$ tapping mode SFM image of the surface of a GC substrate after etching through a TEM grid pattern that was transferred to a layer of photoresist. The line traversing the image corresponds to the cross sectional profile below the image. (B) SEM image of micro-wells etched in GC.

Ross and coworkers analyzed the reaction products formed following anodic dissolution of carbon black in alkaline solution [45]. The authors used ^{14}C -labeled carbon black and established that O_2 , CO and CO_2 gaseous products were formed. We observe a copious discharge of gas bubbles originating at the electrode surface during the etching process. Analysis of the headspace atmosphere of the electrochemical cell revealed the presence of O_2 but no significant amount of CO_2 above the electrolyte solution after etching. Two possible sources of O_2 under the alkaline conditions employed include the oxidation of OH^- via,



as well as the anodic electrolysis of water.



$$E^\circ = 0.238 \text{ V (pH 13)}$$

In addition, for anodization potentials $>2.0 \text{ V}$, small but visible carbon particles are detached from the GC surface and released into solution. The etching electrolyte solution changes color to light brown. These observations and the evolution of O_2 are identical to the observations of Kozlowski and Sherwood who studied the oxidation of carbon fibers. These authors proposed the following process to account for the breakdown of the carbon fiber lattice during the anodic treatment in NaOH ,

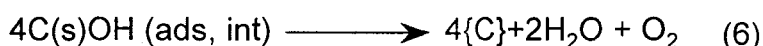


where, C(s) implies an intact carbon lattice, C(s)OH(ads) refers to –OH groups chemisorbed to the GC surface and {C} indicates a carbon material removed from the substrate [44]. A number of intermediate reactions may exist to account for the break-up of the carbon lattice.

The mechanism that results in the removal of carbon material upon anodization in base is not well understood. Several studies have reported the injection of anions between graphite layers following anodic treatment [46-49]. Smyrl and co-workers proposed that anodization of GC in a NaOH solution lead to the intercalation of OH⁻ between the planes of the graphitic microcrystallites [50-52]. This caused localized build up of stress, swelling, and the formation of mesa-like protrusions [50]. Intercalation of other anions under similar conditions has been observed to induce swelling of graphite [46]. The amount of anions intercalated between graphite layers increases with anodization potential [48, 53]. If intercalation of OH⁻ plays a role in the etching procedure, the applied potential is expected to be an important parameter in determining the rate at which carbon material is removed from the GC surface.

Figure 2.3A contains a plot of the etch depth vs. anodization potential for experiments in stagnant solutions of 0.1 M NaOH. In this case, the feature depth was measured from SFM images of patterns similar to those shown in Figure 2.2. From the plot, it is apparent that the amount of carbon removed from the GC substrate increases with potential, which is consistent with an intercalation mechanism. We thus believe that intercalation of OH⁻ may be an additional step

in the mechanism proposed by Kozłowski and Sherwood. For example, in addition to the chemisorption step (reaction 3) it is possible that a fraction of the OH⁻ intercalates into the GC lattice. The GC-20 used here is characterized by an intraplanar microcrystallite size, L_a, of 2.5 nm [10], which represents the maximum depth that OH⁻ can intercalate. Although this is not an appreciable depth relative to anion intercalation into the edge of graphite (>1 μm) [47], it is sufficient to increase the stress at the surface of the material. A combination of chemisorbed and intercalated OH⁻ is oxidized to form O₂. As the O₂ is liberated, it extricates carbon from the lattice hence the tiny carbon particles that are visualized during the anodization process. Thus, the combination of reaction (3) above with,



where C(s)OH (int) corresponds to intercalated OH⁻, is a more complete description of the etching process. This combination of processes is consistent with our observations of low surface oxidation, potential dependent etch depth, and O₂ evolution.

Plots of current in response to potential steps of various magnitude are shown in Figure 2.3B for GC (curves a, b and c) and Pt (curve d). In all cases the current increases rapidly due to double layer charging and then decays to a

steady-state value due to the convection induced by the evolution of O₂ gas. The shapes of the current responses at GC are similar to Pt (curve d), although a higher current is generated at Pt for a given potential (curve d, 2.0 V), than at GC (curve a, 2.0 V). These observations imply that reactions (1) and (2) above, which are expected to occur at a higher rate at Pt, are responsible for the majority of the current in Figure 2.3B. Figure 2.3B also shows that the magnitude of the steady-state current at GC increases with potential. This is not only due to a higher rate of solvent electrolysis but also an increased rate of etching as reflected in Figure 2.3A.

Without a doubt, the majority of the detected O₂ in the headspace is generated by reactions (1) and (2). Although we expect the rate of these reactions to be much lower on GC than on a noble metal like Pt, it is difficult to determine the contribution of reaction (6) to the total O₂ produced. For example, a 15 min. anodization at 2.5 V at a Pt foil electrode, where reactions (1) and (2) are the only source of O₂, produces approximately the same amount of headspace O₂ (19 ± 2%), as at a GC electrode of the same area (23 ± 2%). This is reasonable since the stoichiometry for all O₂ generating reactions (1, 2, 6) is similar (4e⁻/O₂).

Because the etching process is accompanied by a large amount of gas evolution and a visible breakup of the GC lattice, it is reasonable to expect the process to roughen the surface. Scanning tunneling microscopy (STM) imaging was employed to compare topography of the GC surface after etching with that of

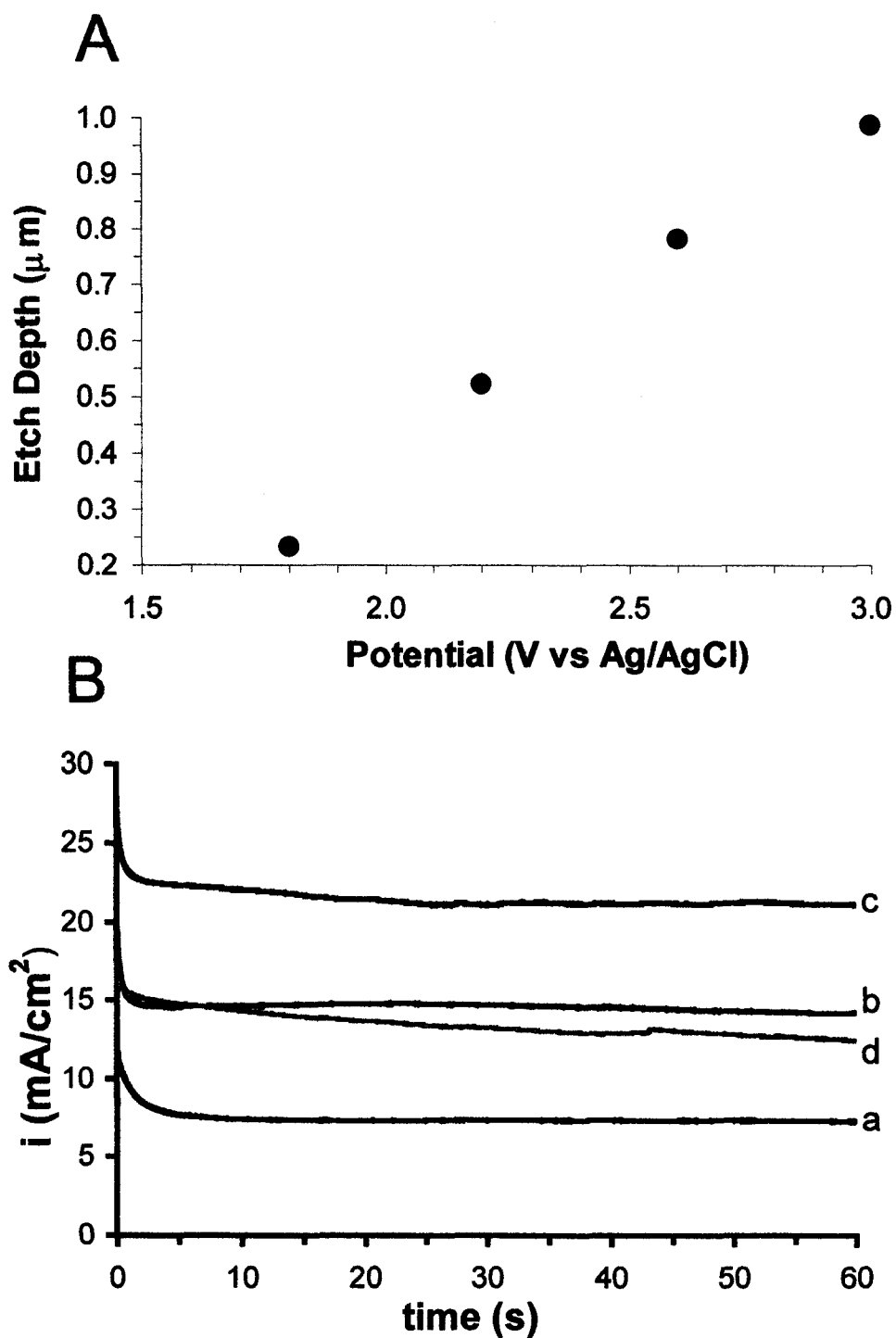


Figure 2.3 (A) Plot of etch depth vs. anodization potential at a constant time of 2 min. The depths were measured with SFM (B) Plots of current vs. time in response to a potential step. (a) GC 2.0V vs. Ag/AgCl, (b) GC, 2.5V, (c) GC, 3.0V, (d) Pt, 2.5V.

the initial polished surface. Figure 2.4A is a $10 \times 10 \mu\text{m}$ constant current STM image of a polished GC surface. A number of linear scratches due to the polishing procedure are visible. Roughness analysis of a number of $10 \times 10 \mu\text{m}$ areas yielded a root-mean-square (RMS) roughness of $5.4 \pm 0.9 \text{ nm}$.

Figure 2.4B is a $10 \times 10 \mu\text{m}$ constant current STM image of a GC surface that was etched for 8 min. at 2.0 V. Polishing scratches are not apparent in this image because the conditions employed are sufficient to etch beyond the depth of these features. The RMS roughness of the etched surface was measured to be $4.5 \pm 1.0 \text{ nm}$. Thus, the etching process does not increase the roughness of the resulting surface.

In most microfabrication applications, a process for controlling the depth of etching is desirable. Figure 2.3 suggests that anodization potential can be used to control etch depth. Figure 2.5 shows that the extent of GC etching can also be controlled by anodization time. The depth of etched features were measured from SEM images as shown in the inset of Figure 2.5A. The angle at which SEM images were collected was kept constant at 60° with respect to the detector and consequently, the measured depths are consistent from sample to sample. Figure 2.5B plots etch depth vs. time for a constant potential of 2.5 V while Figure 2.5C plots depth vs. charge passed for etching at a constant current of 100 mA. In both cases the measured depth increases with etch time and depths of $50 \mu\text{m}$ are achieved in a reasonable time frame (25-30 min.). It is clear from these figures that a targeted feature depth can be obtained by pre-selecting an

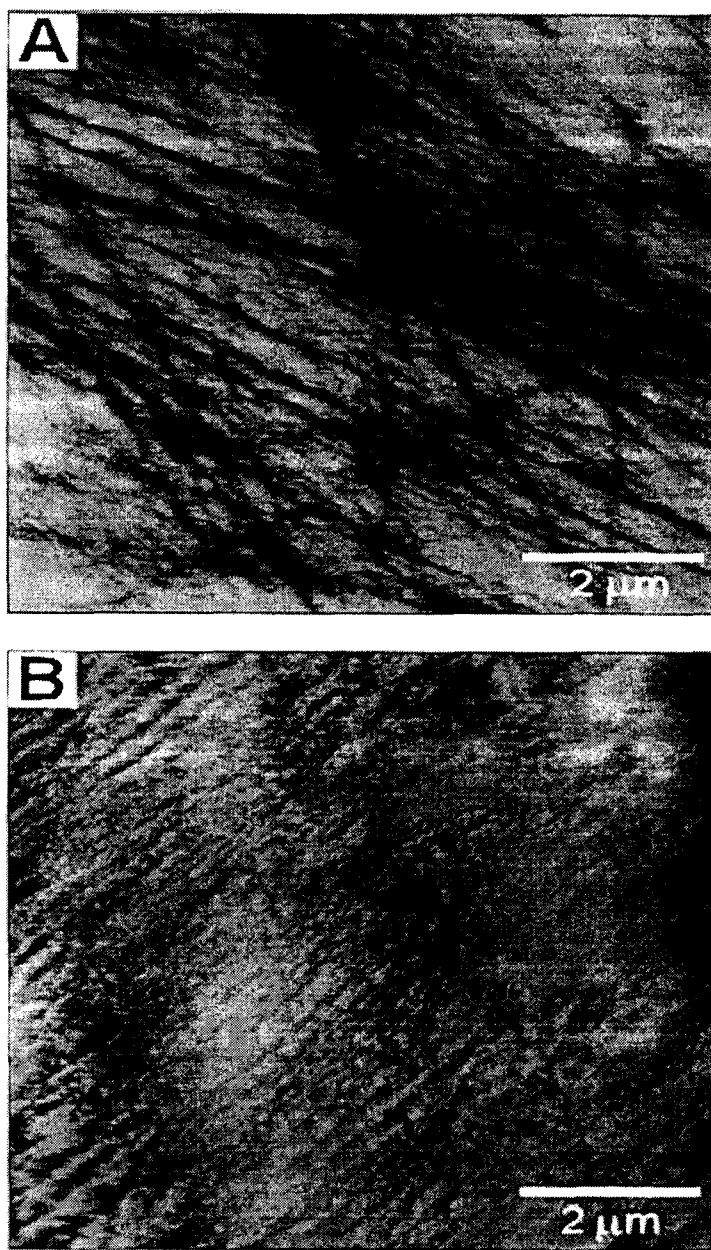


Figure 2.4 10 x 10 μm STM images of GC. (A) As polished GC, rms = 5.4 ± 0.9 nm. (B) Following GC etching for 8 min at 2.0V, rms = 4.5 ± 1.0 nm.

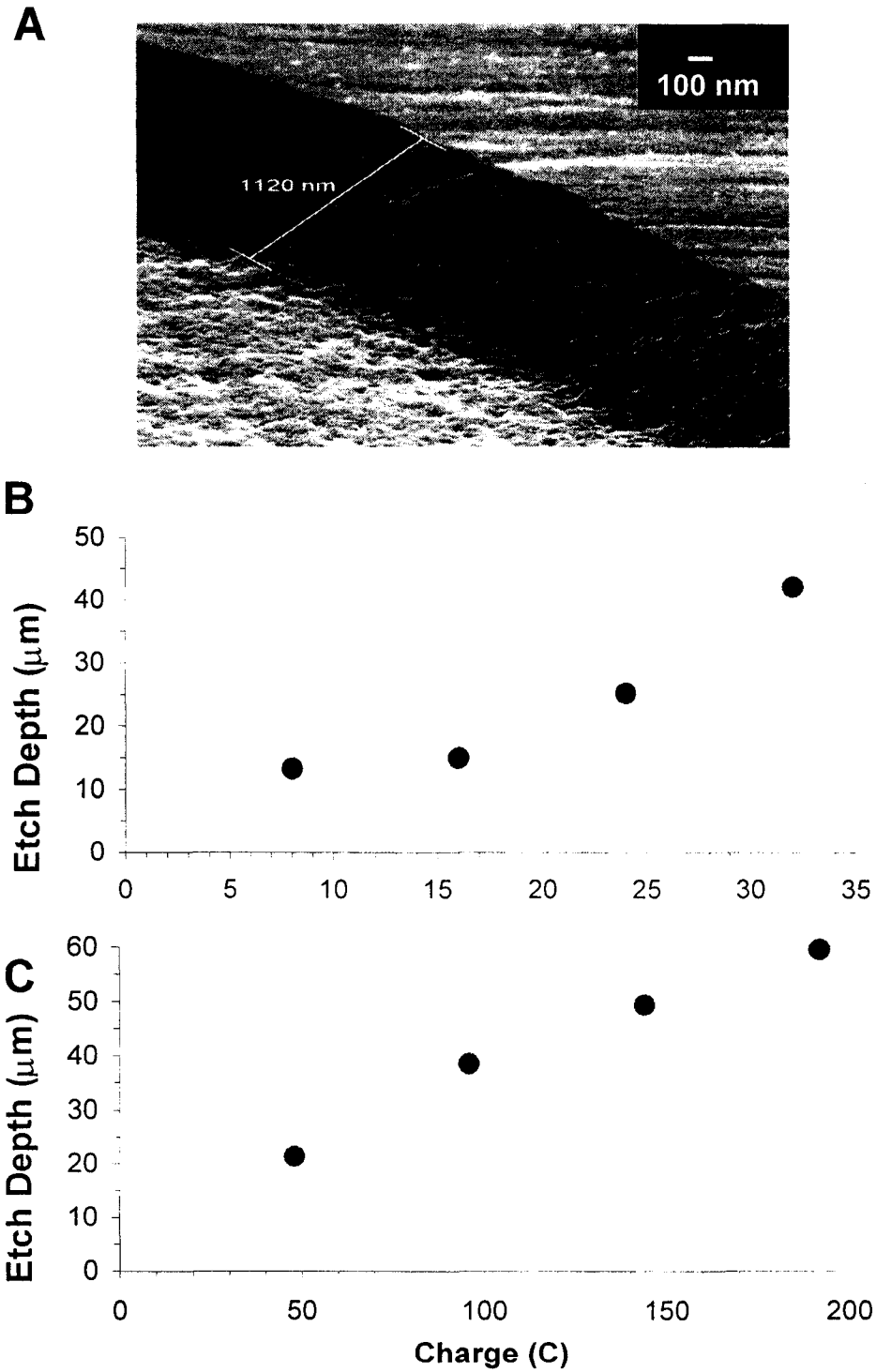


Figure 2.5 (A) SEM image illustrating the measurement of etch depth for a channel etched for 20 min at 2.5 V. (B) Plot of etch depth vs. time at a constant potential of 2.5 V. (C) Plot of etch depth vs. charge. Experiment was carried out at a constant current of 100mA.

appropriate potential or current and anodizing for an appropriate time.

The microstructure of GC is comprised of nanometer sized graphite crystallites arranged in random orientations [10]. Consequently, GC is isotropic even though graphite is an anisotropic material. Therefore, we expected the etching of GC to be isotropic. Figure 2.6 is an SEM image of a channel exhibiting a semicircular cross-section, which is strong evidence for isotropic etching. The channel depth is 15 μm while the width at the top of the channel measures $\sim 44 \mu\text{m}$. The exposed opening in the patterned photoresist for this channel was 20 μm wide, indicating that the etching undercut the mask by 12 μm on each side, a distance similar to the depth of the channel. This observation is consistent with isotropic etching.

The channel shown in Figure 2.6 suggests that anodic etching of GC may be useful for the fabrication of microfluidic or “lab-on-a-chip” devices. Over the past 10-15 years, glass has been the most widely used substrate for these devices. Recently, researchers have been developing “single-use” devices fabricated from polymeric materials [54]. The materials properties of GC, such as density, melting point, Young’s modulus, and conductivity, are vastly different than glass. In addition, the surface chemistry of GC differs substantially from glass and several convenient methods exist to chemically modify the surface of GC [16-19]. These statements are meant to imply that GC may be an interesting alternative material for the fabrication of microfluidic devices.

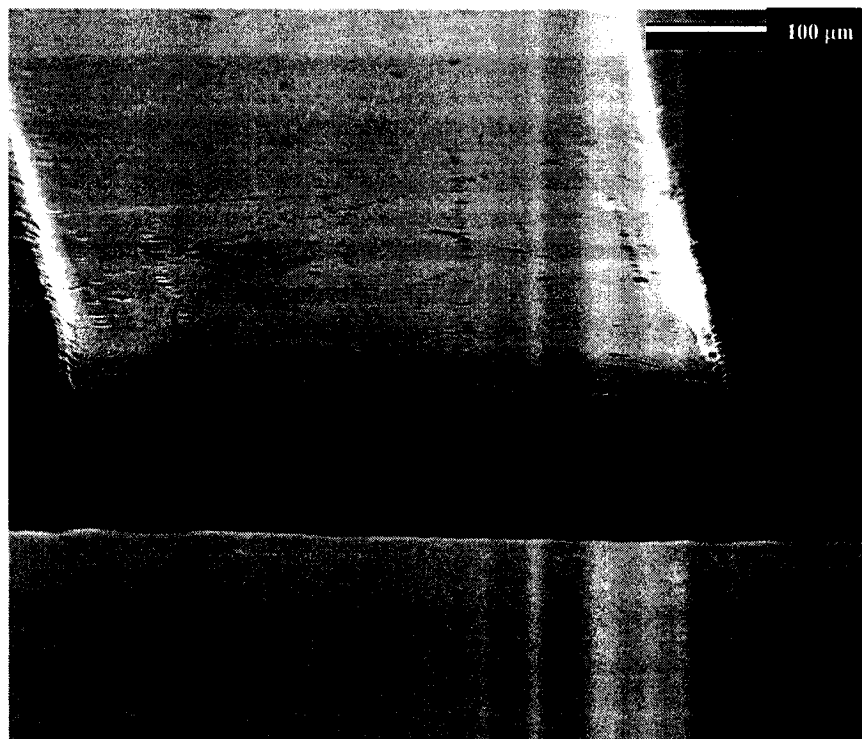


Figure 2.6 SEM image of the fractured end of a microchannel etched in GC at 2.0V for 30min. The semicircular profile is indicative of isotropic etching.

2.4 CONCLUSION

This chapter shows that lithographic pattern transfer and anodic etching in 0.1 M NaOH can be combined to microfabricate features in GC. The etching process is accompanied by the evolution of O_2 and likely involves the intercalation of OH^- into the GC lattice. The etched depth following anodization in basic media is dependent on anodization potential, current and time. Therefore, the etched depth can be controlled over different timescales and electrochemical conditions. In general, we employ an anodization potential between 2.0 and 2.5 V for between 20 and 60 min. to etch structures with depths on the order of tens of microns. The results discussed here show that the anodic process is isotropic due to the microstructure of GC and that a number of interesting structures, such as arrays of microwells and microchannels, can be etched into GC.

2.5 REFERENCES

1. Harrison, D.J., et al., *Capillary Electrophoresis and Sample Injection Systems Integrated on a Planar Glass Chip*. *Analytical Chemistry*, 1992. **64**(17): p. 1926-1932.
2. Harrison, D.J., et al., *Micromachining a Miniatuized Capillary Electrophoresis-Based Chemical Analysis System on a Chip*. *Science*, 1993. **261**: p. 895-897.
3. Bustillo, J.M., R.T. Howe, and R.S. Muller, *Surface Micromachining for Microelectromechanical Systems*. *Proceedings of the IEEE*, 1998. **86**(8): p. 1552-1574.
4. Janata, J., et al., *Chemical sensors*. *Analytical Chemistry*, 1998. **70**(12): p. 179R-208R.
5. Gopel, W., *Ultimate Limits in the Miniaturization of Chemical Sensors*. *Sensors and Actuators A*, 1996. **56**(1-2): p. 83-102.
6. Kumar, A., H.A. Biebuyck, and G.M. Whitesides, *Patterning Self-Assembled Monolayers-Applications in Materials Science*. *Langmuir*, 1994. **10**(5): p. 1498-1511.
7. Xia, Y.N., X.M. Zhao, and G.M. Whitesides, *Pattern Transfer: Self-Assembled Monolayers as Ultrathin Resists*. *Microelectronic Engineering*, 1996. **32**(1-4): p. 255-268.

8. Kiema, G.K., G. Fitzpatrick, and M.T. McDermott, *Probing Morphological and Compositional Variations of Anodized Carbon Electrodes with Tapping-Mode SFM*. Analytical Chemistry, 1999. **71**: p. 4306-4312.
9. Kiema, G.K., M. Aktary, and M.T. McDermott, *Preparation of Reproducible Glassy Carbon Electrodes by Removal of Polishing Impurities*. Journal of Electroanalytical Chemistry, 2003. **540**: p. 7-15.
10. McCreery, R.L., *In Electroanalytical Chemistry*, A.J. Bard, Editor. 1991, Marcel Dekker: New York. p. 221-374.
11. Kinoshita, K., *Carbon, Electrochemical and Physicochemical Properties*. 1988, John Wiley & Sons Inc.: New York. p. 226 - 292.
12. Engstrom, R.C., *Electrochemical Pretreatment of Glassy Carbon Electrodes*. Analytical Chemistry, 1982. **54**(13): p. 2310-2314.
13. van der Linden, W.E. and J.W. Dieker, *Glassy Carbon as Electrode Material in Electroanalytical Chemistry*. Analytica Chimica Acta., 1980. **119**(1): p. 1-24.
14. Yamada, S. and H. Sato, *Physics-Some Physical Properties of Glassy Carbon*, Nature, 1962. **193**(4812): p. 261.
15. Jenkins, G.M. and K. Kawamura, *Structure of Glassy Carbon*. Nature, 1971. **231**(5299): p. 175-&.
16. Delamar, M., et al., *Covalent Modification of Carbon Surfaces by Grafting*

- of Functionalized Aryl Radicals Produced From Electrochemical Reduction of Diazonium Salts*. Journal of the American Chemical Society, 1992. **114**: p. 5883 - 5884.
17. Dienhammer, R.S., et al., *Electrochemical Oxidation of Amine-Containing Compounds: A Route to the Surface Modification of Glassy carbon Electrodes*. Langmuir, 1994. **10**(4): p. 1306-1313.
 18. Anne, A., et al., *Facile Derivatization of Glassy Carbon Surfaces by N-Hydroxylsuccinamide Esters in View of Attaching Biomolecules*. Langmuir, 1998. **14**: p. 2368 - 2371.
 19. Liu, Y.-C. and R.L. McCreery, *Reactions of Organic Monolayers on Carbon surfaces Observed with Unenhanced Raman Spectroscopy*. Journal of the American Chemical Society, 1995. **117**: p. 11254-11259.
 20. Kariuki, J.K. and M.T. McDermott, *Nucleation and Growth of Functionalized Aryl Films on Graphite Electrodes*. Langmuir, 1999. **15**(19): p. 6534-6540.
 21. Kostecki, R., X. Song, and K. Kinoshita, *Electrochemical Analysis of Carbon Interdigitated Microelectrodes*. Electrochemical and Solid-State Letters, 1999. **2**(9): p. 465-467.
 22. Frackowiak, E. and F. Beguin, *Carbon materials for the Electrochemical Storage of Energy in Capacitors*. Carbon, 2001. **39**(6): p. 937-950.

23. Hierlemann, A., et al., *Application-specific sensor systems based on CMOS chemical microsensors*. Sensors and Actuators B, 2000. **70**(1-3): p. 2-11.
24. Nomoto, S., et al., *Advanced Capacitors and their Application*. Journal of Power Sources, 2001. **97-98**(8): p. 807-811.
25. Schueller, O.J.A., S.T. Brittain, and G.M. Whitesides, *Fabrication of Glassy Carbon Microstructures by Soft Lithography*. Sensors and Actuators A, 1999. **72**: p. 125-139.
26. Schueller, O.J.A., S.T. Brittain, and G.M. Whitesides, *Fabrication of Glassy Carbon Microstructures by Pyrolysis of Microfabricated Polymeric Precursors*. Advanced Materials, 1997. **9**(6): p. 477-480.
27. Schueller, O.J.A., et al., *Fabrication and Characterization of Glassy Carbon MEMS*. Chemistry of Materials, 1997. **9**: p. 1399-1406.
28. Shimizu, Y. and K. Morita, *Microhole Array Electrode as a Glucose Sensor*. Analytical Chemistry, 1990. **62**(14): p. 1498-1501.
29. Morita, K. and Y. Shimizu, *Microhole Array for Oxygen Electrode*. Analytical Chemistry, 1989. **61**: p. 159-162.
30. Ranganathan, S., et al., *Photoresist-Derived Carbon for MEMS and Electrochemical systems*. Journal of the Electrochemical Society, 2000. **147**(1): p. 277-282.

31. Ranganathan, S. and R.L. McCreery, *Electroanalytical Performance of Carbon films with Near-Atomic Flatness*. Analytical Chemistry, 2001. **73**: p. 893.
32. Kepley, L.J. and A.J. Bard, *Ellipsometric, Electrochemical, and Elemental Characterization of the Surface Phase Produced on Glassy Carbon Electrodes by Electrochemical Activation*. Analytical Chemistry, 1988. **1988**(60): p. 1459-1467.
33. McDermott, C.A., K.R. Kneten, and R.L. McCreery, *Electron Transfer Kinetics of Aquated Fe, Eu, and V at Carbon Electrodes: Inner Sphere Catalysis by Surface Oxides*. Journal of Electrochemical Society, 1993. **140**(9): p. 2593 - 2599.
34. Downard, A.J. and A.D. Roddick, *Effect of Electrochemical Pretreatment on Protein Adsorption at Glassy-Carbon Electrodes*. Electroanalysis, 1994. **6**(5-6): p. 409-414.
35. Yang, Y. and Z.G. Lin, *In-situ FTIR Characterization of the Electrooxidation of Glassy Carbon Electrodes*. Journal of Applied Electrochemistry, 1995. **25**: p. 259-266.
36. Bielby, A.L., T.A. Sasaki, and H.M. Stern, *Electrochemical Pretreatment of Carbon Electrodes as a Function of Potential, pH, and Time*. Analytical Chemistry, 1988. **67**(5): p. 976 - 980.

37. Wang, J., et al., *In situ Characterization of Electrochemically Activated Glassy Carbon Electrodes with Scanning Tunneling Microscopy*. Journal of Electroanalytical Chemistry, 1990. **278**(1-2): p. 379-386.
38. Engstrom, R.A. and V.A. Strasser, *Characterization of Electrochemically Pretreated Glassy Carbon Electrodes*. Analytical Chemistry, 1984. **56**(2): p. 136-141.
39. Heiduschika, P., A.W. Munz, and W. Gopel, *Impedance Spectroscopy and Scanning Tunneling Microscopy of Polished and Electrochemically Pretreated Glassy Carbon*. Electrochimica Acta., 1994. **39**(14): p. 2207-2223.
40. Freund, M.S., et al., *Scanning Tunneling Microscopy and Atomic Force Microscopy in the Characterization of Activated Graphite Electrodes*. Analytical Chemistry, 1991. **63**(10): p. 1047-1049.
41. Bowling, R.J., R.T. Packard, and R.L. McCreery, *Activation of Highly Ordered Pyrolytic Graphite for Heterogeneous Electron Transfer : Relationship between Electrochemical Performance and Carbon Microstructure*. Journal of the American Chemical Society, 1989. **111**: p. 1217-1223.
42. Anjo, D.M., et al., *Electrochemical Activation of Carbon Electrodes in Base: Minimization of Dopamine Adsorption and Electrode*. Analytical Chemistry, 1989. **61**: p. 2603-2608.

43. Korshin, G.V., *Investigation of the oxidation of Glassy Carbon by the Method of Electroreflectance - Relevance to Activation Processes*. Journal of Electroanalytical Chemistry, 1998. **446**(1-2): p. 13-18.
44. Kozlowski, C. and P.M. Sherwood, *X-Ray Photoelectron-spectroscopic Studies of Carbon-fiber Surfaces*. Journal of the Chemical Society, Faraday Trans. 1, 1985. **81**: p. 2745-2756.
45. Ross, P.N. and H. Sokol, *The Corrosion of Carbon-Black Anodes in Alkaline Electrolyte .1. Acetylene Black and the Effect of Cobalt Catalyzation*. Journal of the Electrochemical Society, 1984. **131**(8): p. 1742-1750.
46. Alliata, D., et al., *Anion intercalation into Highly Oriented Pyrolytic Graphite studied by Electrochemical Atomic Force Microscopy*. Electrochemistry Communications, 1999. **1**(1): p. 5-9.
47. Nishitani, R., Y. Sasaki, and Y. Nishina, *Kinetics of Staging Transition in H₂SO₄-Graphite Intercalation Compounds*. Synthetic Metals, 1990. **34**(1-3): p. 315-321.
48. Alsmeyer, D.C. and R.L. McCreery, *In-situ Raman Monitoring of Electrochemical Graphite-Intercalation and Lattice Damage in Mild Aqueous Acids*. Analytical Chemistry, 1992. **64**(14): p. 1528-1533.
49. Schnyder, B., et al., *Electrochemical Intercalation of Perchlorate Ions in*

HOPG: An SFM/LFM and XPS study. Applied Surface Science, 2001. **173**(3-4): p. 221-232.

50. Smyrl, W.H., et al., *Surface Injection Catalysis at Glassy-Carbon Electrodes*. Journal of Electroanalytical Chemistry, 1989. **267**(1-2): p. 67-81.
51. Smyrl, W.H., et al., *Morphology Changes Due to Anodic Treatment of Glassy Carbon Electrodes*. Journal of Electroanalytical Chemistry, 1989. **264**: p. 301-304.
52. Firouzi, A., R.T. Atanasoski, and W.H. Smyrl, *Surface-Topography of Anodically Treated Glassy-Carbon Electrodes*. Journal of Electroanalytical Chemistry, 1992. **330**(1-2): p. 369-380.
53. Alliata, D., et al., *In situ AFM Study of Interlayer Spacing during Anion Intercalation into HOPG in Aqueous Electrolyte*. Langmuir, 1999. **15**(24): p. 8483-8489.
54. Becker, H. and L.E. Locascio, *Polymer microfluidic devices*. Talanta, 2002. **56**: p. 267-287.

CHAPTER 3

ELECTROCHEMICAL FABRICATION OF MICROFLUIDIC NETWORKS IN CARBON SUBSTRATES

3.1 INTRODUCTION

Microfluidic devices have found increasing application as analytical systems, and as tools for fundamental research in chemistry and biochemistry. The application of processes such as photolithography, etching techniques, molding, imprinting, and casting to a variety of materials has enabled, for example, the development of lab-on-a-chip devices [1, 2], microelectromechanical systems (MEMS) [3], and miniaturized sensor systems [4]. Some of these processes have also led to methods of easily and reliably patterning surfaces [5, 6]. Since the onset of the microfluidic era, most devices have used glass as a substrate for their fabrication [2, 7]. However, in recent years, researchers have developed "single-use" devices fabricated from polymeric materials [8]. As the field of microfluidics continues to grow, there remains a growing need to expand the materials with which these devices can be fabricated.

Graphitized carbon, such as glassy carbon (GC), has physical properties that are vastly different from glass and most polymeric material. These include density, melting point, Young's modulus, and conductivity. In addition, the surface chemistry of GC differs substantially from that of the substrates mentioned above. Several methods have been explored to chemically modify the surface of GC [9-12]. Graphitic carbon can therefore act as an alternate or complementary material to glass and polymeric material for the fabrication of microfluidic devices. Implementation of processes for the microfabrication of

graphitized carbon materials may lead to new applications of microfluidics.

GC is produced by the pyrolysis of organic polymeric precursors and is considered to be a disordered graphitic material as discussed in Chapter 1. The term “glassy” has little to do with structure but refers instead to the fracture characteristics of the material. The microstructure of GC is characterized by randomly oriented 0.2-0.5 nm graphitic domains that are thought to follow a ribbon-like pattern as a consequence of the precursor polymer backbone. GC has been a widely utilized material in electrochemistry due to a number of attractive properties [13-17]. The physical properties of GC include good electrical conductivity, excellent thermal stability and low gas permeability. These provide a framework for GC as an appealing complementary material to glass and most polymeric material for designing miniaturized systems. Given that there are a number of methods that have been reported to chemically modify the surface of GC, the microfabrication of GC is postulated to open pathways for the development of microsensors and microsystems for controlled fluid flow [9-12, 18]. In the future, micro-machined GC structures may also find applications in microbatteries [19] and micro-capacitors [20-22].

Ultra-flat graphitic carbon films have recently found use in electroanalytical chemistry in the form of pyrolyzed photoresist films (PPF) [23]. The surface of PPF is exceptionally smooth (< 5.0nm rms) when compared to other carbon electrode surfaces, such as polished GC (4.1nm rms), and heat-treated GC disks (4.5nm rms) [24, 25]. In addition, the PPF surface exhibits a low oxygen/carbon

atomic (O/C) ratio [23]. The smoothness and low O/C ratio result in a surface with a low capacitance, contributing to the low background current observed in the cyclic voltammograms acquired on these films [24]. The ability to microfabricate channels and structures by electrochemical etching of carbon films, through lithographically patterned photoresist, could open up many useful possibilities for carbon-based chip design. For example, the preparation of micron sized parallel or circular carbon microelectrodes could lead to the integration of these films into the mass production processes utilized to manufacture components of microchips.

Relevant to the work presented in this Chapter, Schueller and coworkers have reported the fabrication of GC microchannels by a procedure based on reactive ion etching (RIE) through a patterned nickel mask in an oxygen plasma [26]. This procedure is extremely successful at fabricating complex structures with high aspect ratio [26] and even freestanding microstructures [27]. However, the etched surface of the glassy carbon microstructures becomes extensively oxidized during the plasma-etch. This leads to a decrease in the number of applications for which devices fabricated with RIE etched GC can be used [28-30]. Also, ultra-flat photoresist-derived carbon films have been evaluated extensively for their use in MEMS [40], and as lithographically patterned electrodes in microchip capillary electrophoresis devices [41].

The work described herein demonstrates initial efforts aimed at micro-machining glassy carbon (GC) and pyrolyzed photoresist films (PPF) via a

combination of photolithographic pattern transfer and anodic etching in basic media. The application of anodic potentials to GC electrodes in basic media has been shown to remove the thin ubiquitous layer of impurities from a polished GC electrode to produce a reproducible electrode surface [31, 32]. Chapter 2 discussed and hypothesized the mechanism of carbon removal from two carbon substrates, and the resultant morphology of the carbon surface [33]. In this chapter two methods are used. First, scanning electron microscopy (SEM) is used to assess the resultant structures etched in the carbon substrates. Secondly, flow injection analysis with laser-induced fluorescence (FIA-LIF) detection is used to evaluate the performance of the fabricated microfluidic networks. Results obtained in this study show that this etching procedure can be implemented for the fabrication of real microfluidic devices.

3.2 EXPERIMENTAL

3.2.1 Materials.

Sodium hydroxide pellets and HPLC grade methanol (Fisher, Nepean, ON) and fluorescein (Aldrich, Milwaukee, WI) were used as received. Aqueous NaOH solutions were prepared in distilled/deionized (18 M Ω /cm) water (Nanopure, Barnstead, Dubuque, IA) and purged with nitrogen gas for 10 min prior to use. Fluorescein solutions between 1 and 10 μ M were prepared in methanol. FITC labeled anti-mouse IgM [1mg/ml] (Sigma-Aldrich, Canada) was diluted into 50 ml of 10mM PBS buffer (pH 7.4). Glassy carbon plate (10 \times 10 cm, 3 mm thick) were obtained from Tokai Carbon Co., Ltd. (Tokai GC-20S, Tokyo,

Japan) and diced into various sizes. GC-20 refers to a pyrolysis temperature of 2000°C. The positive photoresist (Microposit SJR 5740) was obtained from OCG Chemicals (Providence, RI).

3.2.2 Mask Preparation

Masks for specific microchannels were created by designing the initial pattern in L-Edit TM Student Version software (Pasadena, CA). The design was then written on a Nanofilm chrome photomask blank (Westlake Village, CA) using a Heidelberg Instruments DWL 66 (Heidelberg, Germany) mask generator. After the mask generation, photoresist was developed 354 developer (Shipley) and the chromium etched using chrome etch semi-grade (Arch Chemicals Inc., Norwalk CT). The remaining photoresist was removed with HPLC grade acetone (Fisher).

3.2.3 Etching and Sealing of GC Substrates

The GC substrates were polished with successive slurries of 1.0, 0.3, and 0.05 μm alumina (Buehler) in distilled/deionized (dd) water on polishing microcloth (Buehler). The GC plates were sonicated in dd water for 10 min between polishing and then dried with a stream of argon. Mask patterns were transferred to polished GC substrates as shown in Figure 3.1. The SJR 5740 photoresist was twice spin-coated on the surface. The coated GC substrate was illuminated through a lithographic mask with UV light (~405 nm) and then the photoresist was developed with Shipley 354 developer. Electrochemical anodization of the surface was accomplished in a three-electrode cell with a

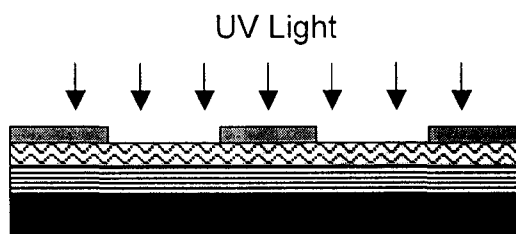
1. GC Substrate



2. Deposit 2 Layers of Photoresist



3. Pattern



4. Develop Photoresist in 0.01M NaOH



5. Anodize in 0.1M NaOH



6. Remove Photoresist



Figure 3.1 Schematic diagram describing the procedure used to generate microchannels in glassy carbon by electrochemical-wet etching.

Ag/AgCl (3 M KCl) reference electrode and a Pt foil counter electrode. A positive potential (≥ 2.0 V) was applied to the GC surface for a controlled period of time (≥ 8 min) in 0.1 M NaOH solution (pH ~ 13) at 23°C. For all fabricated microchannels the entire substrate was immersed in the electrolyte solution. The cell was connected to a Model AFCBP1 (Pinechem Instrument Co., PA) bipotentiostat. Anodized GC substrates were sonicated in acetone for 10 min to remove the remaining photoresist, rinsed, and then further sonicated in dd water for 5 min.

A polydimethylsiloxane (PDMS) substrate was fabricated according to established methods. Briefly, the polydimethylsiloxane prepolymer and cross-linker (Sylgard 184, Dow Corning; Midland, MI) were mixed in a container in a 10:1 by weight ratio. The mixture was then poured into a flat glass dish and allowed to cure overnight at ambient temperature and pressure. After trimming the bulk polymer into manageable pieces, a piece of the PDMS was brought in conformal contact with the GC substrate and through-bored at the ends to allow fluids access to the channels on the GC. Fluid flow was driven by vacuum applied through a pipette tip to one access point of the microchannel while the other end was connected to a reservoir of solution as shown in Figure 3.2.

For substrates sealed with glass, after drying under argon the GC substrate was carefully coated with a very thin layer UV-curable adhesive (Henkel Loctite, Rocky Hill, CT). A 1 mm thick microscope glass slide (President's Choice, Montreal, PQ) in which access holes had been drilled was

then placed on top of the microchip. The entire assembly was clamped together, ensuring that there was no adhesive in the channels, and exposed to UV light using a UV lamp, for 3 min. The device was cleaned as previously described [34] and sonicated in distilled water before use as shown in Figure 3.2.

Pyrolyzed photoresist films (PPF) were prepared on silicon substrates as described previously [23, 24]. The procedure entails dicing a silicon wafer into 1.2×1.2 cm pieces. The surface oxide layer was stripped from the silicon substrates by immersing it into a 10:1 buffered oxide etch solution (10 parts 40% NH_4F and 1 part 49% HF). Two coatings of positive photoresist (SJR 5740) were spin-coated onto each substrate at 2000 rpm. The samples were soft baked at 115°C in argon to remove excess solvent, and then pyrolyzed in a tube furnace at 1000°C for 1 hour under flowing forming gas (95% N_2 :5% H_2). After cooling under forming gas to 23°C , the substrates were patterned as described above.

3.2.4 Microscopy.

Scanning electron microscopy (SEM) of the GC substrates were carried out using a JEOL model 6301FXV scanning electron microscope at an acceleration voltage of 3.5 kV. The samples were attached to a silver holder with conductive carbon tape. Image analyses were performed with commercial software (Image Tool, version 2.00, University of Texas Health Science Center in San Antonio) for measuring the dimensions of the features.

1. Etched GC



2. Etched GC sealed by conformal contact with PDMS or spin-coated with UV-cured adhesive and bonded with glass cover.



3. Covered GC Microchip

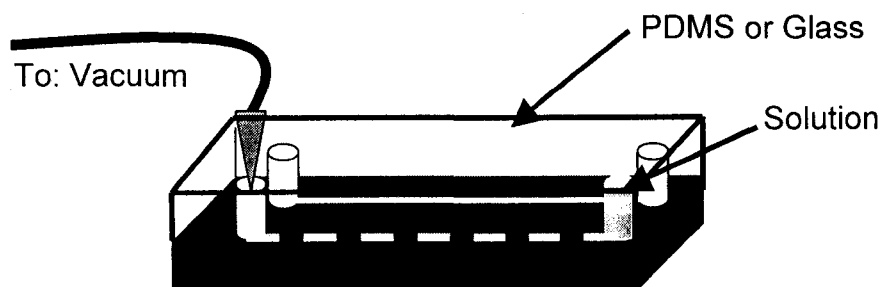


Figure 3.2 Schematic describing the procedure used to prepare PDMS sealing and glass bonding for a GC microchip for fluorescence detection. For glass bonding, after etching was completed, adhesive was applied and cured with a UV lamp.

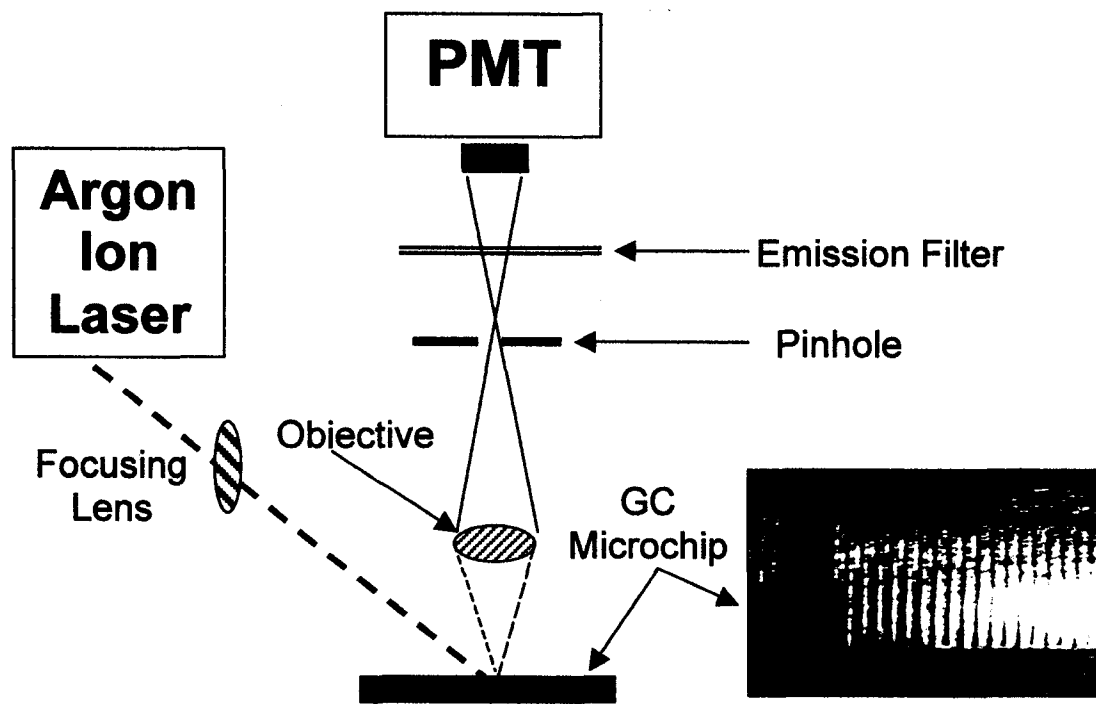


Figure 3.3 The experimental set-up for the flow injection analysis with laser induced fluorescence of fluorescein. An argon ion laser was used as the source, followed by a focusing lens, GC microchip and the emitted light focused into a PMT detector. The optical image shown illustrates a top view of the glassy carbon microchip used for the described in this experiment.

An Olympus Fluoview™ scanning laser confocal microscope was used to obtain fluorescence from the GC channels. All samples were covered with either PDMS elastomer or a bonded cover glass. A 50mW, 488nm argon ion laser beam was focused onto the sample through a 50X(0.55NA) achromatic microscope objective lens. A 0.25m spectrometer with a CCD detector array was used to collect fluorescence with a 40 second acquisition time.

3.2.5 Instrumentation for Flow Injection Analysis

The work presented in this section was carried out in the laboratory of Dr. D. Jed Harrison. The optical instrumentation setup is illustrated in Figure 3.3. The computer used to collect the data used in-house written LabVIEW software (National Instruments, Austin, TX). An air-cooled 488 nm Argon ion laser (Model 2214-105 L, Uniphase, San Jose, CA) operated at 4mW, was used as a source. Emitted fluorescence was collected at a 45° angle to the incident beam using a 25X, 0.35 N.A. microscope objective (Leitz, Wetzlar, Germany). A 600 nm pinhole, 530 nm emission filter and a photomultiplier tube (PMT) (R1477: Hamamatsu, Bridgewater, NJ) biased at 500V were used for detection. The PMT signal was amplified with a homemade transresistance current amplifier, filtered (25Hz Butterworth) and sampled at 50Hz. Solution flow was achieved via a low-pressure vacuum system to yield a flow of ~1mL/min with mobile phase consisting of 100% HPLC grade methanol. Fluorescence was detected after the sample flowed past the spot where the laser was focused.

3.3 RESULTS AND DISCUSSION

The procedure for combining lithographic pattern transfer and electrochemical etching to microfabricate features in GC is shown in Figure 3.1. The parameters used are described in the first paragraph in the results and discussion section of Chapter 2. Figure 3.4 is an SEM image illustrating the result of this procedure. A channel with a width of $\sim 130 \mu\text{m}$ was fabricated in GC by anodization at 2.0V for 30min in a stirred solution. As observed, the slanted walls of the microchannels are indicative that the photoresist used to mask the GC was undercut at several times during the etching of GC, indicating that the process was isotropic as shown in Chapter 2. In most microfabrication applications, a procedure for controlling the etching process is always desirable. In Chapter 2 we found that the dimensions of GC structures fabricated by electrochemical anodization can be varied by three parameters [33]: the anodization potential, anodization time, and charge passed for a constant current. A comparison between constant potential and constant current etching is shown in Figure 3.4 and 3.5. The channel shown in Figure 3.4 was fabricated using a constant anodization potential of 2.0V, while the microchannel presented in Figure 3.5 was etched under constant current conditions of 100 mA. The total charge passed for the channel in Figure 3.5 was 480 Coulombs. The inset SEM image of the channel in Figure 3.5 shows a semicircular edge with respect to the bottom of the channel wall. From these figures, it can be concluded that both constant potential and constant current electrochemical etching of GC produces

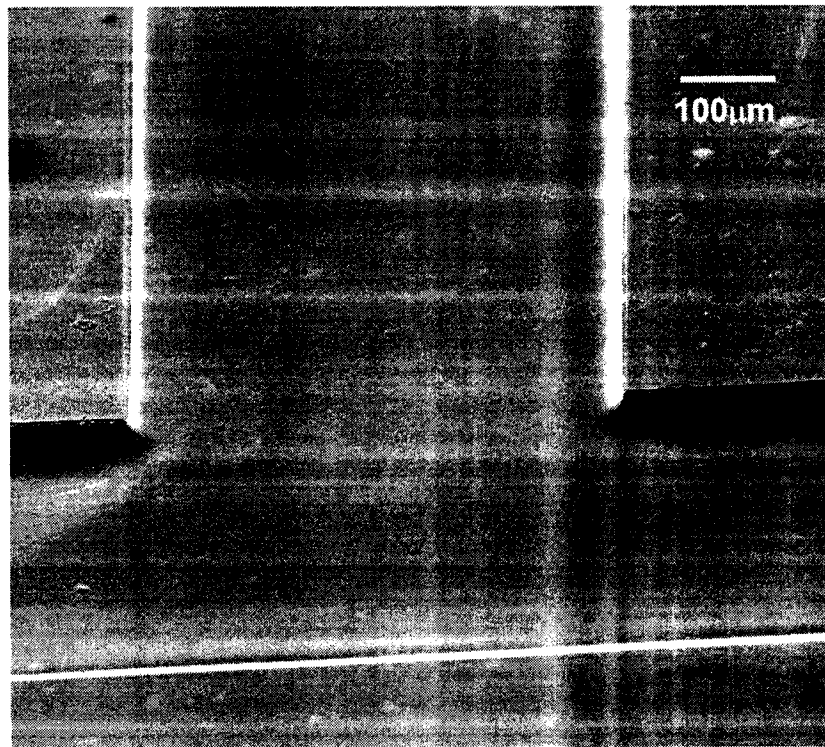


Figure 3.4 SEM image of a single "T" glassy carbon microchannel fabricated by electrochemical etching at 2.0V for 30 min

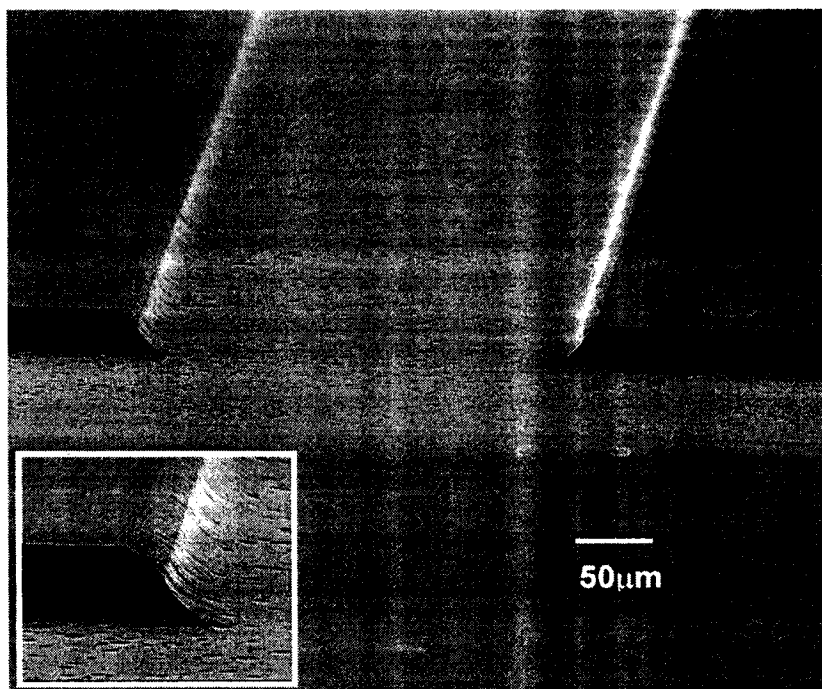


Figure 3.5 SEM image of a single "T" microchannel fabricated in glassy carbon at a constant current of 100mA for 80 min. The inset shows a close-up view of the slanted channel wall which was indicative of mask undercutting.

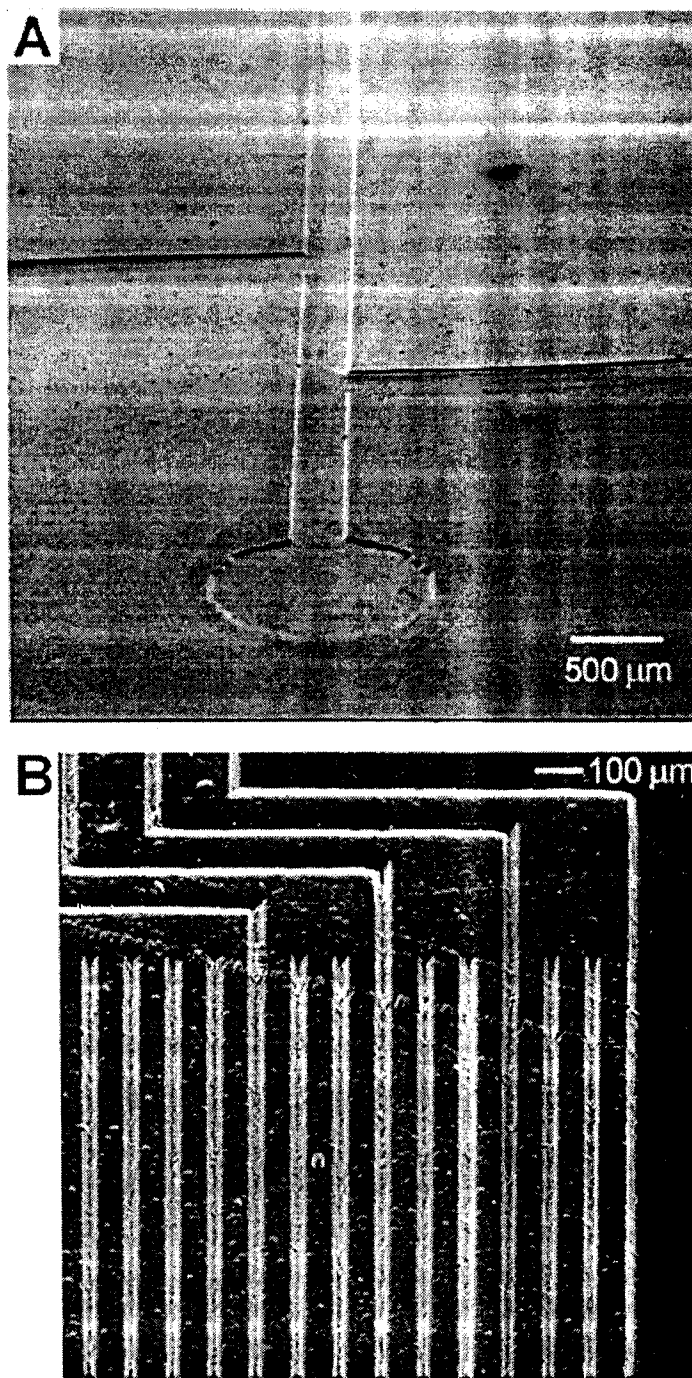


Figure 3.6 SEM image of a microchannel networks etched in GC at 2.0V for 30min.

well-defined channel structures. The wall shape observed within these electrochemically etched channels is similar with those observed in isotropically etched glass substrates [1, 2]. The remainder of the channels discussed in this chapter have been etched at constant potential.

The next objective was to investigate the feasibility of etching various channel designs and entire devices in GC. Figure 3.6 shows that microfluidic channels can be fabricated in GC via anodic etching. Figure 3.6A shows a circular reservoir and a “double-T” injector, originally reported by Harrison and coworkers [2] that has been etched into GC. The channels in this design are 300 μm wide and 30 μm deep, similar to dimensions that are fabricated in glass substrates. A more complex channel system is shown in Figure 3.6B. The images presented in Figure 3.6 prove that channel networks fabricated in glass can also be fabricated into GC. Figure 3.7 illustrates a complete device fabricated in GC via electrochemical anodic etching. The device was etched into a 1 cm x 2.5 cm GC substrate in 0.1 M sodium hydroxide under a constant voltage of 2.0V for 80 min. A rectangular double reservoir for the electrolytic generation of gas bubbles and a chevron barrier developed by Harrison and coworkers [35] was etched into GC. The channels on the device are ~30 μm deep and either 300 μm or 600 μm wide as illustrated by the two different line widths.

Having shown the viability of micromachining miniaturized analytical devices in GC as shown in Figure 3.7, we explored procedures to seal the top of

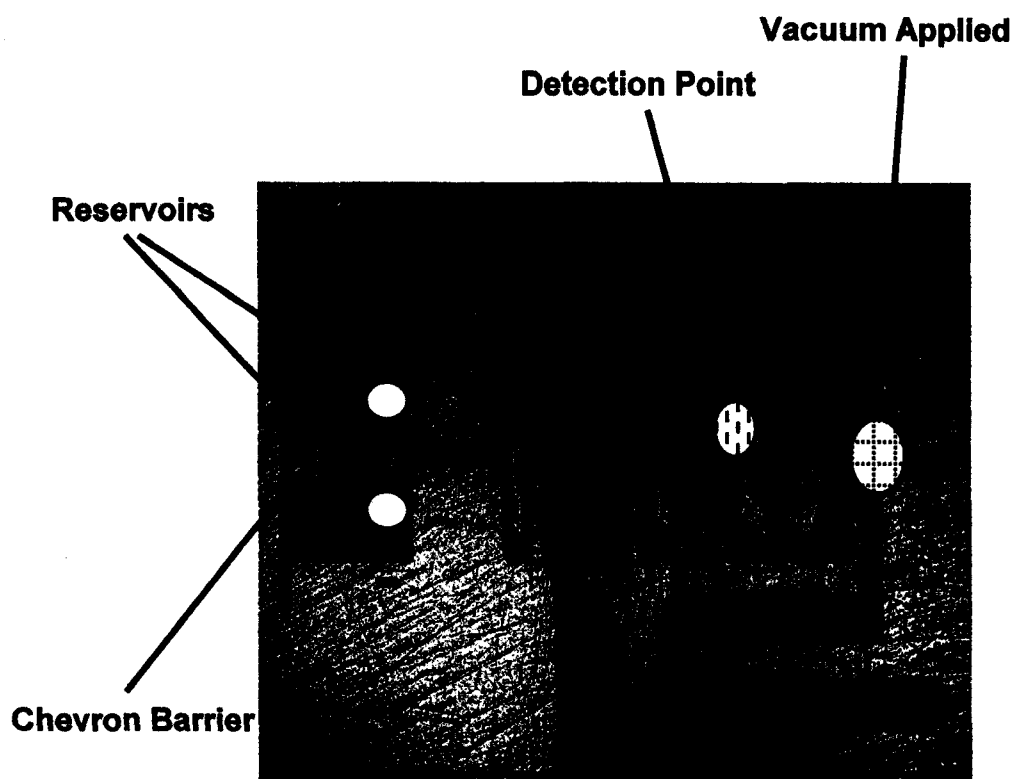


Figure 3.7 SEM image of a 1cm x 2.5 cm glassy carbon chip showing an etched electrolysis pump device. Channels are $\sim 30\mu\text{m}$ deep and either $300\mu\text{m}$ or $600\mu\text{m}$ wide as illustrated by the 2 different line widths. The chevron barrier is shown to the left of the device. Anodization was carried out at 2.0V for 80 min.

the fabricated microchannels to allow liquid flow. In glass microfluidic networks, closed microchannels were initially formed by bonding a glass cover plate to the substrate in a process that was carried out in a muffle furnace at 620°C [1]. Later, a direct bonding technique was developed by which the glass substrate and cover plate were first hydrolyzed, joined by hydrogen bonding, and then annealed at 500°C [36]. However, the high temperature bonding process hindered the fabrication of devices that contain temperature-sensitive materials or material with different coefficients of thermal expansion. Consequently, several techniques have been studied and developed for low temperature [37] and room temperature [38] glass bonding. Also, several methods such as the application of UV cured adhesive between substrate and cover plate [34] have been explored to solve the problem of thermal coefficient incompatibilities experienced during thermal bonding.

Initially, we experimented with sealing the fabricated GC microchannels by covering them with poly(dimethyl)siloxane (PDMS) elastomer. PDMS has been shown to form excellent conformal seals of surfaces such as glass and gold [39]. Figure 3.8 is a scanning laser confocal fluorescence micrograph of a microchannel in GC sealed with a PDMS cover. The channel contains a 10 mM solution of FITC labeled mouse IgM that was pressure driven through the channel. Significant leakage of the solution between the PDMS cover and the GC substrate was observed. We find that flow rates >1mL/min, over 50% of seals made with PDMS showed leakage. We therefore explored other methods

to seal microchannels fabricated into GC. We avoided thermal bonding techniques as it was difficult to find materials that had a matching thermal expansion coefficient to that of GC, lending to a plausible substrate-cover plate pair. After consulting the literature, a method reported by Divakar and coworkers was adopted for GC [34]. A schematic representation is given in Figure 3.2

FITC labeled mouse IgM [1mg/mL] and 10mM PBS buffer were pressure driven through different channels and results of the detected sample shown in Figure 3.9. Figure 3.9 shows a scanning laser confocal image of adjacent channels on a GC microchip. The image shows a channel containing the 10mM PBS buffer solution (gray) to the left, and a channel containing fluorescent FITC labeled anti-mouse IgM (green) to the right, separated by a barrier. Although the solution in the microchannel was stagnant when the image was acquired, higher flow rates were achievable relative to PDMS covers.

Using the same device as shown in Figure 3.7, we performed an analysis of several fluorescein samples. Our aim was to gauge whether a micromachined GC substrate could be used for the detection of solutions under hydrodynamic flow. Solutions of various concentrations of fluorescein in methanol were aliquoted into the device at the reservoirs. The vacuum was applied at the location noted in Figure 3.7 to induce a fluid flow of ~5mL/min. Methanol, ~2mL, was initially flowed through the system before the various solutions of fluorescein were introduced into the reservoirs. Each plug of the fluorescein was detected at the “detection point” on the device. In essence, the device was functioning as a

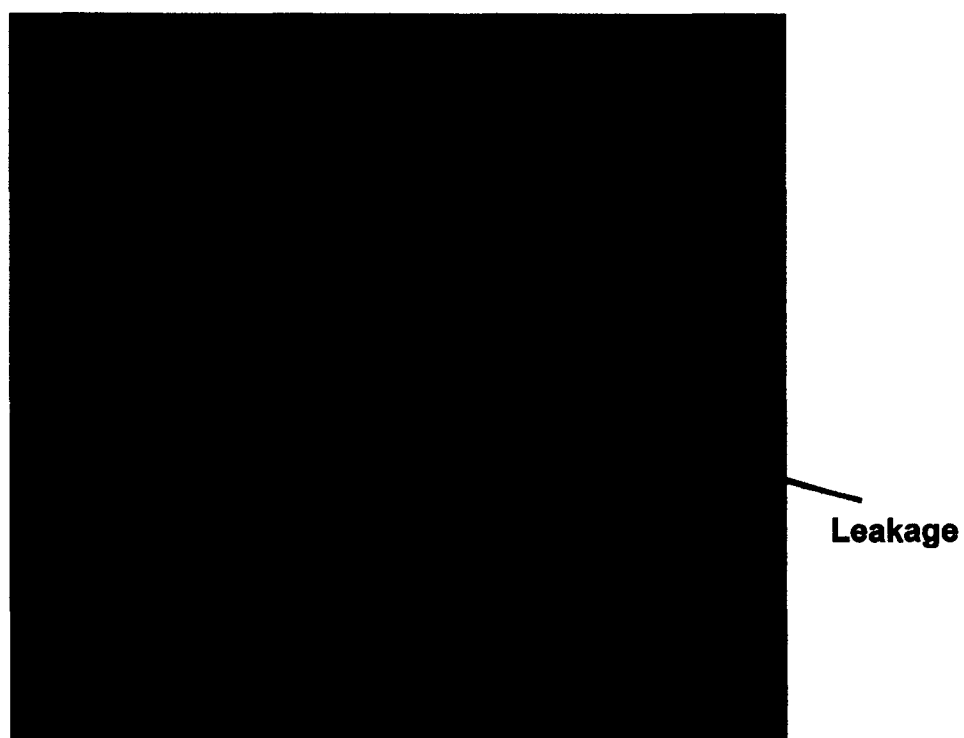


Figure 3.8 Fluorescence micrograph of a single microchannel containing FITC labeled IgM. The channel is $\sim 300\mu\text{m}$ wide and shows the resultant poor seal achieved with PDMS elastomer.

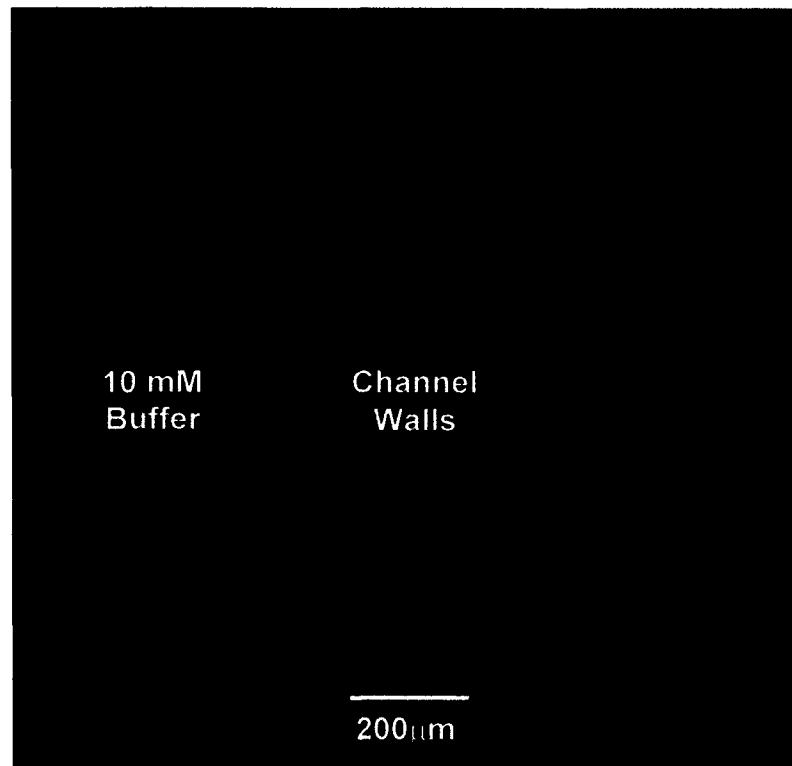


Figure 3.9 Fluorescence micrograph of 2 channels containing 10mM PBS buffer and FITC labeled IgM. The channels, which illustrate excellent sealing achieved using bonded glass are also $\sim 300\mu\text{m}$ wide and are separated by a barrier wall that was $\sim 600\mu\text{m}$ wide.

simple flow injection analysis device.

The results of the experiment are shown in Figure 3.10. Shown are plots of fluorescence intensity as a function of time. Effort was made to synchronize data collection with sample introduction. It should be noted that at the end of the experiment, a blank fluorescein free methanol solution, was run to ensure that the fluorescence was predominantly due to the fluorescein. In terms of quantitation, although peak shape observed in Figure 3.10 was poor due to the formation of bubbles as the solution was driven past the point of detection, the detected fluorescence intensity scaled linearly with concentration as evident with the least-squares linear regression equation and correlation factor that are given on Figure 3.11. From the results presented in the previous sections, it can be concluded room temperature UV-cured adhesive can be successfully implemented in sealing GC microdevices. The data given herein extends the feasibility of implementing this method in sealing “real” devices.

Figure 3.12 is a SEM image of a section of a photolithographically patterned PPF. The microchannel etched at an anodization potential of 2.0V for 8 min. The width and depth of the channel are 300 μm and 2.5 μm respectively. Most of the PPF film at the base of the channel has been etched through to the silicon substrate. The shape of the channel as shown in the inset, results from the undercutting of the photoresist during the etching process, as were observed during the etching of GC. This attribute will be exploited for the fabrication of microelectrode arrays in Chapter 5. In addition, the morphology of the PPF

channel wall as seen in the inset, is different as compared to GC in Figure 4.3B. We attribute the roughness of the wall to incomplete graphite domain formation during pyrolysis.

3.4 CONCLUSION

We have demonstrated that lithographic pattern transfer and anodic etching in 0.1 M NaOH can be combined to fabricate microfluidic networks features in GC and PPF films. Our results show that the anodic process is isotropic due to the microstructure of GC, and can be controlled with anodization potential or current. Carbon material is known to be resistant to acids, bases, oxidizing and reducing agents, most solvents, and generally have low surface energies. Even though a significant drawback to GC as a substrate is the difficulty in effecting any on-chip electrophoretic separations, we conclude that the use of carbon materials would still prove well suited for use in microfluidic devices. The fabricated micro-devices presented here and elsewhere [42] show that GC can be useful in analytical chemistry not just as an electrode. We believe that these devices will open a new frontier of "lab-on-a-chip" devices based on carbon materials.

The wet etching technique presented here is the only technique currently applicable for the fabrication of microfluidic devices in carbon materials. The technique is relatively inexpensive and results in channel structures that are comparable with those achieved in glass or silicon etching. Channel widths as small as 1 μm [data not shown] to as large as 300 μm have been achieved.

We believe our approach provides advantages over the photolithographic approach that is used to fabricate microchannels in glass, and the reactive ion etching (RIE) approach used to fabricate microstructures in GC [26]. It does not require the use of a metal layer, gold, nickel or chromium, which are required for the etching of glass or GC to produce comparable features. Furthermore, the bonding of a cover slide to the carbon material has proved easy. This could be advantageous if thousands of similar devices were to be produced. Carbon is relatively inexpensive, has a high mechanical stability, wide potential window, and applicability to a wide range of redox systems; the application of this lithographic patterning and electrochemical etching will provide new pathways to the use of carbon material in microfluidics. A novel application that uses this electrochemical technique is discussed in the next chapter.

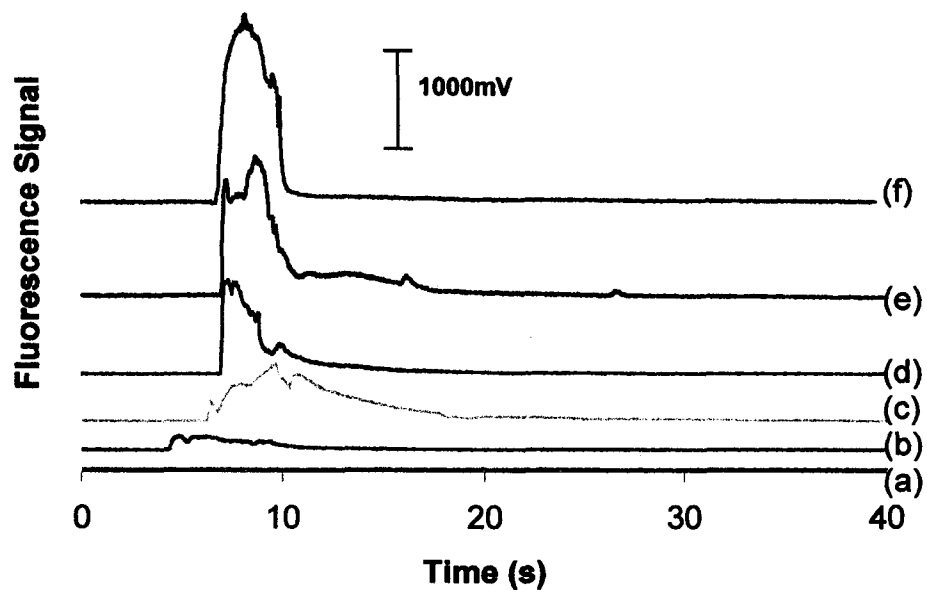


Figure 3.10 Flow injection analysis (FIA) of (a) 100% methanol (b) $1\mu\text{M}$ fluorescein, (c) $2\mu\text{M}$ fluorescein, (d) $5\mu\text{M}$ fluorescein, (e) $7\mu\text{M}$ fluorescein, (f) $10\mu\text{M}$ fluorescein at 530nm following suction of fluorescein samples through GC chip. FIA was performed in a mobile phase composed of 100% methanol.

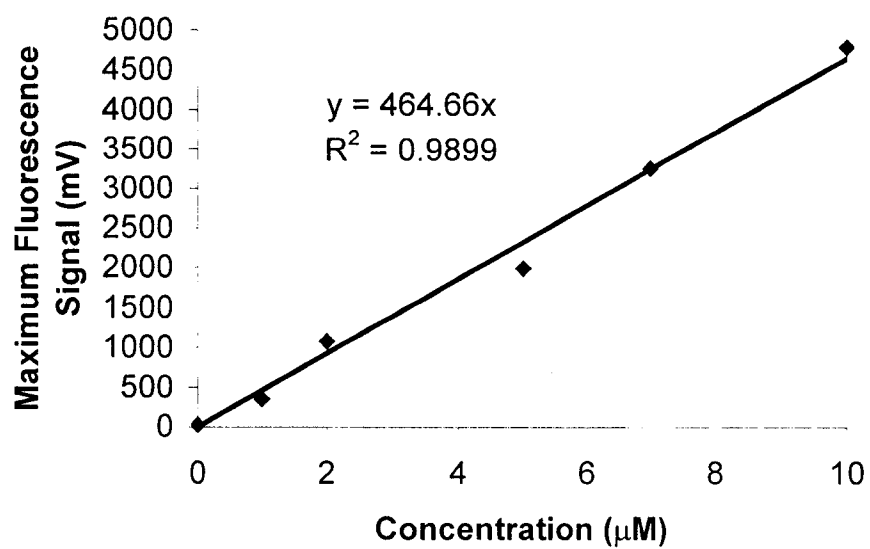


Figure 3.11 A calibration curve of the various fluorescein solutions that were pressure driven a channel of the GC based FIA-LIF device shown in figure 3.7.

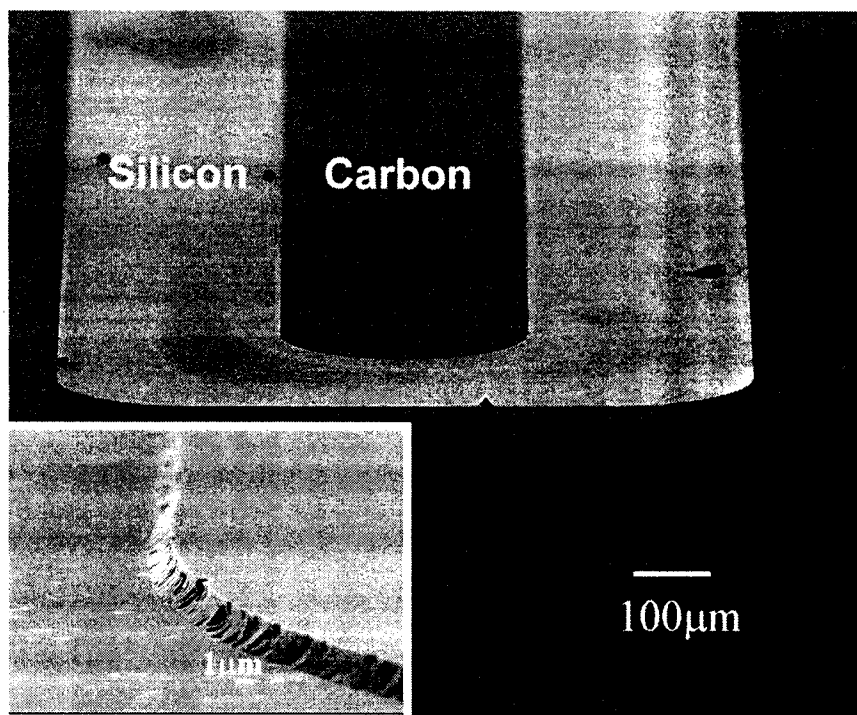


Figure 3.12 SEM image of a single meandering microchannel fabricated in a pyrolyzed photoresist film (PPF). The inset shows a close-up view of the channel wall from which we can observe its morphology. Anodization was carried out at a constant voltage of 2.0V for 8 min.

3.5 REFERENCES

1. Harrison, D.J., et al., *Capillary Electrophoresis and Sample Injection Systems Integrated on a Planar Glass Chip*. Analytical Chemistry, 1992. **64**(17): p. 1926-1932.
2. Harrison, D.J., et al., *Micromachining a Miniaturized Capillary Electrophoresis-Based Chemical Analysis System on a Chip*. Science, 1993. **261**: p. 895-897.
3. Bustillo, J.M., R.T. Howe, and R.S. Muller, *Surface Micromachining for Microelectromechanical Systems*. Proceedings of the IEEE, 1998. **86**(8): p. 1552-1574.
4. Gopel, W., *Ultimate Limits in the Miniaturization of Chemical Sensors*. Sensors and Actuators A, 1996. **56**(1-2): p. 83-102.
5. Kumar, A., H.A. Biebuyck, and G.M. Whitesides, *Patterning Self-Assembled Monolayers-Applications in Materials Science*. Langmuir, 1994. **10**(5): p. 1498-1511.
6. Janata, J., et al., *Chemical Sensors*. Analytical Chemistry, 1998. **70**(12): p. 179R-208R.
7. Manz, A., et al., *Planar Chips Technology for Miniaturization and Integration of Separation Techniques into Monitoring Systems - Capillary Electrophoresis Chip*. Journal of Chromatography A, 1992. **593**(1-2): p. 253-258.

8. Becker, H. and L.E. Locascio, *Polymer Microfluidic Devices*. *Talanta*, 2002. **56**: p. 267-287.
9. Dienhammer, R.S., et al., *Electrochemical Oxidation of Amine-Containing Compounds: A Route to the Surface Modification of Glassy Carbon Electrodes*. *Langmuir*, 1994. **10**(4): p. 1306-1313.
10. Delamar, M., et al., *Covalent Modification of Carbon Surfaces by Grafting of Functionalized Aryl Radicals Produced From Electrochemical Reduction of Diazonium Salts*. *Journal of the American Chemical Society*, 1992. **114**: p. 5883 - 5884.
11. Liu, Y.-C. and R.L. McCreery, *Reactions of Organic Monolayers on Carbon surfaces Observed with Unenhanced Raman Spectroscopy*. *Journal of the American Chemical Society*, 1995. **117**: p. 11254-11259.
12. Anne, A., et al., *Facile Derivatization of Glassy Carbon Surfaces by N-Hydroxylsuccinamide Esters in View of Attaching Biomolecules*. *Langmuir*, 1998. **14**: p. 2368 - 2371.
13. McCreery, R.L., *In Electroanalytical Chemistry*, A.J. Bard, Editor. 1991, Marcel Dekker: New York. p. 221-374.
14. Yamada, S. and H. Sato, *Physics-Some Physical Properties of Glassy Carbon*, *Nature*, 1962. **193**(4812): p. 261.
15. Jenkins, G.M. and K. Kawamura, *Structure of Glassy Carbon*. *Nature*,

1971. **231**(5299): p. 175-&.
16. van der Linden, W.E. and J.W. Dieker, *Glassy Carbon as Electrode Material in Electroanalytical Chemistry*. Analytica Chimica Acta., 1980. **119**(1): p. 1-24.
 17. Kinoshita, K., *Carbon, Electrochemical and Physiochemical Properties*. 1988, John Wiley & Sons Inc.: New York. p. 226 - 292.
 18. Kariuki, J.K. and M.T. McDermott, *Nucleation and Growth of Functionalized Aryl Films on Graphite Electrodes*. Langmuir, 1999. **15**(19): p. 6534-6540.
 19. Kostecki, R., X. Song, and K. Kinoshita, *Electrochemical Analysis of Carbon Interdigitated Microelectrodes*. Electrochemical Solid-State Letters., 1999. **2**(9): p. 465-467.
 20. Hierlemann, A., et al., *Application-Specific Sensor Systems based on CMOS Chemical Microsensors*. Sensors and Actuators B, 2000. **70**(1-3): p. 2-11.
 21. Frackowiak, E. and F. Beguin, *Carbon Materials for the Electrochemical Storage of Energy in Capacitors*. Carbon, 2001. **39**(6): p. 937-950.
 22. Nomoto, S., et al., *Advanced Capacitors and their Application*. Journal of Power Sources, 2001. **97-98**(8): p. 807-811.
 23. Ranganathan, S., et al., *Photoresist-Derived Carbon for MEMS and*

- Electrochemical Systems*. Journal of the Electrochemical Society, 2000. **147**(1): p. 277-282.
24. Ranganathan, S. and R.L. McCreery, *Electroanalytical Performance of Carbon Films with Near-Atomic Flatness*. Analytical Chemistry., 2001. **73**: p. 893.
 25. McDermott, M.T. and R.L. McCreery, *Scanning Tunneling Microscopy of Ordered Graphite and Glassy Carbon Surfaces: Electronic Control of Quinone Adsorption*. Langmuir, 1994. **10**: p. 4307-4313.
 26. Schueller, O.J.A., S.T. Brittain, and G.M. Whitesides, *Fabrication of Glassy Carbon Microstructures by Soft Lithography*. Sensors and Actuators A, 1999. **72**: p. 125-139.
 27. Schueller, O.J.A., S.T. Brittain, and G.M. Whitesides, *Fabrication of Glassy Carbon Microstructures by Pyrolysis of Microfabricated Polymeric Precursors*. Advanced Materials, 1997. **9**(6): p. 477-480.
 28. Durkic, T., et al., *Boron and Phosphorus Doped Glassy Carbon: Surface Properties*. Carbon, 1997. **35**: p. 1567-1572.
 29. Cho, D., et al., *Microscopic Behaviour on the Protection of Polyacrylonitrile-based Carbon Fibers from Thermal Oxidation*. Polymer Journal, 1997. **29**: p. 959-963.
 30. Criscione, J.M., H.F. Volk, and A.W. Smith, *Protection of Graphite from*

- Oxidation at 2100C*. AIAA Journal, 1966. **4**: p. 1791-1797.
31. Kiema, G.K., M. Aktary, and M.T. McDermott, *Preparation of Reproducible Glassy Carbon Electrodes by Removal of Polishing Impurities*. Journal of Electroanalytical Chemistry, 2003. **540**: p. 7-15.
 32. Kiema, G.K., G. Fitzpatrick, and M.T. McDermott, *Probing Morphological and Compositional Variations of Anodized Carbon Electrodes with Tapping-Mode SFM*. Analytical Chemistry, 1999. **71**: p. 4306-4312.
 33. Kiema, G.K., S. Ssenyange, and M.T. McDermott, *Microfabrication of Glassy Carbon by Electrochemical Etching*. Journal of the Electrochemical Society, 2004. **151**(2): p. C142-C148.
 34. Divakar, R., D. Butler, and I. Papautsky, *Room Temperature Low-Cost UV-Cured Adhesive Bonding for Microfluidic Biochips*, in *MicroTotal Analysis Systems*, J.M.R.a.A.v.d. Berg, Editor. 2001, Kluwer Academic Publishers. p. 385-386.
 35. Furdui, V.I., J.K. Kariuki, and D.J. Harrison, *Microfabricated Electrolysis Pump System for Isolating Rare Cells in Blood*. Journal of Micromechanics and Microengineering, 2003. **13**: p. S164-S170.
 36. Jacobson, S.C., et al., *Effects of Injection Schemes and Geometry on the Performance of Microchip Electrophoresis Devices*. Analytical Chemistry, 1994. **66**(7): p. 1107-1113.

37. Wang, H.Y., et al., *Low Temperature Bonding for Microfabrication of Chemical Analysis Devices*. Sensors and Actuators B, 1997. **45**(3): p. 199-207.
38. Chiem, N., et al., *Room Temperature Bonding for Microfabrication of Chemical Analysis Devices*. Sensors and Actuators B, 2000. **63**(3): p. 147-152.
39. Donzel, C., Geissler, M., Bernard A., Wolf, H., Michel, B., Hilborn, J., Delamarche, E. *Hydrophilic Poly(dimethylsiloxane) Stamps for Microcontact Printing*. Advanced Materials, 2001. **13**(15): p. 1164 - 1167.
40. Kim, J., et al., *Electrochemical Studies of Carbon Films from Pyrolyzed Photoresist*. Journal of the Electrochemical Society, 1998. **145**(7): p. 2314-2319.
41. Hebert, N.E., et al., *Performance of Pyrolyzed Photoresist Carbon Films in a Microchip Capillary Electrophoresis Device with Sinusoidal Voltammetric Detection*. Analytical Chemistry, 2003. **75**(16): p. 4265-4271.
42. Ssenyange, S., et al., *A Glassy Carbon Microchip for Electrospray Mass Spectrometry*. Analytical Chemistry, 2004. In Press.

CHAPTER 4

A GLASSY CARBON MICROCHIP FOR ELECTROSPRAY MASS SPECTROMETRY

A version of this chapter has been published. Ssenyange, S., Taylor, J., Harrison, D. J., McDermott, M. T. *Analytical Chemistry*. **2004**, In Press. "A Glassy-Carbon Microchip for Electrospray Mass Spectrometry"

4.1 INTRODUCTION

Miniaturized analytical instrumentation is attracting growing interest in chemical analysis due to its potential for enhanced sensitivity, ease of automation, high throughput capabilities and reductions in analysis time, sample consumption and system size. Most devices reported to date have been fabricated in glass or silicon using photolithography and wet or dry chemical-etching processes. In recent years, however, interest in polymer-based microchips for chemical analysis has increased due to the availability of methods for accurate plastic replication. Over the past few years the coupling of microchips with mass spectrometric (MS) detection has been developed [1-3]. The flow rates generated within micro-devices are perfectly suited to micro- and nano-electrospray MS, [4] making the two techniques compatible despite the seemingly drastic size comparison. A number of different approaches have been explored in order to optimize the coupling of microfluidic chips to MS.

The first simple interfaces involved electrospray signal directly from the flat edge of the device [5, 6]. In both cases, the electrospray voltage was applied through a fluidic reservoir on the chip. Difficulties in limiting the size and stability of the resulting Taylor cone have ultimately limited the usefulness of this technique. Exploration of coupling transfer lines to ESI sources [7] and of direct coupling of nanospray emitters [8, 9] has proven fruitful, and the majority of chip-MS work over the past years has used one of these two methods. Application of the electrospray voltage often adds further complication to the interface design

and has been the driving force of new developments. Voltage can be applied at the distal end of the electrospray emitter, through a liquid junction either on [10] or off [7] chip. Alternatively, the voltage can be applied at the end of the emitter either through the use of a sheath flow or through a metallic coating [11]. The use of commercial nanospray tips with metallic coatings has proven effective in the past, however, instability of the metallic coating has limited their wide spread use. Recent work has explored the use of metallic emitters as electrospray sources for use in microfluidic devices [12]. The electrospray voltage is easily applied to the stainless steel emitter without concern for metal degradation. Our present study describes the fabrication of a microfluidic device in a conductive substrate, glassy carbon (GC), enabling the application of the electrospray voltage directly to the sample solution avoiding the need for external junctions.

Work presented in Chapters 2 and 3 has shown that the application of anodic potentials to GC electrodes in basic media can be used to etch GC [13, 14]. The physical properties of GC, good electrical conductivity, thermal stability, low coefficient of thermal expansion, and low density provide a framework for GC as an appealing complementary material to glass, silicon and plastic for designing miniature systems. Although the conductive nature of GC inhibits electrokinetic-based separations, other separation methods may be attainable on GC devices. For example, electrochemically modulated liquid chromatography (EMLC) [15, 16] employs a conductive carbon stationary phase and may be implemented on a GC microfluidic device.

microfabricated device in GC. A combination of photolithographic pattern transfer, anodization in basic media and sealing the substrate with a glass cover is used to fabricate a GC chip to be used as a platform for electrospray ionization mass spectrometry (ESI-MS). Results obtained in this study show that anodic GC etching can be implemented for the fabrication of functional microchip ESI-MS interface devices.

4.2 EXPERIMENTAL

4.2.1 Fabrication of GC Device

The device was fabricated in a 6 cm x 2 cm and 3 mm thick glassy carbon (GC) plate (Tokai GC-20S, Tokyo, Japan). The "as received" material exhibits a dull texture and a root-mean-square (RMS) roughness of >50 nm as measured with scanning force microscopy (SFM). The GC plate was polished with successive slurries of 1.0, 0.3 and 0.05 μm alumina (Buehler) in distilled/deionized (dd) (18 M Ω /cm) water (Nanopure, Barnstead, Dubuque, IA) on a polishing microcloth (Buehler). The plate was sonicated in dd water for 10 min between polishing steps and then dried with a stream of argon. This polishing procedure results in a surface with a SFM measured RMS roughness of ~5 nm [14]. The mask pattern was transferred to the polished GC substrate as shown in Figure 4.1. The positive photoresist (Microposit SJR 5740) was twice spin-coated onto the surface. The coated GC substrate was illuminated through a lithographic mask with UV light (~405 nm) and the photoresist was developed with Shipley 354 developer. The entire substrate was immersed in a sodium

hydroxide (Fisher) solution prepared in dd water and purged with nitrogen gas for 10 min prior to use. Electrochemical anodization of the surface was accomplished in a three-electrode cell with a Ag/AgCl (3 M KCl) reference electrode and a Pt foil counter electrode. The cell was connected to a Model AFCBP1 (Pinechem Instrument Co., PA) bipotentiostat. A positive potential (2.5 V) was applied to the GC for 75 min in 0.1 M NaOH solution (pH ~ 13) at room temperature (23°C). The anodized GC substrate was rinsed with dd water then sonicated in acetone for 10 min to remove the remaining photoresist followed by further sonication in dd water for 5 min. As previously in Chapter 2, the SFM measured roughness of the GC surface after etching did not differ appreciably from the original polished GC surface [14]. After drying under argon, the substrate was spin coated with adhesive (Henkel Loctite, Rocky Hill, CT) and bonding of a glass covers slip was carried out as previously described [17].

4.2.2 Chip-MS Interfacing

A commercial uncoated nanospray tip (360 μm o.d., 50 μm i.d., 15 μm tip, New Objective Inc., Woburn, MA) was coupled to the device using previously published methods [18]. In brief, a 368 μm hole was drilled into the edge of the GC device, aligned with the channel. The tip was blunt cut, inserted into the hole and then fixed using silicon rubber (GE Silicones, Mississauga, ON), which has not been seen to lead to MS interferences. A commercial Nanoport™ (Upchurch Scientific, Oak Harbour, WA) device was fixed to the inlet of the device to allow for easy coupling of the transfer capillary (365 μm o.d., 50 μm i.d., Polymicro

Technologies, L.L.C., Phoenix, AZ). Flow was driven using a syringe pump (Harvard Apparatus, Saint-Laurent, QC, Canada) at a flow rate of 0.4 $\mu\text{L}/\text{min}$.

4.2.3 Mass Spectrometry

All MS data was collected using a single quadrupole Sciex API 150EX (Applied Biosystems, Foster City, CA / MDS Sciex, Concord, ON, Canada) in positive ionization mode. The microchip assembly was placed in front and to the side of the orifice at approximately 1.5 cm from the sampling orifice. The electrospray voltage used ranged from 3200-3900 V and was applied directly to the glassy carbon chip as is shown in Figure 4.2. The dwell time was set to 1.0 milliseconds (ms) and the pause time to 2.0 ms. The remaining scan parameters are noted in the caption to each figure. Mass-to-charge is denoted by m/z and the intensity is shown in counts per second (c.p.s.). A polypropylene glycol (PPG) standard was used as supplied from Applied Biosystems. The sample was supplied in 50 % methanol and 50 % water and was buffered with both formic acid and ammonium acetate. The polypropylene glycol concentration was 0.04 % PPG 2000, 0.01% PPG 1000 and 0.0014% PPG 425, by volume. Angiotensin II was obtained from Sigma-Aldrich (Sigma-Aldrich Canada Ltd., Oakville, Ontario, Canada). A stock solution of 0.7 mg/mL was prepared in water and serial dilutions prepared in 50% methanol (Sigma-Aldrich, HPLC grade), 50% water, 0.1 M formic acid (Sigma-Aldrich). The methanol was distilled before use.

4.3 RESULTS AND DISCUSSION

The microchip assembly used to generate electrospray was prepared as described in the experimental section and interfaced with the MS as shown in Figure 4.2. The drawing is not to scale. The relative channel lengths for the experiments discussed below are 28mm from the reservoir to the tapering intersection and 12 mm from the tapering section to the nanospray tip. The nanospray tip was approximately 4 cm in length. As highlighted in the top view profile, Figure 4.2, the various sections of the channel also varied in width. The Nanoport inlet was coupled to a 300 μm wide section of the channel while the channel leading to the nanospray tip tapered to a width of 50 μm . Channel depths were $\sim 20\mu\text{m}$.

Preliminary studies using this device indicated that the signal obtained was easily reproducible. The resulting spectrum from the infusion of polypropylene glycol and associated peak assignments are shown in Figure 4.3. The m/z values for each peak was compared to a vendor-supplied table of masses with no variations noted at the 0.1 amu precision level used for data collection. Long-term stability of the generated ESI signal was monitored at 0.77 spectra s^{-1} over the mass range corresponding to the range where the majority of the analyte and adduct signals were observed ($m/z = 750\text{-}1400$). Figure 4.4 illustrates the total ion current (TIC) for infusion of the polypropylene glycol solution over a period of 87 min. The relative standard deviation (RSD) of the 3982 scans collected was $\sim 2.0\%$. This value is in the same range as those

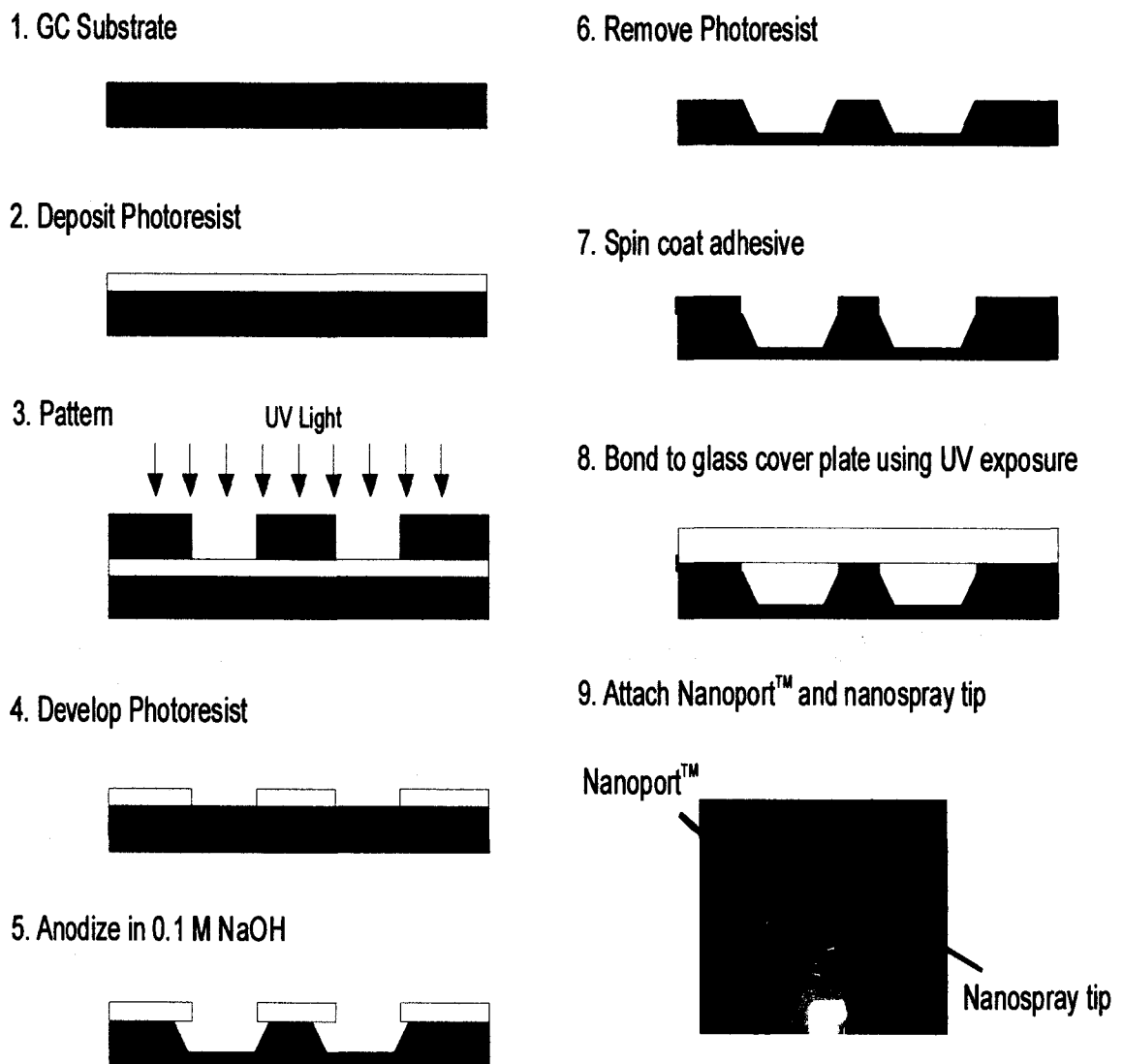


Figure 4.1 Illustration of the scheme used to fabricate the glassy carbon chip.

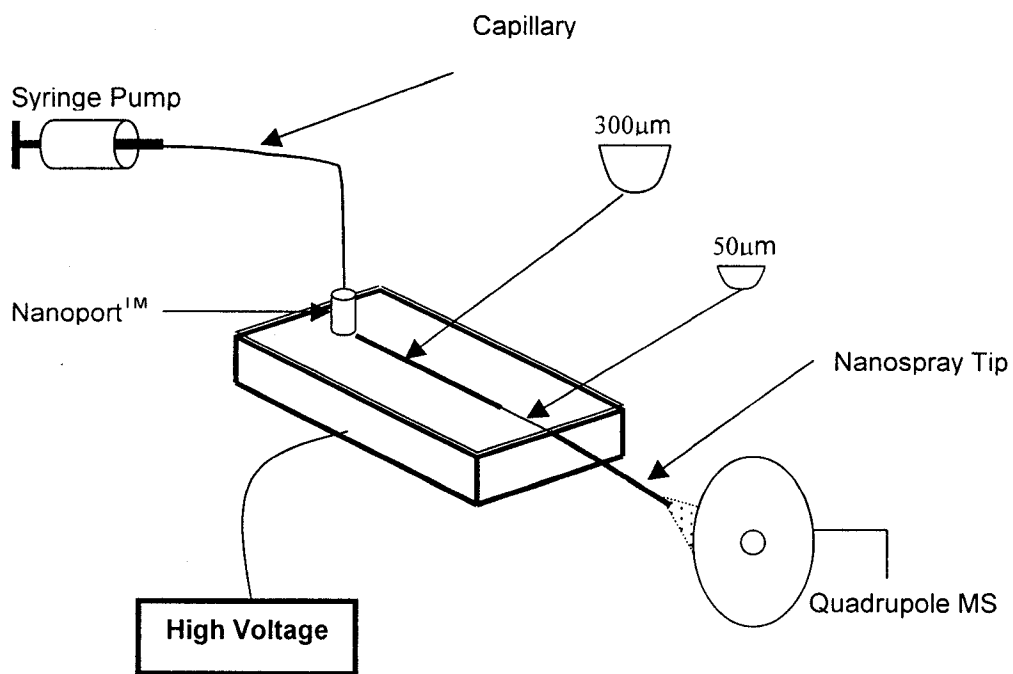


Figure 4.2 Experimental setup of the GC nanoelectrospray device. The sample is introduced via a syringe pump and the high voltage is applied to the glassy carbon chip. The nanospray tip creates a spray that is directed into a quadrupole mass spectrometer.

previously reported for a nanospray tip source, using similar acquisition parameters [4, 19, 20].

In order to test the ability of the system to detect lower concentrations, a series of peptide (angiotensin II) solutions were run. Three concentrations were used and spectra collected over a narrow m/z range, 504-554. The doubly charged state of angiotensin II is seen at 524^{2+} and detection was focused in this range. Spectra shown in Figures 4.5A-C are the result of infusion of 6.69 μM , 134 nM and 26.8 nM angiotensin II, respectively, at a flow rate of 0.4 $\mu\text{L}/\text{min}$. Considering our spectral acquisition time of 0.4 s, these concentrations result in 17.8 fmol, 357 amol and 71.4 amol being electrosprayed during the spectral acquisition. Figures 4.5B-C include a trace for the buffer signal alone (grey) that was collected after buffer rinsing for 10 min. to confirm that no sample carryover due to adsorption impacts the corresponding peptide spectra. We note that the PPG samples required much longer rinsing time (~ 1 hour) to minimize sample carryover. The signal intensity at $m/z = 524.1$ was averaged over 200 scans for both the 26.8 nM angiotensin solution (Figure 4.5C, black trace) and the running buffer (Figure 4.5C, grey trace). Signals of $76,000 \pm 10,000$ c.p.s. and 15300 ± 4600 c.p.s. were observed for the protein and blank solutions respectively. Taking the difference between protein and blank solutions gives a background corrected value of 60,600 c.p.s., which is 13 times the noise, taken as the standard deviation in the buffer signal. This value is well above the limit of detection (3σ) and limit of quantitation (10σ) as defined by standard analytical

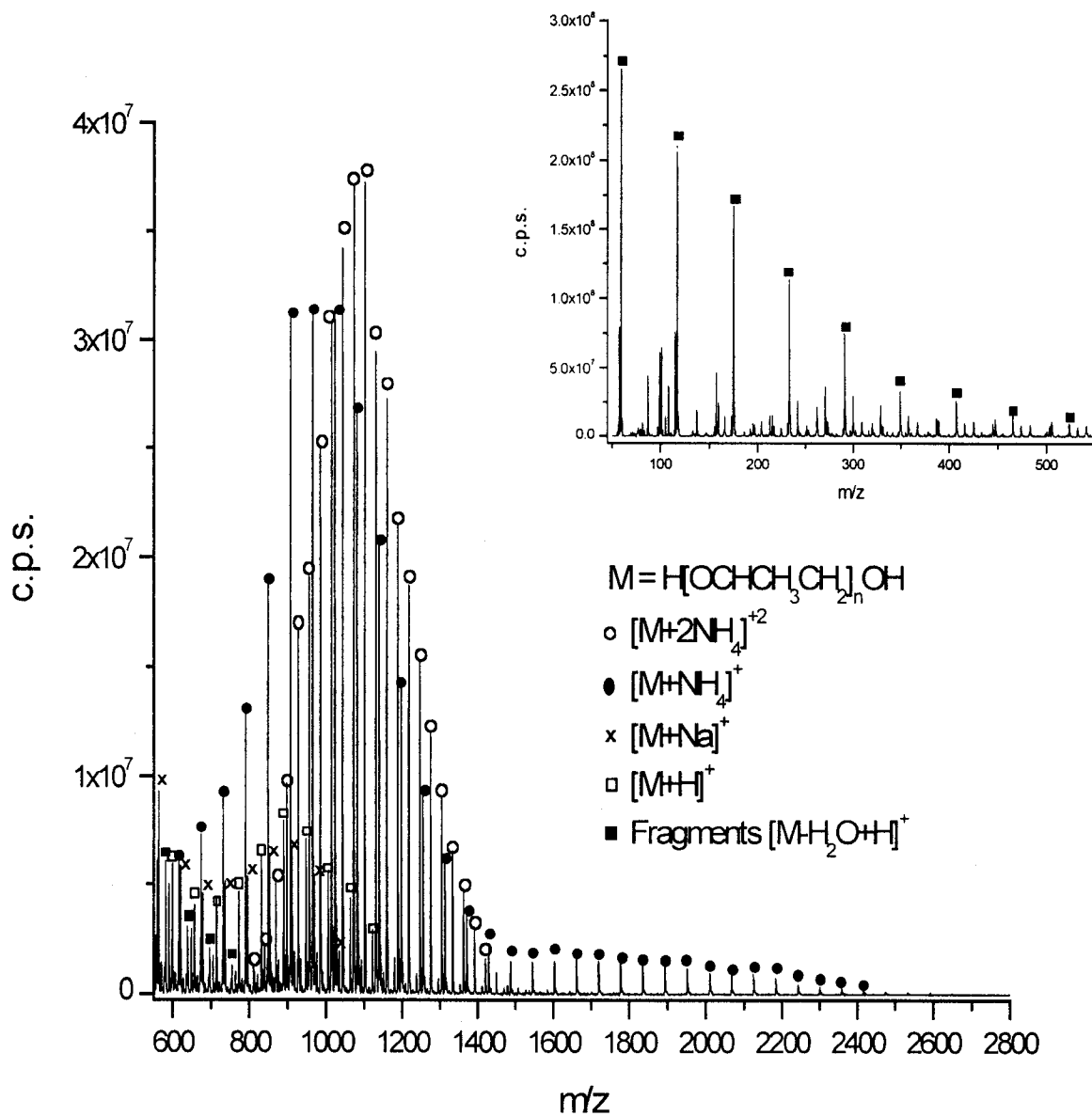


Figure 4.3 Resulting spectrum from infusion of the PPG standard. Spectrum is the sum of 50 scans. The main plot shows m/z range 550 to 2800 and the inset 50 to 550 both at a step size of 0.1 amu. ESI voltage was 3850 V.

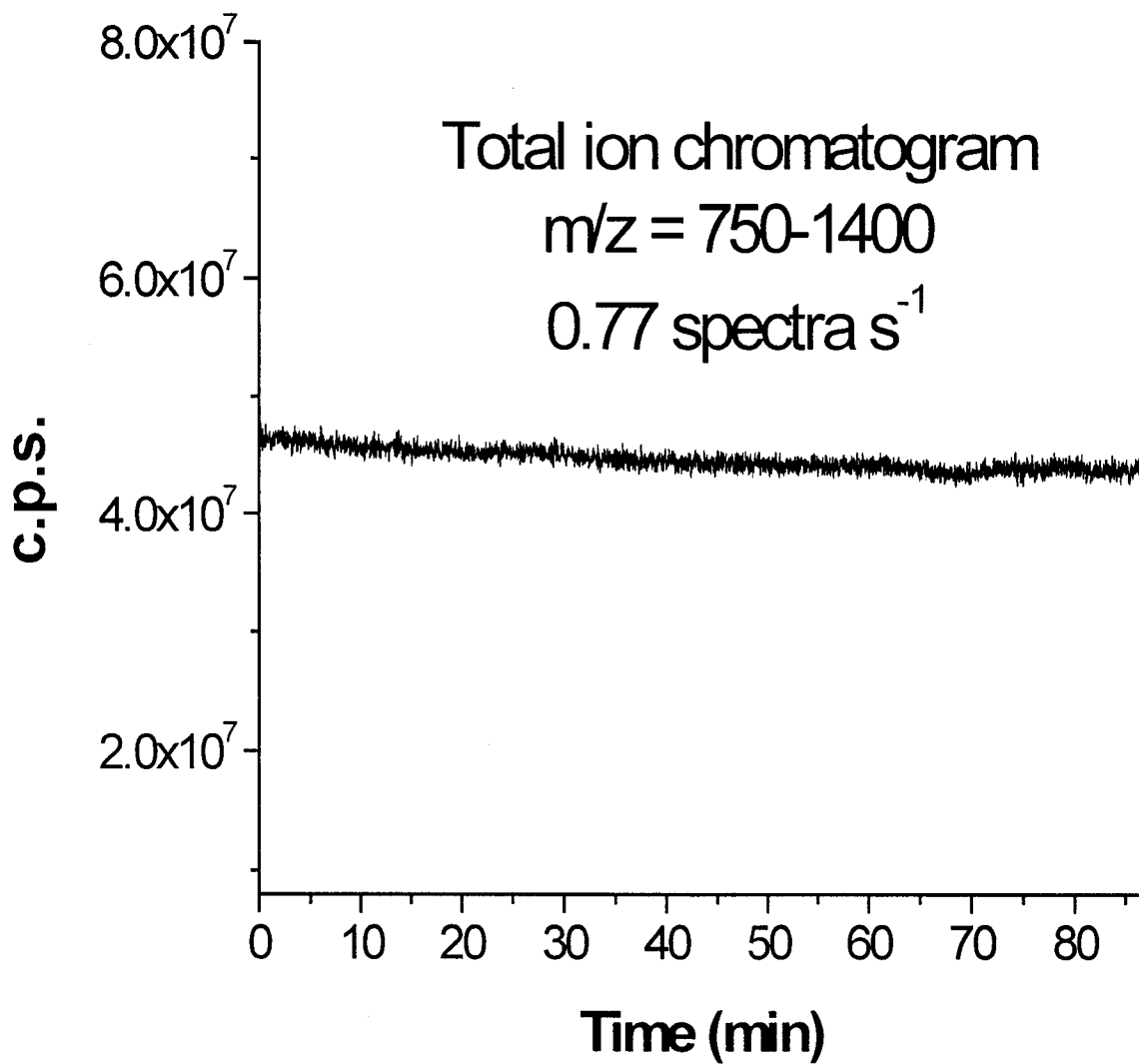


Figure 4.4 Long-term stability of the signal collected from the device for the PPG standard. The m/z range was 750 to 1400 at a step size of 0.5 amu. ESI voltage was 3900V.

practice. The lowest detected concentration of peptide was 26.8 nM for a 0.4 s data acquisition time. It is important to note that this value does not constitute the limit of detection for this microchip-ESI technique and that the spectrometer employed ultimately controlled the sensitivity.

The stability of the spray from the GC device for peptide samples was evaluated with 26.8 nM angiotensin II at higher spectral acquisition rates than in Figure 4.4. Figure 4.5D illustrates the TIC for a spectral acquisition rate of 2.5 spectra s^{-1} over $m/z = 504-544$. The RSD of 4.3% observed for the 2979 spectra collected in Figure 4.5D illustrates the stability of the system at higher acquisition rates, where fewer spectra are summed. This performance is comparable to other chip-MS studies reported for peptides [8, 21, 22].

Some chemical interference was observed that likely stems from the adhesive (Loctite: acrylate esters and modified acrylamide) used to bond the device. A sample of the uncured adhesive was analyzed by conventional ESI-MS and resulted in a series of peaks with a separation of 216 m/z units, indicative of sequential fragmentation of repeat units from both polymers ($m/z = 455.1 + n*216$). After curing the adhesive during device fabrication, no adhesive peaks were observed in the PPG standard sample, Figure 4.3. However, in buffer samples some adhesive derived peaks were visible, at intensities 10 times less than typical buffer impurity peaks (in the peptide samples of Figure 4.5, buffer impurity peaks would be 10 to 100 times less than the peptides). We note that if these peaks were to overlap sample peaks, reduced sample sensitivity

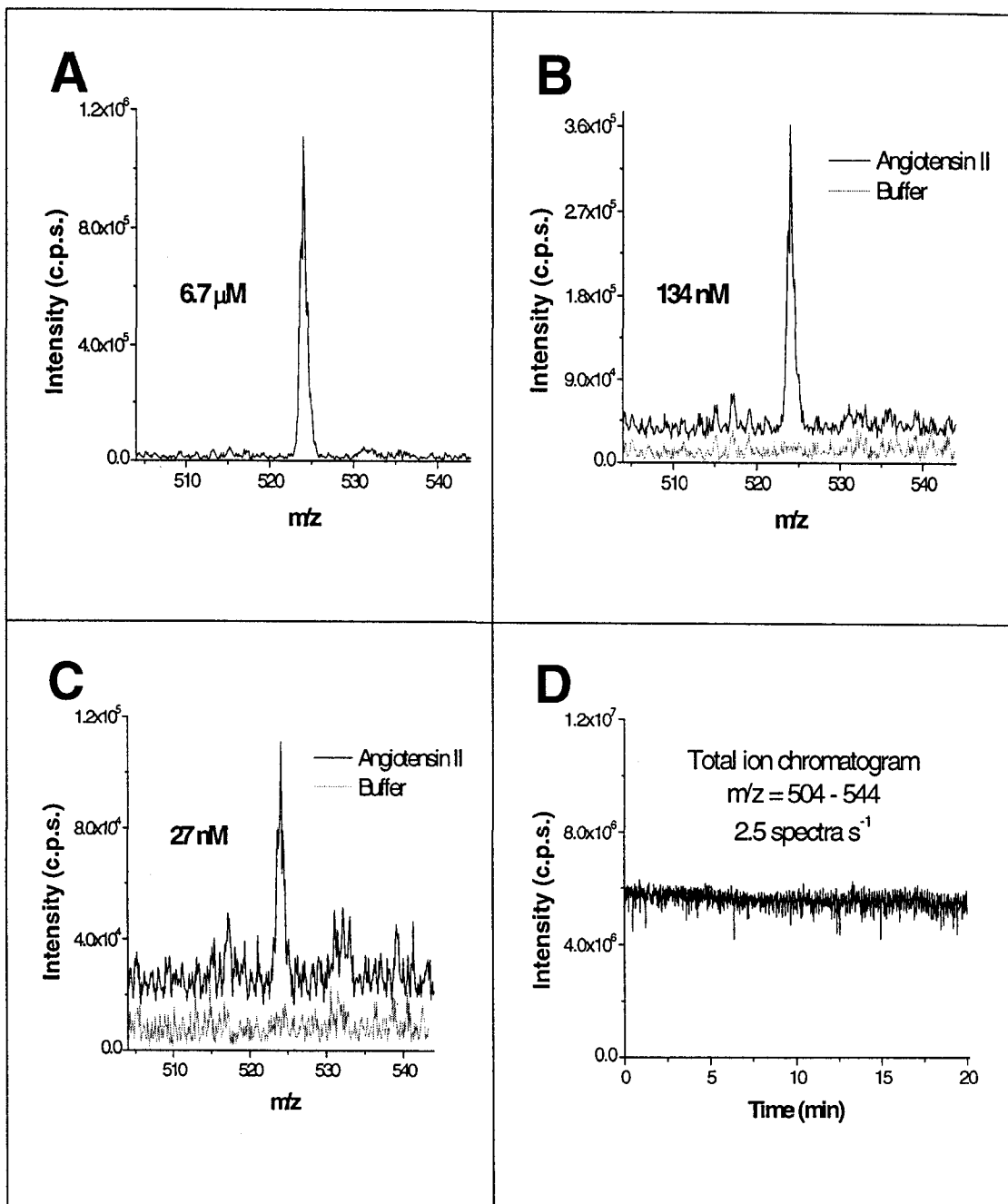


Figure 4.5 Mass spectra from infusion of angiotensin II at various concentrations. A single spectrum is shown in plots A-C. The peak at $m/z = 524$ corresponds to the doubly charged state of angiotensin. In all plots the m/z range was 504-544 at a step size of 0.1 amu and ESI voltage was 3200 V. (A) Infusion of 6.69 μM angiotensin II (B) The black trace represents infusion of 134 nM angiotensin II. The grey trace is the running buffer alone collected immediately before injection. (C) The black trace represents infusion of 26.8 nM angiotensin II. The grey trace is the running buffer alone collected immediately before injection. The black traces in both B and C have been offset in the y direction for ease of comparison to the buffer trace. (D) Total ion chromatogram for infusion of 26.8 nM angiotensin at a scan rate of 2.5 spectra s^{-1} .

would be expected. We are currently investigating new methods for sealing the GC devices.

The novel and advantageous feature for glassy carbon as a microchip-ESI-MS substrate is that the electrospray voltage can be directly applied to the chip without the need for external attachments. In the past, electrospray tips have been coated at the tip end with conductive materials such as metal layers [23, 24], conductive graphite particles [25, 26] or polymers [27], in order to facilitate application of the ESI voltage. However, deposition of these materials at the surface of the tip without clogging the tapered end has proven challenging.

Furthermore, vapor deposited coatings have low durability, thereby requiring regular tip replacement [12, 28]. The use of GC as a substrate for microchip-ESI-MS allows for direct application of the electrospray voltage to the sample solution without the need for conductive coatings, liquid junctions or sheath flows. Its overall simplicity and proven performance makes this microchip-ESI-MS interface noteworthy.

4.4 CONCLUSION

This chapter has shown the successful microfabrication of an electrospray mass spectrometry GC microdevice using a single layer photoresist process, photolithographic pattern transfer and anodic etching in 0.1 M NaOH. Electrospray from the GC channel performed well, with limits of detection for the peptide samples approaching the attomole range at flow rates typical for micro-ESI-MS (0.4 $\mu\text{L}/\text{min}$). The ease of fabrication, assembly and overall operation of this method ranks favorably in comparison to previously reported microchip configurations. The application of a direct ESI voltage to the chip without added apparatus opens new pathways for the implementation of glassy carbon as a microfabrication compatible material for the development of robust chemical analysis systems.

4.5 REFERENCES:

1. Limbach, P.A. and Z.J. Meng, *Integrating micromachined devices with modern mass spectrometry*. *Analyst*, 2002. **127**(6): p. 693-700.
2. de Mello, A.J., *Chip-MS: Coupling the large with the small*. *Lab on a Chip*, 2001. **1**(1): p. 7N-12N.
3. Oleschuk, R.D. and D.J. Harrison, *Analytical microdevices for mass spectrometry*. *Trac-Trends in Analytical Chemistry*, 2000. **19**(6): p. 379-388.
4. Wilm, M. and M. Mann, *Analytical properties of the nanoelectrospray ion source*. *Analytical Chemistry*, 1996. **68**(1): p. 1-8.
5. Xue, Q.F., et al., *Multichannel microchip electrospray mass spectrometry*. *Analytical Chemistry*, 1997. **69**(3): p. 426-430.
6. Ramsey, R.S. and J.M. Ramsey, *Generating electrospray from microchip devices using electroosmotic pumping*. *Analytical Chemistry*, 1997. **69**(6): p. 1174-1178.
7. Figeys, D., Y.B. Ning, and R. Aebersold, *A microfabricated device for rapid protein identification by microelectrospray ion trap mass spectrometry*. *Analytical Chemistry*, 1997. **69**(16): p. 3153-3160.
8. Lazar, I.M., et al., *Subattomole-sensitivity microchip nanoelectrospray source with time-of-flight mass spectrometry detection*. *Analytical Chemistry*, 1999. **71**(17): p. 3627-3631.

9. Li, J.J., et al., *Integration of microfabricated devices to capillary electrophoresis-electrospray mass spectrometry using a low dead volume connection: Application to rapid analyses of proteolytic digests*. *Analytical Chemistry*, 1999. **71**(15): p. 3036-3045.
10. Zhang, B., et al., *Microfabricated devices for capillary electrophoresis-electrospray mass spectrometry*. *Analytical Chemistry*, 1999. **71**(15): p. 3258-3264.
11. Li, J.J., et al., *Rapid and sensitive separation of trace level protein digests using microfabricated devices coupled to a quadrupole-TOF MS*. *Electrophoresis*, 2000. **21**: p. 198-210.
12. Shui, W.Q., et al., *Micro-electrospray with stainless steel emitters*. *Rapid Communications in Mass Spectrometry*, 2003. **17**(14): p. 1541-1547.
13. Kiema, G.K., G. Fitzpatrick, and M.T. McDermott, *Probing Morphological and Compositional Variations of Anodized Carbon Electrodes with Tapping-Mode SFM*. *Analytical Chemistry*, 1999. **71**: p. 4306-4312.
14. Kiema, G.K., M. Aktary, and M.T. McDermott, *Preparation of reproducible glassy carbon electrodes by removal of polishing impurities*. *Journal of Electroanalytical Chemistry*, 2003. **540**: p. 7-15.
15. Harnisch, J.A. and M.D. Porter, *Electrochemically modulated liquid chromatography: an electrochemical strategy for manipulating chromatographic*

retention. *Analyst*, 2001. **126**(11): p. 1841-1849.

16. Deinhammer, R.S., E.Y. Ting, and M.D. Porter, *Electrochemically Modulated Liquid-Chromatography (Emlc) - a New Approach to Gradient Elution Separations*. *Journal of Electroanalytical Chemistry*, 1993. **362**(1-2): p. 295-299.

17. Divakar, R., D. Butler, and I. Papautsky, *Room Temperature Low-Cost UV-Cured Adhesive Bonding for Microfluidic Biochips*, in *MicroTotal Analysis Systems*, J.M.R.a.A.v.d. Berg, Editor. 2001, Kluwer Academic Publishers. p. 385-386.

18. Bings, N.H., et al., *Microfluidic devices connected to fused-silica capillaries with minimal dead volume*. *Analytical Chemistry*, 1999. **71**(15): p. 3292-3296.

19. Hannis, J.C. and D.C. Muddiman, *Nanoelectrospray mass spectrometry using nonmetalized, tapered (50 → 10 μm) fused-silica capillaries*. *Rapid Communications in Mass Spectrometry*, 1998. **12**(8): p. 443-448.

20. Geromanos, S., et al., *Injection adaptable fine ionization source ('JaFIS') for continuous flow nano-electrospray*. *Rapid Communications in Mass Spectrometry*, 1998. **12**(9): p. 551-556.

21. Kim, J.S. and D.R. Knapp, *Miniaturized multichannel electrospray ionization emitters on poly(dimethylsiloxane) microfluidic devices*. *Electrophoresis*, 2001. **22**(18): p. 3993-3999.

22. Gobry, V., et al., *Microfabricated polymer injector for direct mass spectrometry coupling*. Proteomics, 2002. **2**(4): p. 405-412.
23. Barnidge, D.R.N., S.; Markides, K.E., *A design for low-flow sheathless electrospray emitters*. Analytical Chemistry, 1999. **71**(19): p. 4115-4118.
24. Nilsson, S. and K.E. Markides, *On-column conductive coating for thermolabile columns used in capillary zone electrophoresis sheathless electrospray ionisation mass spectrometry*. Rapid Communications in Mass Spectrometry, 2000. **14**(1): p. 6-11.
25. Svedberg, M., et al., *Sheathless electrospray from polymer microchips*. Analytical Chemistry, 2003. **75**(15): p. 3934-3940.
26. Nilsson, S., et al., *A simple and robust conductive graphite coating for sheathless electrospray emitters used in capillary electrophoresis/mass spectrometry*. Rapid Communications in Mass Spectrometry, 2001. **15**(21): p. 1997-2000.
27. White, T.P. and T.D. Wood, *Reproducibility in fabrication and analytical performance of polyaniline-coated nanoelectrospray emitters*. Analytical Chemistry, 2003. **75**(14): p. 3660-3665.
28. Valaskovic, G.A., et al., *Attomole-Sensitivity Electrospray source for Large-Molecule Mass Spectrometry*. Analytical Chemistry, 1995. **67**(20): p. 3802-3805.

CHAPTER 5

ELECTROCHEMICAL FABRICATION AND CHARACTERIZATION OF PYROLYZED PHOTORESIST CARBON MICRO- AND BAND ARRAY ELECTRODES

5.1 INTRODUCTION

Over the last decade, the analytical use of microvoltammetric and microband electrode arrays has increased in a variety of fields. This has been brought to the forefront by research into low volume electroanalytical sensors, which have become increasingly relevant as engineers and scientists explore the analytical benefits of miniaturization. Several fields of research have seen a significant increase in the use of fabricated microelectroanalytical sensors. These include environmental monitoring [1], biotechnology [2-5], drug discovery [6], and microchip systems [7-10].

Generally, electrodes of small dimensions ($10\mu\text{m}$ or less) are known to possess unique properties, which can make their use in many applications preferable to electrodes of conventional size. For example, in vivo measurements of neurotransmitters require electrodes of small size to minimize damage to neural tissue [11, 12]. Due to their small size, microelectrodes generate extremely small currents and thus, iR drop is minimized. This allows electroanalytical chemistry to be performed in highly resistive media and cyclic voltammetry to be extended to scan rates of greater than 10 kV/s without the need for instrumental corrections [13, 14]. The double layer capacitance on such electrodes is reduced due to the small area of the electrode surface. This results in an electrochemical cell with a small resistive-capacitive (RC) time constant, which has allowed potentiostatic experiments to be performed at

submicrosecond time scales [15].

Another unique property of microelectrodes is the sigmoidal current response obtained in cyclic voltammetry. The sigmoidal response is a result of enhanced mass transport due to spherical diffusion [16]. Faradaic processes at microelectrodes can be time-independent or only weakly time dependent due to steady-state diffusion at slow cyclic voltammetric scan rates. This characteristic, which leads to an increase in the sensitivity of electroanalytical measurements, is useful in sensor applications thereby offering a significant advantage for the use of microelectrodes over conventional macroelectrodes. However, the improved sensitivity and small magnitude of currents detected has resulted in instrumental difficulties in the measurement of dilute concentrations when using microelectrodes. Therefore, researchers have examined the use of arrays of microelectrodes for resultant larger currents in the electrochemical analysis of dilute samples.

Lithographically patterned arrays of microelectrodes have been fabricated using materials such as iridium, platinum, gold, and carbon on silicon [17]. Carbon materials are considerably useful in electroanalytical chemistry due to their favorable properties. Directly relevant to the current work in this chapter, carbon exhibits lower background currents over a wide potential window [18], a rich and modifiable surface chemistry, and tunable surface reactivity resulting from a number of developed pretreatment methods [19]. These properties make carbon materials good candidates for the fabrication of microelectrode and

microband arrays.

Research into the use of carbon as a microelectrode material in electroanalysis traces back to the early 1970s when Adams and coworkers recognized that neurotransmitters, molecules that relay information between neurons, are easily oxidized, and thus should be detectable with carbon electrodes [20]. The most common carbon material used in microelectrode fabrication has been carbon fibers. Carbon fibers range in diameter from 0.1 to 100 μm with a typical range of 5-25 μm . Electrodes are fabricated by embedding the length of the fiber in a non-conductive filler (e.g. epoxy) and using the ends of the fibers as the electrode surface. Carbon fiber microelectrodes have been used in applications such as general microelectrode studies [11], single cell analysis [21], and electrochemical detection after liquid chromatography separation [12].

Arrays of carbon fibers, each 5 μm in radius, have been shown to have sufficiently high sensitivity for trace analysis following liquid chromatography separation [22]. The fabrication process involves the placement of carbon fibers between two glass plates and applying an epoxy resin between the "sandwich" assembly to firmly secure the fibers onto the glass. The procedure could be repeated on a single glass substrate, with the curing of the epoxy after each step, until a multi-layered sandwich containing five layers of carbon fibers was constructed. The problem with the fabrication of such arrays was that spacing between adjacent carbon fibers was irregular and diffusional cross-talk between

neighboring electrodes was unavoidable.

A variety of other carbon-based materials have also been investigated as microelectrodes. An ensemble of randomly spaced microelectrodes formed from reticulated vitreous carbon and epoxy has been reported [23]. Arrays of microelectrodes have been fabricated using techniques such as the suspension of carbon fibers or particles within an insulator, and the impregnation of the pores of a host membrane with conducting carbon particles [24-25]. Also, pyrolytic carbon [12, 26], and sputtered thin-film carbon [27] arrays have received considerable attention.

Electrode arrays that are fabricated by techniques such as those given above are subject to great variability in their electrochemical characteristics. This is due to the fact that these arrays, with the exception of sputtered thin-film carbon, are difficult to reproducibly fabricate in a format with individually addressable electrodes [28]. It had proved difficult to fabricate an array of regularly spaced, individually addressable carbon microelectrodes until photolithographic techniques were used in the assembly of carbon microarray electrodes [29, 30]. Now, carbon microarray electrodes including microdisk [31], microbands [32, 33], and interdigitated array electrodes [34, 35] have been fabricated using these techniques. Another advantage gained from using conventional photolithographic microfabrication techniques is that fabrication of the microelectrode arrays is reproducible and mass production of micron to submicron-sized features are also possible.

This group has reported a method for etching glassy carbon and pyrolyzed photoresist films (PPF) for the fabrication of microchannel structures [36]. The work described in this chapter expands on the use of photolithographic pattern transfer and anodization of the underlying carbon substrate in basic media, to reliably and reproducibly fabricate high-density microelectrode and microband arrays from PPF. We employed scanning electron microscopy (SEM) as well as linear and cyclic sweep voltammetry to visualize and characterize the electrochemical behavior of the microarrays, respectively. Results obtained in this study show that the electrochemical etching procedure presented can be implemented in the fabrication of functional microelectroanalytical electrodes from pyrolyzed carbon films.

5.2 EXPERIMENTAL

5.2.1 Reagents and Materials

Sodium hydroxide (NaOH), potassium chloride (KCl) (EM Science, USA), dopamine (Sigma-Aldrich, Canada) and potassium ferricyanide ($K_3Fe(CN)_6$) (Caledon Ltd., Canada) were all used as received. Aqueous NaOH and $K_3Fe(CN)_6$ solutions were prepared in distilled/deionized (18 M Ω /cm) water (Nanopure, Barnstead, Dubuque, IA) and purged with nitrogen gas for 10 min prior to use to remove the oxygen in solution. Highly doped silicon (100mm, n-type, <1-0-0> oriented, 0.002-0.004 Ω -cm) and low-pressure chemical vapor deposited (LPCVD) silicon nitride wafers were obtained from Addison Engineering, Inc. (San Jose, CA) and diced into various sizes. The positive

photoresist, Microposit SJR 5740, was obtained from OCG Chemicals (Providence, RI).

5.2.2 Mask Preparation

Masks used in the photolithography for the microelectrode arrays were created as described in Chapter 2.

5.2.3 Preparation of the Carbon Films

Pyrolyzed photoresist films (PPF) were prepared on silicon and silicon nitride substrates as described previously [37, 38]. The procedure entails dicing a silicon wafer into 1.2×1.2 cm pieces. The surface oxide layer was stripped from the silicon and silicon nitride substrates by immersing it into a 10:1 buffered oxide etch solution (10 parts 40% NH_4F and 1 part 49% HF). One coating of the positive photoresist (Microposit SJR 5740) was spin-coated onto each substrate at 4000 rpm. The samples were soft baked at 115°C in argon to remove excess solvent, pyrolyzed in a tube furnace at 1000°C for 1.5 hours under flowing forming gas (95% N_2 :5% H_2) and cooled under the same gas to room temperature (23°C).

5.2.4 Electrode Fabrication

The typical process for electrode fabrication is given in Figure 5.1. The fabrication process began by twice spin-coating a layer of photoresist onto the surface of the films. This was followed by illumination of the photoresist through a lithographic mask with UV light (~ 405 nm) and then the photoresist was

developed with Shipley 354 developer. Electrochemical anodization of the exposed surface was accomplished in a three-electrode cell with a Ag/AgCl (3 M KCl) reference electrode and a Pt foil counter electrode. A positive potential (≥ 2.0 V) was applied to the PPF surface for a controlled period of time in 0.1 M NaOH solution (pH ~ 13) at 23°C while stirring the solution. For both the microelectrode and microband arrays, the entire substrate was immersed in the electrolyte solution and the cell connected to a Model AFCBP1 (Pinechem Instrument Co., PA) bipotentiostat. Anodized substrates were then sonicated in acetone for 30 seconds to remove the remaining photoresist and rinsed for 5 min in dd water before use.

5.2.5 Carbon Film Derivatization

4-Nitrobenzene (NB) 4'-diazonium tetrafluoroborate salts were prepared as previously described [39]. Electrochemical derivatization was performed using an aqueous 0.1M H₂SO₄ solution containing 2.5 mM diazonium salt. The solution was purged with argon for 20 min before derivatization. Deposition conditions were chosen such that samples of a single NB thickness were prepared. The applied potential was scanned at 100 mV/s for one cycle from +600 to -100 mV versus Ag/AgCl. These conditions produced a NB layer covalently bonded to the PPF.

5.2.5 SEM Characterization

Scanning electron microscopy (SEM) images of the etched PPF films were using the same instrument as described in Chapter 2.

5.2.6 Electrochemical Experiments

Cyclic voltammetry (CV) was performed using a Model AFCBP1 (Pinechem Instrument Co., PA) bipotentiostat. The reference was a homemade aqueous Ag/AgCl (3M NaCl) electrode. Platinum wire was used as an auxiliary electrode in CV experiments. Voltammograms were collected using, 5mM, 500 μ M potassium ferricyanide in 1M potassium chloride (KCl) and a 1mM dopamine in 0.1M sulfuric acid. CV measurements were in ~10mL of each solution with scan rates varied from 0.010V/s to 5V/s for each run. The triangular wave was performed between +0.30V and -0.60V vs Ag/AgCl for ferricyanide and +0.10V and +0.90V vs Ag/AgCl when dopamine was used.

5.3 RESULTS AND DISCUSSION

We believed that the combination of our electrochemical etching of carbon and photolithography would provide a flexible procedure for producing arrays of microelectrodes of various sizes and shapes. Our idea involves the etching of thin carbon films (PPF). Following, the transfer of a mask pattern to a layer of photoresist deposited on a PPF, the carbon was etched completely through to the underlying silicon or silicon nitride substrate as shown in Figure 5.1. This procedure results in an array of carbon islands on the silicon substrate. The carbon islands are separated from each other by a ~100nm thick native oxide layer.

The results of this procedure are shown in Figure 5.2. Figure 5.2A shows an SEM image showing that carbon islands can be fabricated over wide areas

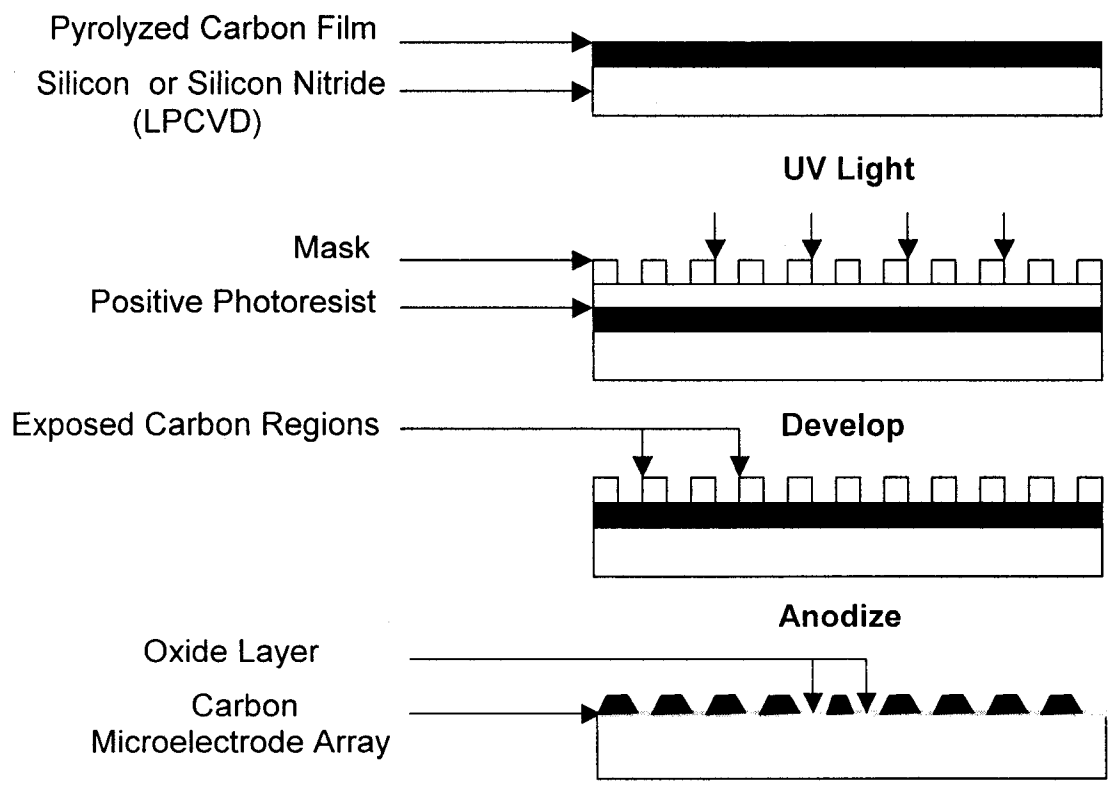


Figure 5.1 Schematic showing the lithographic and electrochemical procedure used to fabricate the microband and microelectrode arrays.

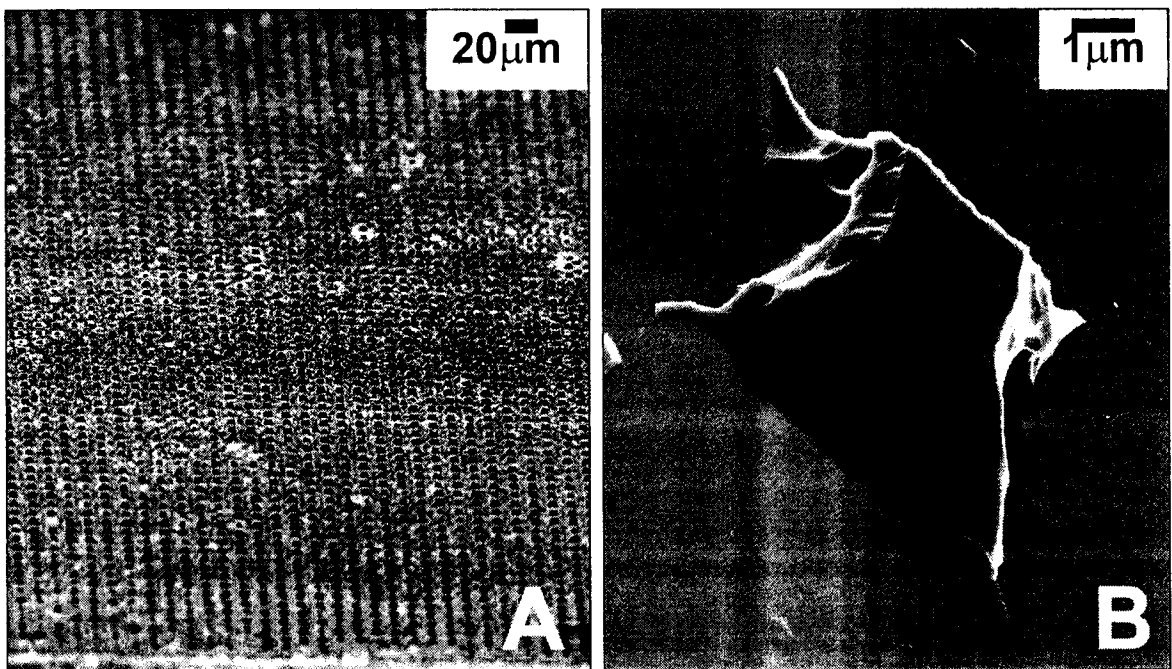


Figure 5.2 Scanning electron micrographs of electrochemically etched carbon microelectrode arrays. A) SEM image of ~1600 carbon microelectrode arrays. B) SEM image of a single cube shaped carbon microelectrode.

using this method. Figure 5.2B is a higher magnification image of a single carbon island that has a width of $\sim 4\mu\text{m}$. Note that the island is isolated from other neighboring islands. Since the substrate is highly doped and conductive silicon, electrical contact to the carbon islands can be made through the substrate. Due to the formation of a native oxide layer on the surface of the silicon, the regions between the carbon microelectrodes will be inactive.

As shown in the previous chapters, varying the etching time can control the extent of carbon etching. Thus, a significant benefit of this procedure is that the size of the carbon islands can be controlled. This is shown in Figure 5.3. The arrays in Figure 5.3 were created with the same lithographic mask. The array in Figure 5.3A was fabricated by etching the PPF for 30 min resulting in islands with an average diameter of $3.5\mu\text{m}$. The array depicted in Figure 5.3B was etched for 60 min and consists of particles as small as 600nm in diameter, as seen in the inset. Therefore, in addition to controlling the shape of the array electrodes using a specific design on the lithographic mask, the size of the features in an array can be varied by a choice of an appropriate etch time.

The electrochemical behaviour of microelectrode arrays is governed by three mass transport regimes [40]. The regimes are defined by the diffusion layer thickness, X_D , which is equal to $(\pi Dt)^{1/2}$. D is the diffusion coefficient and t is the time scale of the experiment. The value that is calculated for X_D thickness is then compared to the dimensions of the array to determine the expected microarray behaviour. The dimensions of the arrays are defined by the radius of each

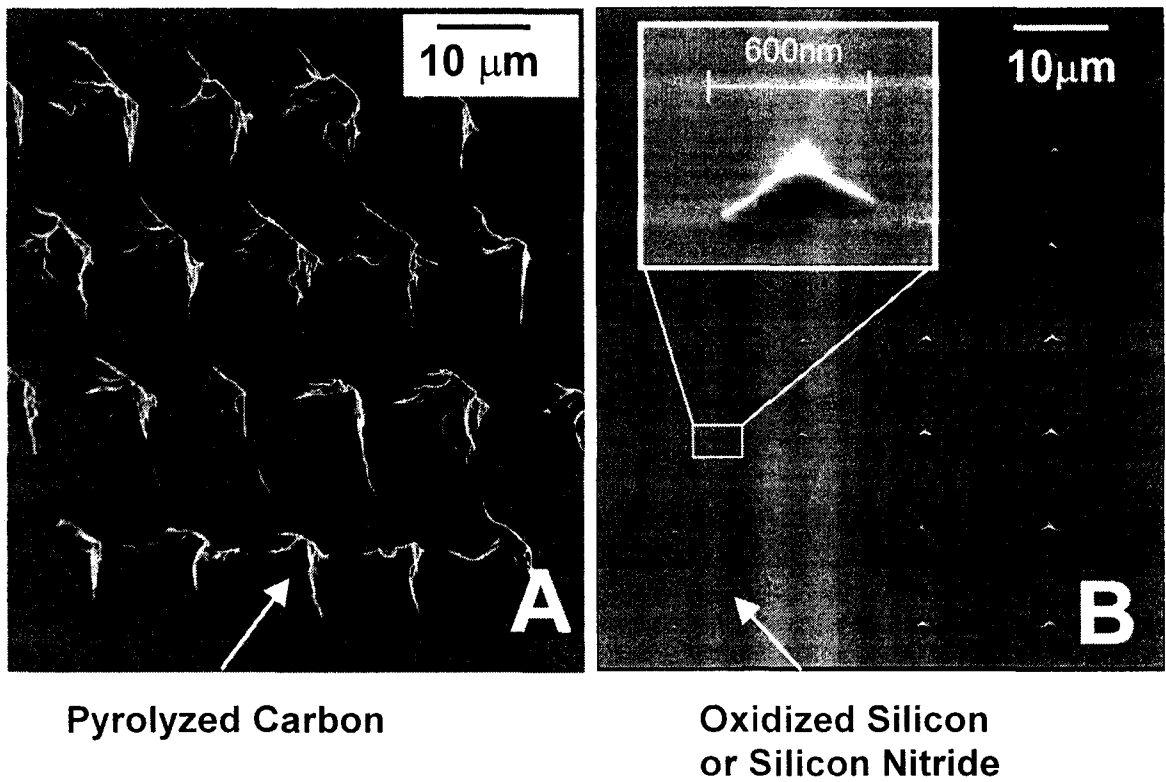


Figure 5.3 Two sets of microelectrode arrays etched for two different periods of time in identical solutions. The SEM image in (A) is an illustration of an array etched for 30min while the one in (B) represents an array etched for 60 min.

electrode element, r_0 and the center-to-center distance between the electrodes, d as depicted in Figure 5.4. Figure 5.4A illustrates an instance when $X_D \gg d$ and r_0 . The spherical diffusion layers around each electrode overlap and the array behaves like a planar electrode. Cyclic voltammetry performed within this diffusion regime shows peak-shaped voltammograms. When $r_0 < X_D < d$, mass transport is dominated by spherical diffusion to each electrode and the array behaves as a collection of individual microelectrodes. The voltammograms become sigmoidal in shape as depicted in Figure 5.4B. The third regime occurs when, $X_D \ll r_0, d$ and planar diffusion at each microelectrode observed. In linear or cyclic voltammetry, the experiment timescale, t and thus X_D is easily controlled by the scan rate where $t = RT/Fv$.

Cyclic voltammetry was used to examine the electrochemical behavior of arrays like those shown in Figure 5.2. Figure 5.5 illustrates CV's of $\text{Fe}(\text{CN})_6^{3-}$. Curve a, is a voltammogram on a Si substrate. As noted above, although the Si used here is highly doped, the native oxide layer passivates the surface towards electrochemical reactions as is shown. Curves b and c were collected on an array of $r_0 = 2 \mu\text{m}$ and $d = 20 \mu\text{m}$. At lower scan rates, curve b, a voltammetric wave is observed with current peaks corresponding to the reduction and re-oxidation of the redox couple. The peak-shaped voltammogram is characteristic of mass transport dominated by planar diffusion. At high scan rates, curve c, the voltammogram exhibits a more sigmoidal shape reflecting significant contribution by spherical diffusion at the surface of the microelectrode array.

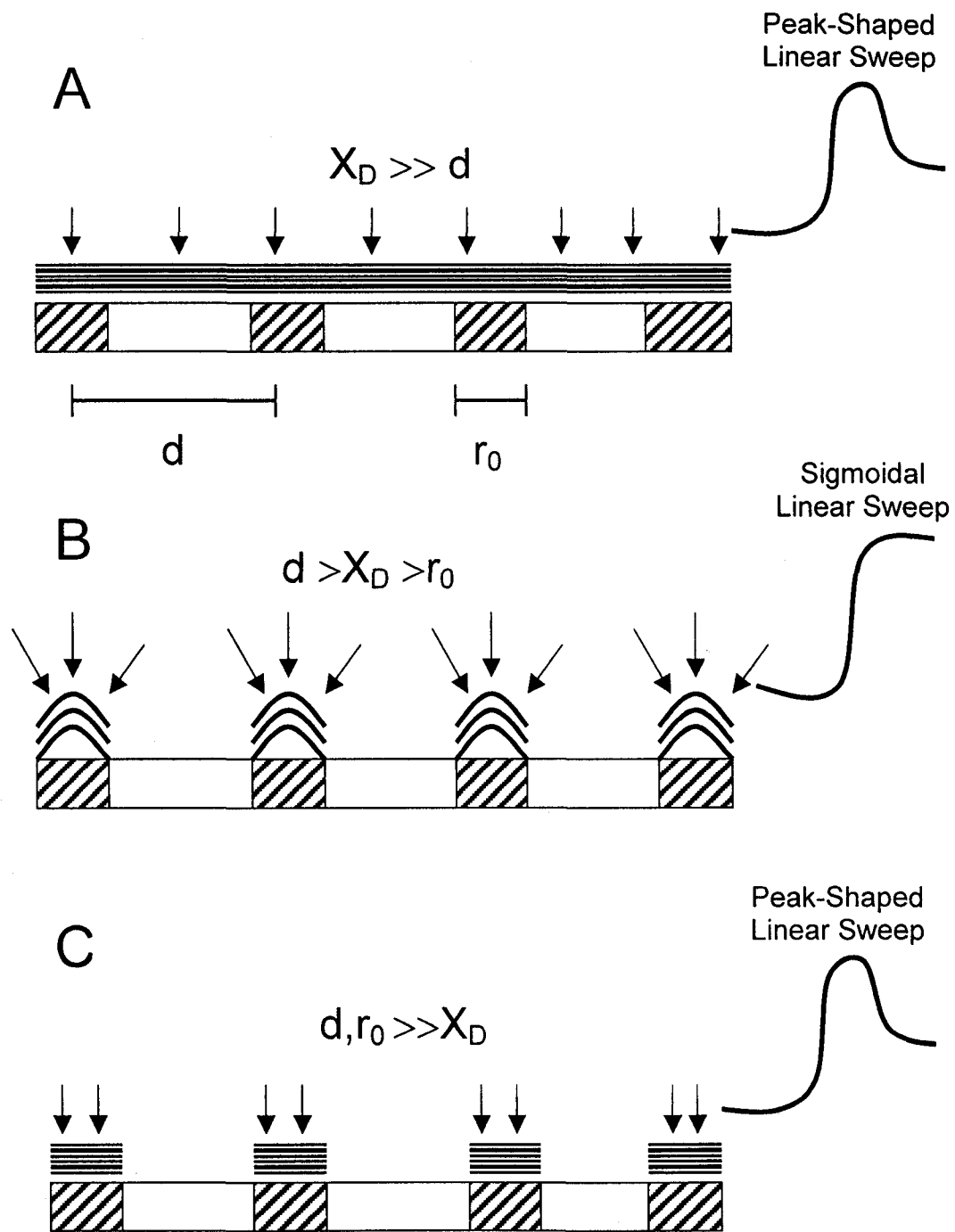


Figure 5.4 Schematic illustrating the three diffusion regimes associated with microelectrode arrays. (a) overlapping radial diffusion to microelectrodes (b) radial diffusion to microelectrodes and (c) linear-active diffusion to microelectrodes

Cyclic Voltammetry of 5mM $\text{Fe}(\text{CN})_6^{3-}$ (1M KCl)

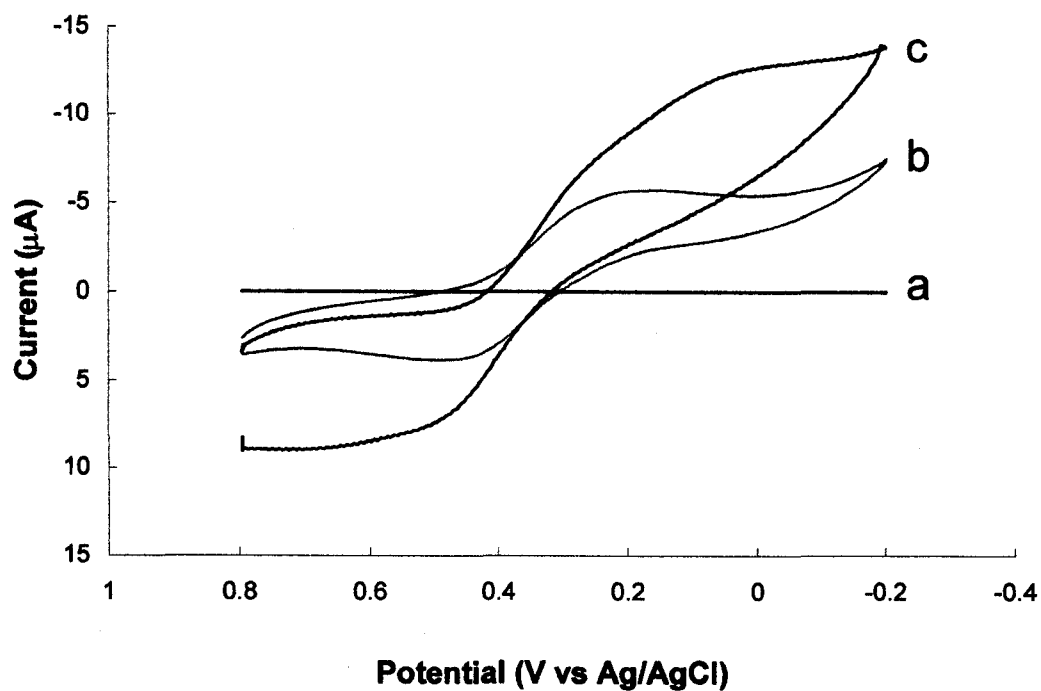


Figure 5.5 Typical cyclic voltammograms acquired with a carbon microelectrode array using potassium ferricyanide and 1M KCl. (a) CV of silicon substrate at 100mV/s (b) CV collected at 20mV/s and (c) CV collected at 200mV/s.

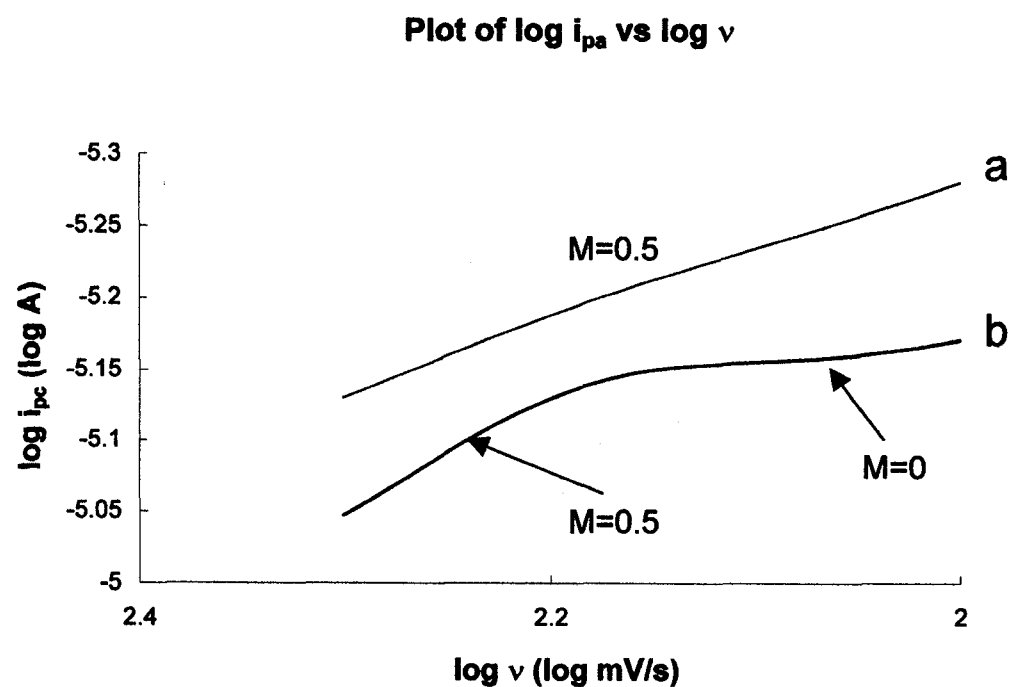


Figure 5.6 Log (cathodic peak current) vs. Log (scan rate) for cyclic voltammograms of 5mM ferricyanide in potassium chloride. Curve a represents the theoretically expected relation where $m=0.5$ while curve b, represents the observed relationship when data was collected using the carbon microelectrode arrays.

The results achieved in this study correlate well with the expected diffusion regimes. The calculated X_D value for curve b, which was collected at a scan rate of 20mV/s is 55 μ m. The array employed has dimensions of $r_0 = 2\mu$ m and $d = 20\mu$ m. Thus, $X_D \gg r_0$ and d and planar diffusion is expected to dominate. The peak shaped voltammogram observed agrees with this expectation. Curve c was collected at a scan rate of 200mV/s and X_D was calculated to be 18 μ m. Therefore, for an identical array, spherical diffusion is expected to dominate. Curve c agrees fairly well with this expectation.

To probe the electrochemical response more thoroughly, the logarithm of the maximum cathodic peak current (i_{pc}) was plotted against the logarithm of the scan rate (ν) as depicted in Figure 5.6. For a voltammogram under planar diffusion control, $i_{pc} \propto \nu^{1/2}$ and a plot of $\log i_{pc}$ vs $\log \nu$ would be expected to be linear with a slope of 0.5. Spherical diffusion is a much more efficient mode of mass transport and the current observed is independent of ν . Shown in Figure 5.6 are two plots. Plot a, is the theoretical linear curve with a slope of 0.5 provided as a visual reference. This curve was not constructed using any detailed voltammetric data. Plot b is a least squares fit to the data derived from CV's of $\text{Fe}(\text{CN})_6^{3-}$ like those shown in Figure 5.5. The curve has two distinct sections. The first section of the represents a time domain where planar diffusion while the second section is representative of a time domain where spherical diffusion is dominant. For the microelectrode arrays used in this study, this result agrees well with the expected slope of the $\log i_{pc}$ vs $\log \nu$ curve. This is because

as the shift from low to high scan rates was made, a transition from planar diffusion where $m=0.5$ to spherical diffusion where $m=0$ was expected. This is what was observed.

Also evident in the shapes of the CV's shown in Figure 5.5 was the deviation from the theoretically expected curve shapes as the transition was made from low to high scan rates. We attribute this observation to the edge effects associated with the third dimension (i.e., height) of the microelectrode arrays and/or the separation between adjacent microelectrodes within the array. Since the explanation of the microelectrode array behavior given in Figure 5.4 does not consider the effect of electrode height [the theory is based on inlaid disks] and the separation between the microelectrodes might not have been at its optimal distance, theoretically expected curves were not observed.

Contact resistance between the silicon substrate and the patterned carbon film was found to be high when scan rates higher than 100mV/s were used in this electrochemical study. This was clear in the "stretching" observed in CV's collected at higher scan rates as seen in Figure 5.5C. In an attempt to circumvent this obstacle, we adopted fabricated microband array electrodes that were connected to a carbon pad on silicon nitride. This would ensure that the voltage applied would be delivered directly onto the carbon instead of traversing the silicon-carbon interface, as was the case with the microelectrode array.

The microband array electrodes used for this study were fabricated with the combination photolithography and electrochemical-etching method that

previously presented in Figure 5.1. For all the arrays, only LPCVD silicon nitride was used as substrate for the PPF. The results of this procedure are shown in Figure 5.7. All the arrays presented in this figure were etched at 2.5V for 50 min.

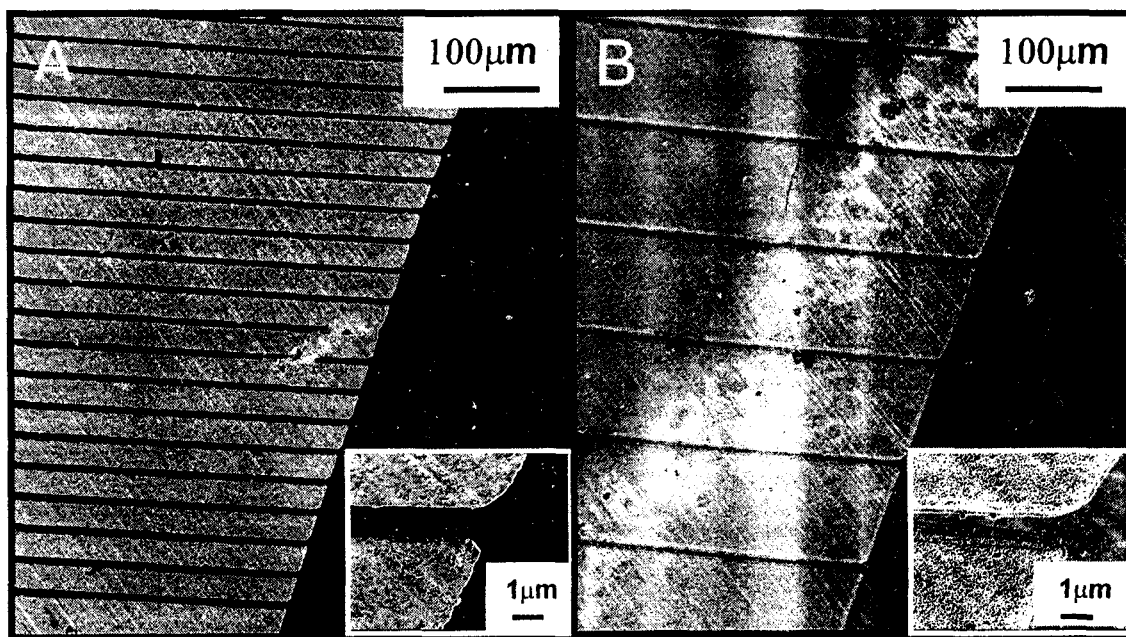
Figure 5.7A shows an SEM image showing that carbon bands can also be fabricated over wide areas. The inset to Figure 5.7A is a higher magnification image of a single carbon band that measures $\sim 8\mu\text{m}$ wide. The height of the band was measured to be $\sim 1.5\mu\text{m}$. Note that the band is attached to a PPF pad where electrical contact was made. Just as was the case of the microelectrode arrays, a native oxide layer passivated the surface of the silicon nitride regions between the carbon microband electrodes. This region is electrically inactive.

As discussed in the section detailing the microelectrode arrays, the interband distance and size of the microband electrodes can be controlled with etch time or by the design on the photolithographic mask. This section presents results achieved by use of a mask with different feature sizes. This is shown in Figure 5.7B. The microband arrays in Figure 5.7B were created with a lithographic mask that is different than that used for the array in Figure 5.7A. The dimensions of the microbands were measured to be $\sim 18\mu\text{m}$ wide, $\sim 1.5\mu\text{m}$ high, and have an interband distance of $\sim 200\mu\text{m}$.

Cyclic voltammetry was also used to examine the electrochemical behavior of band arrays like those shown in Figure 5.7. Figure 5.8 contains CV's of $500\mu\text{M Fe(CN)}_6^{3-}$ using the array shown in Figure 5.7A. Curves a and b were

CV's collected on the PPF microband arrays at 100mV/s and 500mV/s respectively. At lower scan rates, curve a, a voltammetric wave is observed with current peaks corresponding to the reduction and re-oxidation of the redox couple. The peak-shaped voltammogram is characteristic of mass transport dominated by planar diffusion as was the case with microelectrode arrays. At high scan rates, curve b, the voltammogram exhibits a more sigmoidal shape. For microband arrays depicted in 5.7B, the results are presented in Figure 5.9. At 100mV/s, a peak-shaped voltammogram is observed. This indicates planar diffusion due to overlapping spherical diffusion. As the scan rate is increased, a transition in the shape of the voltammograms, from peak-shaped to quasi-sigmoid is observed. Quasi-sigmoid diffusion is observed at scan rates higher than 1000mV/s indicating a predominant hemicylindrical diffusion regime.

Generally speaking, microband electrode arrays resulted in higher currents than those of microelectrode arrays when solutions of the same concentration were used and their CV's exhibited a quasi-sigmoid shape when spherical diffusion was predominant. This was to be expected as the surface area of the electrode increases when microband arrays were in use. Also for microbands, there is no spherical diffusion as would be expected for microelectrode array. Instead, there exists a hemicylindrical diffusion regime, which leads to quasi-sigmoidal curve shape. Hemicylindrical diffusion can be visualized as half a cylinder type of projection for the diffusing species [41]. Planar diffusion for microbands would be similar to that of microelectrode arrays.



Microband Width = 10 μm
Interband Distance = 50 μm

Microband Width = 20 μm
Interband Distance = 200 μm

Figure 5.7 SEM image of electrochemically etched carbon microband arrays. A) Array with width $\sim 8 \mu\text{m}$ and an interband distance of $\sim 52 \mu\text{m}$. The inset represents the junction between the bulk PPF pad and a single microband electrode. B) Array with band width of $\sim 12 \mu\text{m}$ and an interband distance of $\sim 200 \mu\text{m}$. The inset represents the junction between the bulk PPF pad and a single microband electrode.

Cyclic Voltammetry of 500 μ M Fe(CN) $_6^{3-}$ (1MKCl)

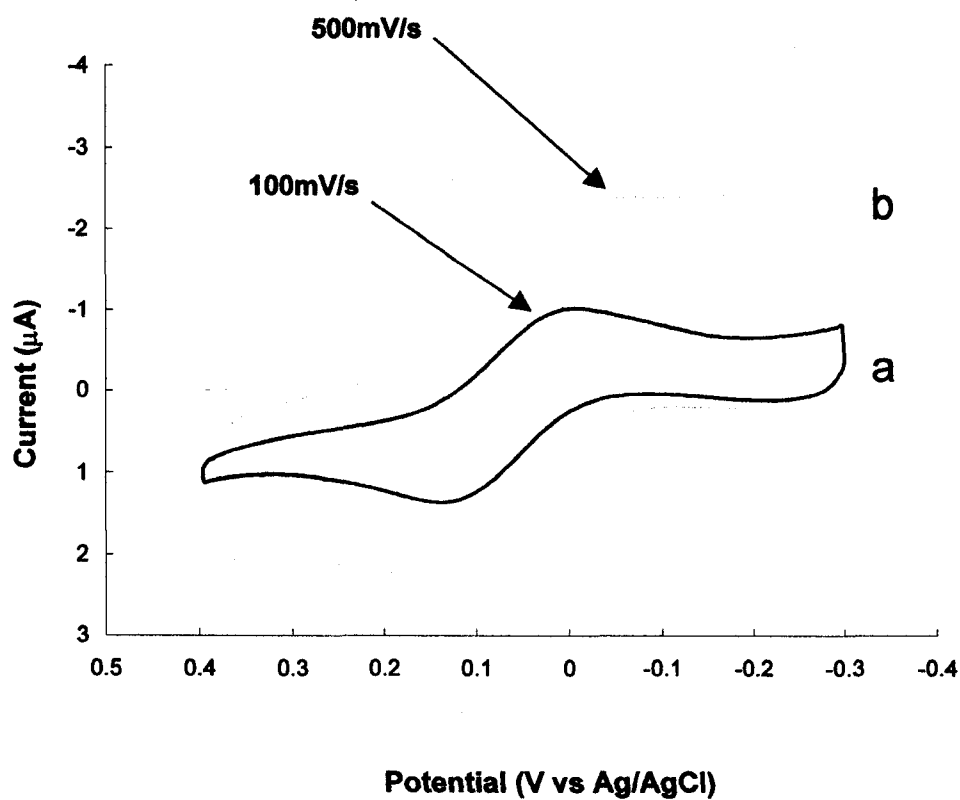


Figure 5.8 Cyclic voltammograms acquired with carbon microband array electrodes as shown in Figure 5.7A using 500 μM potassium ferricyanide and 1M KCl.

Cyclic Voltammetry of $500\mu\text{M Fe(CN)}_6^{3-}$ (1M KCl)

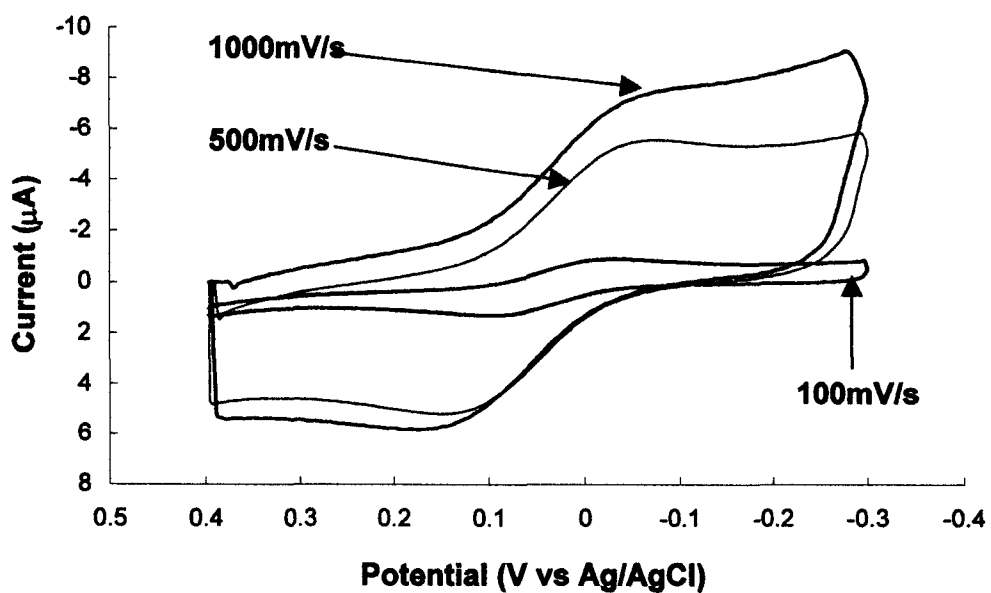


Figure 5.9 Cyclic voltammograms acquired with carbon microband array electrodes as shown in Figure 5.7B using $500\mu\text{M}$ potassium ferricyanide and 1M KCl .

Electrochemically assisted covalent modification of carbon surfaces is a relatively recent development in modified electrode research. Pinson et al. were the first to report on the electrochemical generation of an *in situ* radical, which appeared to couple to the carbon surface, forming a covalent bond between a surface carbon and the modifier [42]. Specific to this work, they demonstrated that the reduction of aryl diazonium salts at carbon surfaces resulted in a strongly attached surface layer of aromatic functionalities and suggested that a covalent bond had formed between an aryl radical and the graphitic moiety on the carbon surface [43]. Previously, our group has shown the nucleation and growth of functionalized aryl films on ordered graphite [44], the formation of multi-layered aryl films on glassy carbon electrodes, [45] and more recently, McCreery and coworkers have applied this diazonium salts methodology for the attachment of functionalized and conjugated carbon films on PPF.

For the application presented in this section, we attached a monolayer of an aryl diazonium to the fabricated carbon microband array electrodes and tested the modification of the carbon electrode using the benchmark dopamine system. Figure 5.10 illustrates the reduction of 4-nitrobenzene (NB) diazonium tetrafluoroborate in 0.1M H₂SO₄, on the microband array electrodes, which were shown in Figure 5.7A, at a scan rate of 100mV/s. The voltammogram labeled (a) shows a wave, corresponding to the reduction of nitrobenzene on the carbon surface, followed by a smaller wave (b) on the second scan.

To test for defects and pinholes within the deposited monolayer, cationic

dopamine was cycled on the modified electrode. The triangular wave, applied over a potential window of +0.9 to -0.1V showed no dopamine signal. This signified the blocking of the PPF surface with nitrobenzene (NB). Dopamine voltammetry was employed due to the fact that electron transfer between dopamine and the carbon electrode can only occur if the electrode is bare. Since no redox waves were observed on the voltammogram in Figure 5.11A, we concluded that NB strongly blocked the electron transfer reaction of dopamine. From this observation, it can be concluded that no defects or pinholes were present within the NB monolayer that was deposited on the carbon microband electrodes. For comparison purposes, Figure 5.11B shows a dopamine CV with the characteristic redox waves acquired on an unmodified (bare) microband array electrodes.

5.4 CONCLUSIONS

This chapter has demonstrated a reliable and reproducible process for the fabrication of novel carbon film microband and microelectrode arrays for electroanalysis using lithographic pattern transfer and anodic etching in 0.1 M NaOH. The electrochemical characteristics of such carbon microarray electrodes have been presented. The work also demonstrates the first successful fabrication of functional, electrochemically etched carbon array electrodes and extends on work that has previously been done on thin-film carbon microelectrode fabrication and shows that these microarray electrodes can be used for the detection of various benchmark electro-active species.

Deposition Waves of 4-Nitrobenzene on 20-200 μm Microband Electrodes

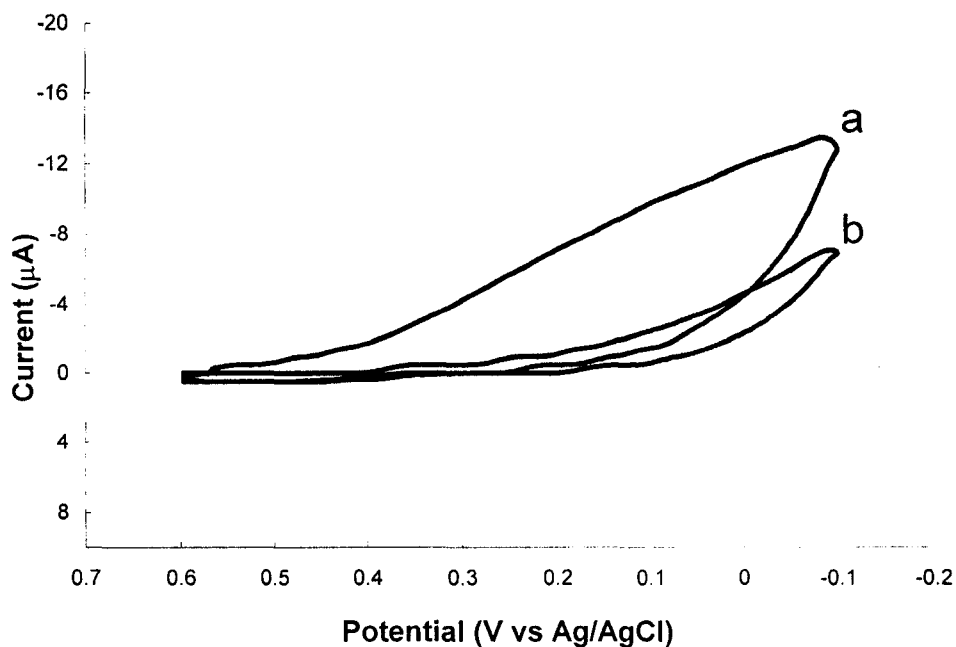


Figure 5.10 Cyclic voltammograms for the reduction of 4-nitrobenzene (NB) diazonium tetrafluoroborate in 0.1M H_2SO_4 (a) A wave corresponding to the reduction of nitrobenzene on the carbon surface and (b) A smaller wave on a second scan after the initial deposition wave was acquired. All CV's were acquired at a scan-rate of 100mV/s.

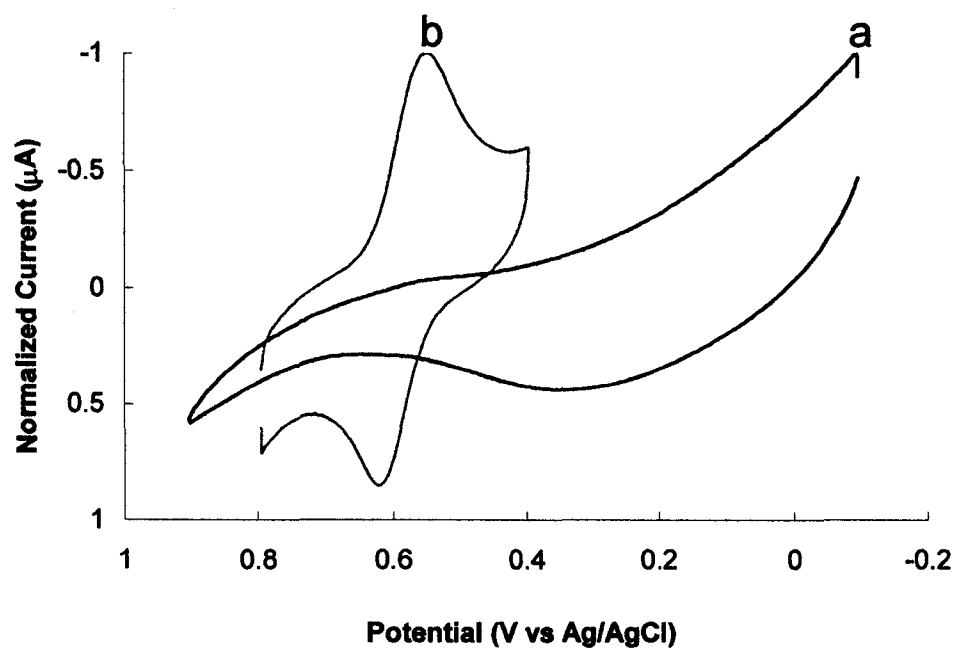


Figure 5.11 Cyclic voltammograms showing the blocking of the surface by NB of the carbon microband arrays as diagnosed with dopamine voltammetry (A) and the typical dopamine voltammogram acquired with unblocked (bare) carbon microband array electrodes. The microband array used was as shown in Figure 5.7B. All CV's were acquired at a scan-rate of 100mV/s.

5.5 REFERENCES

1. Fleet, B. and H. Gunasingham, *Electrochemical Sensors for Monitoring Environmental-Pollutants*. *Talanta*, 1992. **39**(11): p. 1449-1457.
2. Cahill, P.S., Q.D. Walker, and R.M. Wightman, *Microelectrodes for the measurement of catecholamines in biological systems*. *Analytical Chemistry*, 1996. **68**(18): p. 3180-3186.
3. Davis, C.B. and W.G. Kuhr, *Multiplexed immobilization of biomolecules onto a gold band electrode array*. *Abstracts of Papers of the American Chemical Society*, 2001. 221: p. U84-U84.
4. Davis, B.C., et al., Independently-addressable micron-sized biosensor elements. *Biosensors and Bioelectronics*, 2003. 18: p. 1299-1307.
5. Pihel, K., Q.D. Walker, and R.M. Wightman, Overoxidized polypyrrole-coated carbon fiber microelectrodes for dopamine measurements with fast-scan cyclic voltammetry. *Analytical Chemistry*, 1996. **68**(13): p. 2084.
6. Keusgen, M., *Biosensors: new approaches in drug discovery*. *Naturwissenschaften*, 2002. **89**(10): p. 433-444.
7. Chen, R.S., et al., *Carbon fiber nanoelectrodes modified by single-walled carbon nanotubes*. *Analytical Chemistry*, 2003. **75**(22): p. 6341-6345.
8. de Silva, J.A.F., *Electrochemical detection in capillary electrophoresis*. *Quimica Nova*, 2003. **26**(1): p. 56-64.

9. Tanyanyiwa, J., S. Leuthardt, and P.C. Hauser, *Conductimetric and potentiometric detection in conventional and microchip capillary electrophoresis*. *Electrophoresis*, 2002. **23**(21): p. 3659-3666.
10. Hebert, N.E., et al., *Performance of pyrolyzed photoresist carbon films in a microchip capillary electrophoresis device with sinusoidal voltammetric detection*. *Analytical Chemistry*, 2003. **75**(16): p. 4265-4271.
11. Wightman, R. M., *Microvoltammetric Electrodes*. *Analytical Chemistry*, 1981. **53** (9): p 1125A-1134A.
12. Ewing, A. G., Dayton, M. A., Wightman, R. M., *Pulse Voltammetry with Microvoltammetric Electrodes*. *Analytical Chemistry*, 1981, **53** (12): 1842-1847.
13. Howell, J. O and Wightman, R. M., *Ultrafast Voltammetry and Voltammetry in Highly Resistive Solutions with Microvoltammetric Electrodes*. *Analytical Chemistry*, 1984, **56** (3) 524-529.
14. Lines, R. and Parker, V. D., *Voltammetry in Benzene and Chlorobenzene Behaviour of Ions of Aromatic Compounds in Nonpolar Media*. *Acta Chemica Scandinavica Series B-Organic Chemistry and Biochemistry*, 1977. **31** (5): 369-374
15. Robinson, R. S., McCreery, R. L., *Submicrosecond Spectroelectrochemistry Applied to Chlorpromazine Cation Radical*

- Charge Transfer Reactions*. Journal of Electroanalytical Chemistry, 1985. **182** (1) 61-72.
16. Dayton, M. A., Brown, J. C., Stutts, K. J., Wightman, R. M., *Faradaic Electrochemistry at Micro-Voltametric Electrodes*, 1980. Analytical Chemistry, **52** (6): 946-950 1980.
 17. Feeney, R. and S.P. Kounaves, *Microfabricated Ultramicroelectrode Arrays: Developments, Advances, and Applications in Environmental Analysis*. Electroanalysis, 2000. **12**(9): p. 677-684.
 18. Niwa, O. and H. Tabei, *Voltammetric Measurements of Reversible and Quasi-Reversible Redox species using Carbon-Film Based Interdigitated Array Microelectrodes*. Analytical Chemistry, 1994. **66**(2): p. 285-289.
 19. McCreery, R. L., *Carbon Electrodes: Structural Effects on Electron Transfer Kinetics*, in *Electroanalytical Chemistry*, A. J. Bard, Editor. 1991, Marcel Dekker Inc. New York. p.221-374.
 20. Adams, R.N., *Probing Brain Chemistry with Electroanalytical Techniques*. Analytical Chemistry, 1976. **48**(14): p. 1126A-1138A.
 21. Travis, E., Wightman, R. M., *Spatio-Temporal Resolution of Exocytosis from Individual Cells*, in *Annu. Rev. Biophys. Biomol. Struct.* 1998, **27**, 77-103.
 22. Caudill, W. L., Howell, J. O., Wightmann, R. M. *Flow-Rate Independent*

- Amperometric Cell*, Analytical Chemistry, 1982. **54**(14) 2532-2535
23. Sleszynski, N., Osteryoung, J., Carter M., *Arrays of very Small Voltammetric Electrodes Based on Reticulated Vitreous Carbon*, Analytical Chemistry, 1984 **56** (2) 130-135.
 24. Wang, J. and B.A. Freiha, *Vitreous Carbon-Based Composite Electrode as Electrochemical Detector for Liquid-Chromatography*. Journal of Chromatography A, 1984. 298: p. 79-87.
 25. Fletcher, S. and M.D. Horne, *Random Assemblies of Microelectrodes for Electrochemical Studies*. Electrochemistry Communications, 1999. 1: p. 502-512.
 26. Rojo, A., A. Rosenstratten, and D. Anjo, *Characterization of a Conductive Carbon-Film Electrode for Voltammetry*. Analytical Chemistry, 1986. **58**(14): p. 2988-2991.
 27. Sreenivas, G., et al., *Fabrication and Characterization of Sputtered-Carbon Microelectrode Arrays*. Analytical Chemistry, 1996. 68: p. 1858-1864.
 28. Starr, A., K.D. Wise, and J. Csongradi, *Evaluation of Photoengraved Microelectrodes for Extracellular Single-Unit Recording*. IEEE Transactions in Biomedical Engineering, 1973. **20**(4): p. 291-293.
 29. Reller, H., E. Kirowa-Wisner, and E. Gileadi, *Ensembles of*

- Microelectrodes - Digital Simulation by the Two Dimensional Expanding Grid Method - Cyclic Voltammetry, IR Effects and Applications*. Journal of Electroanalytical Chemistry, 1984. **161**(2): p. 247-268.
30. Kittlesen, G.P., H.S. White, and M.S. Wrighton, *A Microelectrochemical Diode with Sub-Micron Contact Spacing based on the Connection of 2 Microelectrodes using Dissimilar Redox Polymers*. Journal of the American Chemical Society, 1985. **107**(25): p. 7373-7380.
31. Cassidy, J., et al., *Simulation of the Edge Effects in Electroanalytical Experiments by Orthogonal Collocation. 6. Cyclic Voltammetry at Ultramicroelectrode Ensembles*. Electrochimica Acta, 1986. **31**(6): p. 629-636.
32. Bard, A.J., et al., *Digital-Simulation of the Measured Electrochemical Response of Reversible Redox Couples at Microelectrode Arrays- Consequences arising from Nearly Spaced Ultramicroelectrodes*. Analytical Chemistry, 1986. **58**(11): p. 2321-2331.
33. Matsue, T., et al., *Multichannel Electrochemical Detection System for Flow-Analysis*. Analytical Chemistry, 1990. **62**(4): p. 407-409.
34. Niwa, O., M. Morita, and H. Tabei, *Fabrication and Characteristics of Vertically Separated Interdigitated Array Electrodes*. Journal of Electroanalytical Chemistry, 1989. **267**(1-2): p. 291-297.

35. Sanderson, D.G. and L.B. Anderson, *Filar Electrodes - Steady-State Currents and Spectroelectrochemistry at Twin Interdigitated Electrodes*. Analytical Chemistry, 1985. **57**(12): p. 2388-2393.
36. Kiema, G.K., S. Ssenyange, and M.T. McDermott, *Microfabrication of Glassy Carbon by Electrochemical Etching*. Journal of the Electrochemical Society, 2004. **151** (2) C142-C148.
37. Ranganathan, S., et al., *Photoresist-Derived Carbon for Microelectromechanical Systems and Electrochemical Applications*. Journal of the Electrochemical Society, 2000. **147**(1): p. 277-282.
38. Ranganathan, S. and R.L. McCreery, *Electroanalytical performance of carbon films with near-atomic flatness*. Analytical Chemistry, 2001. (5): p. 893-900.
39. Delamar, M., Hitmi, R., Pinson, J., Saveant, J. M., *Covalent Modification of Carbon Surfaces by Grafting of Functionalized Aryl radicals produced from Electrochemical Reduction of Diazonium Salts*. Journal of the American Chemical Society, 1992. **114** (14), 5883-5884
40. Cheng, I.F., L.D. Whiteley, and C.R. Martin, *Ultramicroelectrode Ensembles. Comparison of Experimental and Theoretical Responses and Evaluation of Electroanalytical Detection Limits*. Analytical Chemistry, 1989. **61**: p. 762-766.

41. Drogoff, B.L., et al., *Effect of the Microelectrode Geometry on the Diffusion Behavior and the Electroanalytical Performance of Hg-Electroplated Iridium Microelectrode Arrays Intended for the Detection of Heavy Metal Traces*. *Electroanalysis*, 2001. **13**(18): p. 1491-1496.
42. Barbier, B., et al., *Electrochemical Bonding Of Amines To Carbon Fibers Surface Towards Improved Carbon-Epoxy Composites*. *Journal of the Electrochemical Society*, 1990. **137**(6): p. 1757-1763.
43. Delamar, M., et al., *Covalent Modification of Carbon Surfaces by Grafting of Functionalized Aryl Radicals Produced from Electrochemical Reduction of Diazonium Salts*. *Journal of the American Chemical Society*, 1992. **114**(14): p. 5883-5884.
44. Kariuki, J.K. and M.T. McDermott, *Nucleation and Growth of Functionalized Aryl Films on Graphite Electrodes*. *Langmuir*, 1999. **15**(19): p. 6534-6550.
45. Kariuki, J.K. and M.T. McDermott, *Formation of Multilayers on Glassy Carbon Electrodes via the Reduction of Diazonium Salts*. *Langmuir*, 2001. **17**(19): p. 5947-5951.

CHAPTER 6

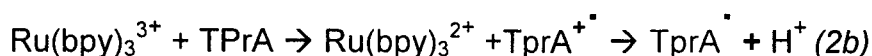
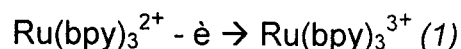
CONCLUSIONS AND FUTURE WORK INVOLVING THE APPLICATION OF ELECTROCHEMICAL ETCHING

As first prototypes, these initial devices fabricated by the electrochemical etching of carbon substrate were successful and many more are plausible. In the future, there are several applications that could utilize electrochemically fabricated glassy carbon or pyrolyzed photoresist films. A few of these applications are described in detail in the following sections.

6.1 ELECTROGENERATED CHEMILUMINESCENCE DETECTION ON A GLASSY CARBON MICROCHIP

Electrogenerated Chemiluminescence (ECL) has grown into a rather established field that includes many different chemical systems and applications. Advances in the area include new co-reactants[1, 2] and new emitters[3]. New applications consist of scanning optical microscopic methods[4], studies of novel organic systems and extensions to the analysis of non-electroactive species. ECL[5] arises from an energetic electron-transfer reaction between electrogenerated redox species, typically radical ions, to form an excited state that emits in the visible region. Historically, ECL has been performed in organic solutions[6]. However, several chemical precursor systems have been reported in aqueous solution[7], one of which has received tremendous study due to the simplicity of the required set-up for ECL. This system requires an anodic oxidation reaction between the inorganic species, tris (2,2'-bipyridyl) ruthenium (II) $[\text{Ru}(\text{bpy})_3^{2+}]$, and an organic co-reactant, tri-n-propylamine (TprA)[1, 2]. The proposed mechanism for this reaction, which exhibits significant ECL upon

oxidation at the glassy carbon electrode[5], is given below:



The principle reason that the use of this ECL system could prove valuable to study in a glassy carbon (GC) microchip format is the fact that the $\text{Ru}(\text{bpy})_3^{2+}/\text{TPrA}$ couple has shown significant sensitivity and selectivity[8] and can be utilized in many analytical applications. The broad relevance of this detection scheme set-up is that if detection of $\text{Ru}(\text{bpy})_3^{2+}$ or other electrogenerated chemiluminescent species, which could be used as labels in immunoassays and as DNA probes, can be accomplished on the GC microchip format, a novel yet simplistic way of detecting such species would have been achieved. Up until now, many steps had to be carried out to microfabricate electrodes onto glass microchips, a process that would entirely be avoided if GC was used. With this unique scheme, the microfabricating process is shortened and the ECL sensitivity increased due to the use of a glassy carbon electrode[9].

6.2 MICROFABRICATED ELECTROLYSIS PUMP SYSTEM

Another application that could benefit from the microfabrication of glassy carbon would be the implementation of a fabricated Twente electrolysis micropump as described by a group at the University of Twente [10, 11]. In this microfabricated electrochemical pump, a gas is formed by electrolysis of a solvent and forms a bubble pump. Low voltages are applied to electrodes, located in a pump chamber, where a sample electrolyte solution is located. Being quite tedious, the device fabrication process usually occurs on a silicon substrate and is a two-mask process. It requires the deposition of a metal layer for the electrodes and isolation of the electrode from the silicon substrate by the growth of a thermal oxide layer. Conversely, adaptation of this device onto a GC substrate would eliminate several of the described steps. Foremost, device fabrication would be reduced to a single mask process. The growth of a thick ($\sim 1\mu\text{m}$) and durable oxide layer would only require a simple cyclic voltammetry sweep as described by Kepley and coworkers [12]. Also, the deposition of metal electrodes would be unnecessary, as the insulated glassy carbon substrate would serve as an excellent electrode for electrolysis.

6.3 MODIFIED CARBON SUBSTRATES FOR ELECTROSPRAY MASS SPECTROMETRY STUDIES

Finally, it would be interesting to repeat the experiments that were presented in chapter 3, but with modified glassy carbon as a substrate. It is

well known that carbon surfaces can be modified using various electrochemically assisted diazonium salt [13] depositions. Studies involving diazonium moieties that present hydrophobic and hydrophilic functionalities would undoubtedly confer useful observations in the electrospray ionization (ESI) mass spectrometry of various peptides and proteins. The data collected during these follow-up experiments would be a valuable addition to the current knowledge about ESI mass spectrometry data available on proteins and peptides.

6.4 REFERENCES

1. Leland, J.K. and M.J. Powell, *Electrogenerated Chemiluminescence - an Oxidative-Reduction Type ECL Reaction Sequence Using Tripropyl Amine*. Journal of the Electrochemical Society, 1990. 137(10): p. 3127-3131.
2. McCord, P. and A.J. Bard, *Electrogenerated Chemiluminescence* .54. *Electrogenerated Chemiluminescence of Ruthenium (II) 4,4'-Diphenyl-2,2'-Bipyridine and Ruthenium (II) 4,7-Diphenyl-1,10-Phenanthroline Systems in Aqueous and Acetonitrile Solutions*. Journal of Electroanalytical Chemistry, 1991. 318(1-2): p. 91-99.
3. Myung, N., Z.F. Ding, and A.J. Bard, *Electrogenerated Chemiluminescence of CdSe Nanocrystals*. Nano Letters, 2002. 2(11): p. 1315-1319.
4. Zu, Y.B., et al., *Scanning Optical Microscopy with an Electrogenerated Chemiluminescent Light Source at a Nanometer Tip*. Analytical Chemistry, 2001. 73(10): p. 2153-2156.
5. Faulkner, L.R. and A.J. Bard, *Electroanalytical Chemistry*, ed. A.J. Bard. Vol. 10. 1977, New York: Marcel Dekker. 1.
6. Mann, C.K., *Cyclic Stationary Electrode Voltammetry of Some Aliphatic*

- Amines*. Analytical Chemistry, 1964. 36(13): p. 2424-2426.
7. Knight, A.W. and G.M. Greenway, *Occurrence, Mechanisms and Analytical Applications of Electrogenenerated Chemiluminescence - Review*. Analyst, 1994. 119(5): p. 879-890.
 8. Richards, T.C. and A.J. Bard, *Electrogenenerated Chemiluminescence .57. Emission from Sodium 9,10-Diphenylanthracene-2-Sulfonate, Thianthrenecarboxylic Acids, and Chlorpromazine in Aqueous-Media*. Analytical Chemistry, 1995. 67(18): p. 3140-3147.
 9. Zu, Y.B. and A.J. Bard, *Electrogenenerated Chemiluminescence. 67. Dependence of Light Emission of the Tris(2,2')bipyridylruthenium(II)/tripropylamine system on Electrode Surface Hydrophobicity*. Analytical Chemistry, 2001. 73(16): p. 3960-3964.
 10. Bohm, S., W. Olthuis, and P. Bergveld, *An Integrated Micromachined Electrochemical Pump and Dosing System*. Journal of Biomedical Microdevices, 1999. 1: p. 121-130.
 11. Bohm, S., et al., *A Closed-Loop Controlled Electrochemically Actuated Micro-dosing System*. Journal of Micromechanical Microengineering, 2000. 10: p. 498-504.
 12. Kepley, L.J. and A.J. Bard, *Ellipsometric, Electrochemical, and Elemental Characterization of the Surface Phase Produced on Glassy Carbon*

Electrodes by Electrochemical Activation. Analytical Chemistry, 1988.
1988(60): p. 1459-1467.

13. Downard, A.J., *Electrochemically Assisted Covalent Modification of Carbon Electrodes*. Electroanalysis, 2000. 12(14): p. 1085-1096.